MODELING OF CIRCULAR COUNTERFLOW SWISSROLL COMBUSTOR FOR MEMS APPLICATION

by

Emre Özgül

B.S., in M.E., Istanbul Technical University, 2005

Submitted to the Institute for Graduate Studies in
Science and Engineering in partial fulfillment of
the requirements for the degree of
Master of Science

Graduate Program in Mechanical Engineering

Boğaziçi University

2008

ACKNOWLEDGEMENTS

I would like to express sincere gratitude to my thesis supervisor Assoc. Prof. Hasan Bedir for his academic support, motivation and the kind guidance he has shown throughout the study.

I am also grateful to TUBITAK for their support.

I am indebted to everybody who helped me during my thesis at the Mechanical Engineering Department of Bogazici University.

Last but not least; I would like to thank my family for their endless support and finding ways to encourage me for accomplishing my thesis.

This thesis has been supported by Bogazici University Scientific Research Project BAP06A602.

ABSTRACT

MODELING OF CIRCULAR COUNTERFLOW SWISSROLL COMBUSTOR FOR MEMS APPLICATION

A two-dimensional numerical model is generated for simulating combustion and heat transfer in "Spiral Swiss roll" combustors. In this research, the most important purpose is to investigate the micro-scale combustion and the extinction limits in such combustors. The momentum, energy, pressure, ideal gas and species equations are numerically modeled for accomplishing this goal. This models couples heat transfer and chemical reaction in the gas and heat diffusion in the conducting walls. Since; there is complexity exists about modeling a Spiral Swiss roll combustor, unwrapped model is preferred for simplicity. Hence; the Spiral Swiss roll geometry is unwrapped in to a straight channel, and the diffusion of heat among the walls is simulated by using heat fluxes and transporting them throughout the geometry. By this way, heat recirculation between the unburnt and burnt gas is taken into consideration appropriately. Besides, the effect of Reynolds number, equivalence ratio, wall thickness, wall conductivity constant and channel height on the temperature distribution and chemical reaction rate is investigated. Also, the extinction limits observed for different channel heights and Reynolds numbers. Propane and Methane are selected as fuel. In the code development, the SIMPLE method is used as the main algorithm, and FORTRAN is used.

ÖZET

DAİRESEL SWISSROLL SİSTEMLERİNİN MODELLENMESİ

Bu çalışmada, Spiral Swiss Döngülü sistemlerde yanma ve ısı transferi iki boyutlu olarak bilgisayar ortamında sayısal olarak modellenmiştir. Bu araştırmanın temel amacı, bu tip yakıcılarda, mikro ölçekte yanmayı ve sönme limitlerini incelemektir. Bu sebeple, momentum, enerji, basınç, ideal gaz ve tür denklemleri modellenmiştir. Bu model gaz ortamında ısı transferini ve kimyasal reaksiyonu birleştirirken, iletken duvarlardaki ısı difüzyonunu da gerçekleştirmektedir. Spiral Swiss döngülü yanıcıların modellenmesindeki zorluklar nedeniyle, döngünün açılarak modellenmesi basitlik açısından kararlaştırılmıştır. Böylece, Spiral Swiss döngülü geometri, düz bir kanal şeklinde açılmış , duvarlar boyunca gerçekleşen ısı difüzyonu da ısı akılarının kullanımı ve bunların geometri boyunca transferi sayesinde gerçekleştirilmiştir. Bu şekilde, yanmış ve taze gazlar arasındaki ısı dolaşımı hesaba katılabilmektedir. Ayrıca, Reynolds değerinin, yakıt hava oranının, duvar kalınlığının, duvar iletim katsayısının ve kanal yüksekliğinin, sıcaklık dağılımı ve kimyasal reaksiyon değeri üzerindeki etkileri incelenmiştir. Sönme limitleri farklı Reynolds değerleri ve kanal uzunlukları için hesaplanmıştır. Propan ve Metan yakıt olarak kullanılmıştır. Gelişme aşamasında, SIMPLE metodu temel algoritma olarak tercih edilirken, FORTRAN programı da kod geliştirilmesinde kullanılmıştır.

TABLE OF CONTENTS

LIST OF FIGURES

LIST OF TABLES

LIST OF SYMBOLS/ABBREVIATIONS

B	Pre-exponential constant
C_P	Specific heat capacity
d	Channel height
Da	Damkohler number
E	Activation Energy
h	Convective heat transfer coefficient
L	Total length of the channel after unwrapping the Swiss roll
L_1	Total length of the outer wall, excluding the fillers
L_2	Total length of the inner wall, excluding the fillers
Le	Lewis number
MW	Molecule weight of air
Nu	Nusselt number
Pe	Peclet number
Q	Heat Flux
R	Universal gas constant
Re	Reynolds number
s	Length of the outer wall exposed to the environment
t	Time
R	Universal gas constant
T	Temperature
x	Streamwise coordinate
y	Coordinate across the channel height
u	X- directional velocity
v	Y-directional velocity
Y	Mass fraction
D	Binary diffusion coefficient
X	Mole fraction
n	Mole
w	Chemical Reaction rate

p	Pressure
m	Channel height value that is used in the code
ss	Wall thickness value that is used in the code
r	Radius
k	Thermal conductivity
L_x	Channel length in x-direction
L_y	Channel length in y-direction
Bi	Biot number
Q_a	Convective heat flux (for the outer wall) from the gas inside the unwrapped channel
Q_b	Convective heat flux (for the outer wall) from the gas outside the unwrapped channel
Q_c	Convective heat flux (for the inner wall) from the gas inside the unwrapped channel
Q_d	Convective heat flux (for the inner wall) from the gas outside the unwrapped channel
S_u	Source in x direction for momentum equation
S_v	Source in y direction for momentum equation
f_k	Body force
a	Spiral equation coefficient
Pe	Peclet number
F	Convective coefficient
h_k	Heat of combustion
$v_{d,k}$	Diffusion velocity
$J_{d,k}$	Diffusion flux
α	Thermal diffusivity
ϵ	Emissivity of the wall
δ	Wall thickness
ϕ	Equivalence ratio
λ	Thermal conductivity
μ	Dynamic viscosity
ν	Kinematic viscosity

ρ	Density
θ	Angle
Y_f	Mass fraction of fuel
T_g	Gas temperature
T_r	Reference temperature
T_{w1}	Outer wall temperature
T_{w2}	Inner wall temperature
nb	Neighbour

1. INTRODUCTION

Combustion or burning is a complex sequence of chemical reactions between a fuel and an oxidant accompanied by the production of heat or both heat and light in the form of flame glows. Combustion is an important transfer mechanism that transforms stored energy of the chemical bonds into heat. In other words; it is a chemical process in which a substance reacts rapidly with oxygen and gives off heat. The original substance is called the fuel, and the source of oxygen is called the oxidizer. The fuel can be a solid, liquid, or gas. The oxidizer, likewise, could be a solid, liquid, or gas. During combustion, new chemical substances are created from the fuel and the oxidizer. These substances are called exhaust. Most of the exhaust comes from chemical combinations of the fuel and oxygen. When a hydrogen-carbon-based fuel (like gasoline) burns, the exhaust includes water and carbon dioxide. But the exhaust can also include chemical combinations from the oxidizer alone.

During the combustion process, as the fuel and oxidizer are turned into exhaust products, heat is generated. Interestingly, some source of heat is also necessary to start combustion. As a result of combustion, combustion products are created and heat is released. You can control or stop the combustion process by controlling the amount of the fuel available, the amount of oxygen available, or the source of heat.

Although it has a complex structure, combustion has a significant effect on human being's daily life. It can be easily said that combustion is a key element of modern society's critical technologies. Statistically, combustion accounts for approximately 85 percent of the world's energy usage and is vital to current way of life. [12]

There are many application areas of combustion. Spacecraft and aircraft propulsion, electric power production, home heating, ground transportation, and materials processing all use combustion to convert chemical energy to thermal energy or propulsive force. Besides; gas turbines and jet engines, rocket propulsion, rocket engines, guns and explosives, boilers and furnaces, flame synthesis of materials (nano- materi-

als), chemical processing, forming of materials, fire hazards and safety are some other application areas. The variety of the application areas shows the importance of combustion in our daily life and proves that combustion and its control are obligations for the existence of humankind.

A relatively new application area of combustion is power production in Micro-Electro-Mechanical Systems (MEMS). The miniaturization of electromechanical devices and the resulting need for micro power generation (mill watts to watts) with low-weight, long-life devices have led to the recent development of the field of micro scale combustion. Especially, that kind of power generation systems may seriously exist in battery replacement applications. Because previous studies proved that the energy storage density of hydrocarbon fuels is higher than classical batteries such as lithium-ion batteries, a micro-scale combustor utilizing from hydrocarbon fuels is superior over batteries about the energy storage density.

However, micro-scale combustion includes some problems that should be solved before the widespread of the technology. Combustion can not be sustained easily in such scales in general due to large heat loss occurring because of large surface to volume ratio. As the size of the combustor is diminished, both rate of heat release and rate of heat loss decrease. But, the heat loss rate becomes more significant as the size decreased. Since the heat loss rate increases by the decrease of the combustor scale, extinction limits get narrower. The temperatures of the cold boundaries become highly important to sustain the combustion. Also, the quenching distance becomes a significant parameter that should be taken into consideration in combustion models.

However, if appropriate thermal management can be made, combustion in such small to micro-scales is possible and it can be utilized for, small scale power generators and small scale heaters that alternate electric heater. A promising combustor type for MEMS applications is heat re-circulating Excess Enthalpy burners. Swiss roll counter-flow combustors are specific examples for that kind of burners. In that type, thermal energy is transferred from products to reactants without mass transfer. Since the total reactant enthalpy is higher in the incoming cold reactants, combustion can be

sustained under conditions that would result as the extinguishment of the flame without recirculation.

2. LITERATURE SURVEY

Sitski, Borer and Ronney [1] have accomplished some experiments on 2D and 3D Swiss Roll burner prototypes. The prototypes were built using a ceramic "rapid prototyping" technique. It was found that combustion could be sustained in a low-temperature "flameless" mode in which no visible flame occurs. For the macro scale devices, the typical channel size of the micro scale test devices is 3 mm vs. 0.13 mm. It was found that the addition of catalytic materials in the combustion region was found to either increase or decrease the range of flammable mixtures, by substantial amounts in both cases, depending on the Re. It is proved that; with catalysts, the extinction limits narrow at higher Reynolds numbers but broaden substantially at lower Re, which are the conditions most relevant to microscale combustion. They also indicate that, combustion in microscale combustion devices at low Reynolds numbers is possible, but require heat recirculation via the "Swiss roll" or similar heat exchanger geometries, as well as catalytic combustion.

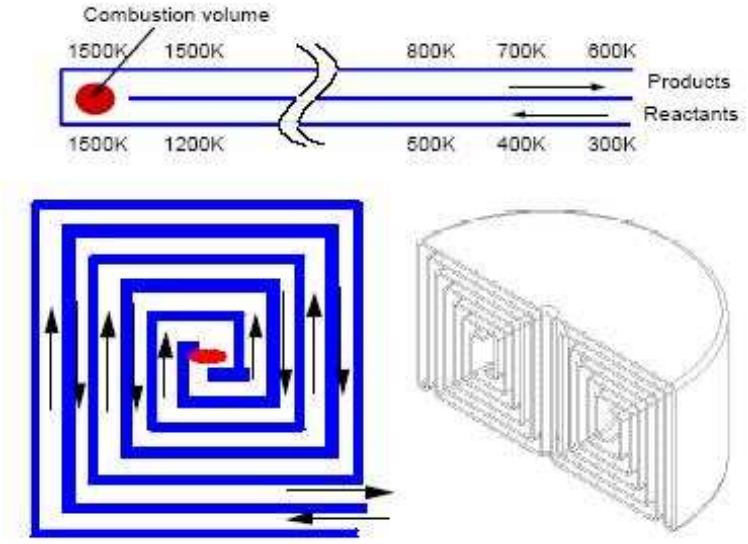

Figure 2.1. Another Swiss Roll geometry [1]

A simple first-principles model of counter- current heat- recirculating combustors is developed by Ronney [4]. The study includes the effects of heat transfer from the product gas stream to the reactant stream, heat loss to ambient and heat conduction in

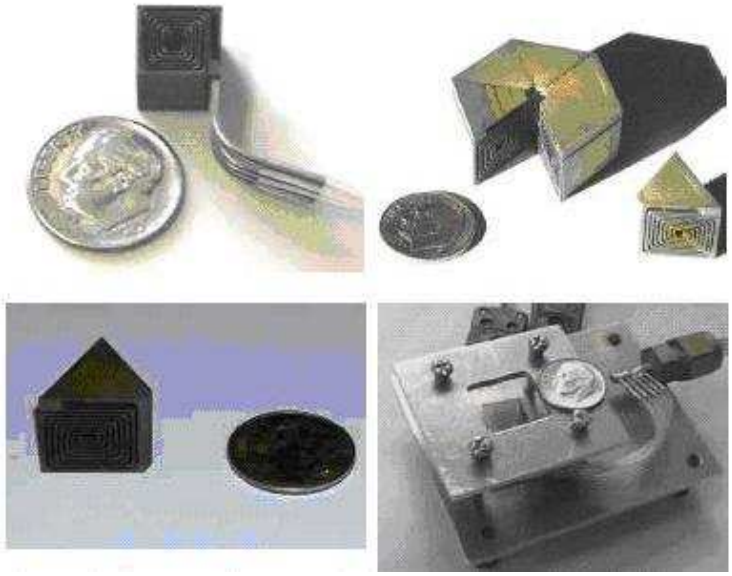

Figure 2.2. Swiss Rolls in different sizes [1]

the stream wise direction through the dividing wall between the reactant and product streams. In the research; heat flux is a significant parameter and denoted as "M". In the study, it is proved that streamwise conduction through wall has a major effect on the operating limits of the combustor, especially at small dimensionless mass fluxes (M) or Reynolds numbers that would be characteristics of micro scale devices. In the research it is also noted that, the wall conduction is not only a heat loss mechanism;it also re-distributes thermal energy within the counter- current heat- recirculating combustor.

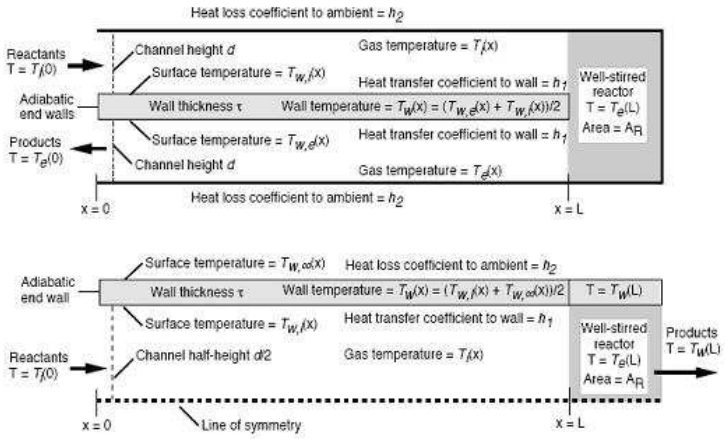

Figure 2.3. U-tube excess enthalpy burner. Upper: counter-current system. Lower: conductive tube [4]

Cui and Matalon [5] have investigated the flame propagation in channels and cracks with applications in many combustion devices. For example, the gas flowing into crevice volumes of an internal combustion engine cools by heat transfer to a temperature that may or may not allow the approaching flame to penetrate the narrow entrance, which has an overall effect on the combustion efficiency with potential contribution to the emission of chemical pollutants. In micro- combustors it is desirable to control the propagation of a flame in gaps that are smaller than the quenching diameter. In the study, the propagation of premixed flames in two-dimensional channels of variable width with a prescribed Poiseuille flow is discussed. The results show that unlike thin flames, known to be affected by the effective Lewis number of the mixture, in narrow channels Lewis number effects are negligible. Also it is shown that; as a result of heat losses to the walls the burning rate is generally reduced; in narrow channels the flame may be totally extinguished when the losses become excessive, but in wide channels there is only local extinction near the walls with the flame surviving in the center.

In another study [7], the characteristics of micro scale combustion were investigated by using a micro channel heated by an external source by Maruta and Parc. Methane-air mixture is used for investigations. The effects of the equivalence ratio and the averaged flow velocity on the characteristics of combustion in the micro channel were examined. Oscillatory combustion was observed at moderate equivalence ratios and lower velocity conditions within the flammability region. A simple analytical model predicting flame oscillations on the basis of the linear analysis of steady solutions is proposed. Combustion of methane-air mixtures in an externally heated micro channel was examined. Results show that; stable combustion can successfully be attained even for mixtures with equivalence ratios outside the conventional flammability limits. It is also shown that; in addition to the steady flame, combustion was also observed for low velocities of the flow. It is also noted that; the stationary stable combustion modes predicted by the theory were observed experimentally.

Dryer and Vican's [2] design is based on a Swiss roll concept of double spiral-shaped channels to facilitate a high level of heat transfer between the reactants and

combustion products and wall surface contact of the flow through the micro reactor body. A global energy balance model was developed to analyze overall reactor performance characteristics. The study has shown that because of the small length scales and flow rates involved in the micro reactor, a nearly uniform reactor body and gas flow temperature is obtained. In a quiescent environment with an un-insulated reactor, significant heat losses from the surface of the reactor via convection and radiation occur. However, it should be noted that even if convection losses were minimized through methods such as vacuum insulation, the radiation losses would continue to play a significant role, unless radiation- shielding approaches are pursued. It is also added that; in the reactor, the catalyst was distributed on the internal channels throughout the reactor body. Future designs are underdevelopment to limit catalyst location to the center regions of the reactor, benefiting some of the possible approaches to reducing heat losses.

The limits to self-sustaining catalytic combustion in a micro-scale channel were studied computationally using a cylindrical tube reactor by K. Maruta [3]. In that study, the tube, 1mm in diameter, 10 mm long and coated with Pt catalyst, was assumed to be thermally thin and the boundary condition on the wall was set to be either adiabatic or non-adiabatic with fixed heat transfer coefficient. Methane-air mixtures were used. They show that, when the wall boundary condition was adiabatic, the equivalence ratio at the extinction limit monotonically decreased with increasing Re. In contrast, for non adiabatic conditions the extinction curve exhibited U-shaped dual limit behavior, that is, the extinction limits increased/decreased with decreasing Re in smaller/larger Re regions, respectively. They also found that by diluting the mixture with N_2 rather than air, the fuel concentration and peak temperatures at the limit decreased substantially for mixtures with fuel to oxygen ratios even slightly rich of stoichiometric due to a transition from O(s) coverage to CO(s) coverage.

In their study [6], a two dimensional model is developed by Chen and Buckmaster to simulate combustion and heat transfer in SRCs. This model couples heat transfer and chemical reaction in the gas and heat diffusion in the conducting walls. The target of the model is to investigate the occurrence of extinction and the ways of preventing

it. In the Chen and Buckmaster's numerical modeling, the "Swiss Roll" geometry is unwrapped into straight channel, with heat recirculation between the unburnt and burnt gas being appropriately taken into account. Besides; the extinction mechanisms and heat transfer characteristics in the combustor are investigated and parametric studies are performed for examining their effects on combustion and extinction. In the experiments, the fuel is limited as propane, also an assumption is made about velocity profile and momentum equations are not solved. They show that; stable combustion in micro-scale combustors can be achieved via SRCs. It is also shown that, for the range of Reynolds numbers and equivalence ratios studied in this paper, as the Reynolds number or equivalence ratio increases, the reaction rate increases and the reaction front moves away from the center of the Swiss Roll towards the inlet.

Kim and Kato [9] investigated the combustion characteristics of a small Swiss-roll combustor that is used as a heater. Three types of Swiss-roll combustors of different designs and two cases of heat transfer conditions were studied. The types are denoted as S, W and D type Swiss-roll combustors and differs from each other due to channel height and channel turn values. The S type Swiss-roll combustor has a channel depth of 6 mm, channel turn of 3 mm and the channel height is 16 mm. The W type Swiss-roll combustor has a channel depth of 6 mm, channel turn of 4 mm and the channel height is 16 mm. The D type Swiss-roll combustor has a channel depth of 15 mm, channel turn of 4 mm and the channel height is 27 mm. The effects of design parameters on the performance of these combustors are also other points of investigation. Kim and Kato show that when the combustor becomes smaller, even tough convective heat transfer becomes larger compared with the radiant heat loss for the same temperature; it requires a higher temperature for flame stabilization. They also state that, it is expected that a flame can be stabilized in a much smaller Swiss-Roll combustor only if the wall temperature of the combustor is sufficiently high. The temperature of the combustor can be controlled by controlling the equivalence ratio or the mean velocity. They also proved that the mean temperatures and the flammable limits of the combustors were governed by both the radiant heat loss from the combustors and the total chemical energy introduced into the combustors.

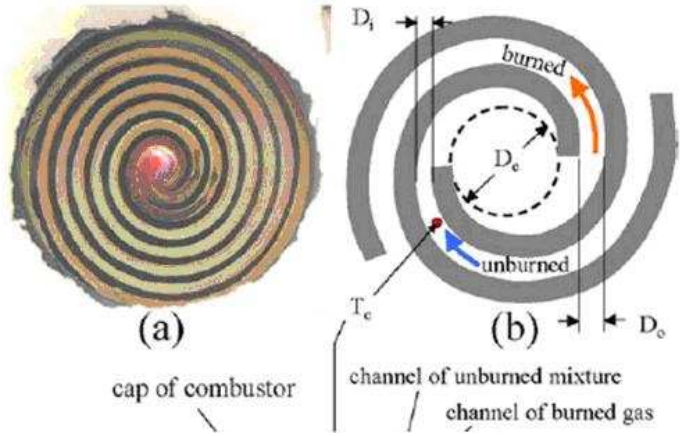

Figure 2.4. Circular excess enthalpy counter flow Swiss Roll burner [9]

Suzuki and Horii [10] have investigated micro-scale catalytic combustion of butane in their study. A ceramic combustor with an embedded ignition heater is also designed and its prototype is fabricated using a high- precision tape-casting technology. The Pt/alumina catalyst layer is successfully integrated onto a ceramic micro channel. In this study, Suzuki and Horii have proved that the system work well for catalytic combustion of butane.

Ronney and Ahn [8] accomplished an experimental study of a spiral counter flow "Swiss Roll" burner which is 7cm x 7 cm x 5 cm tall and 3.5 mm channel height, with investigations on the determination of extinction limits and comparison of results with and without catalysts. In that study, they proved that both lean and rich extinction limits are extended with the catalysts, whereas rich limits extended much further. They also show that Swiss Roll burners are successful in re-circulating thermal energy from high temperature burnt gas to low temperature fresh air- fuel mixture. Results are examined for various Re number values.

In the present research; the Spiral Swiss Roll burners are modeled. The model has some differences relative to the previous studies. First of all, many other researches have preferred finite difference method for evolving the model. However, in this study, finite volume method is used. Also, another significant difference is the SIMPLE Algorithm. This algorithm is used for coupling the momentum, pressure, energy, ideal gas, chemical reaction rate and species equations.

Besides, the most important property of the project is the variable geometry. In the study, various geometries including; Rectangular, 11 parts unwrapped Rectangular, 18 parts unwrapped Rectangular, 11 parts unwrapped Spiral and 18 parts unwrapped spiral Swiss Roll geometries are modeled. It should be noted that, 2D geometry is used. Hence; although in some researches [6] the momentum equations are not modeled; in this project, x and y direction velocities are obtained via solving the equations.

In the following chapters, the unwrapping process is also mentioned in detail. The effects of equivalence ratio, Re number, wall thickness, thermal conductivity and the material of walls on the temperature distribution and chemical reaction rate are investigated. Extinction limits are obtained for different channel lengths and Re numbers. Fuel is also important parameter. During the study, propane is chosen as the primary fuel and methane is also used as a secondary fuel.

3. MATHEMATICAL MODEL

3.1. Swiss Roll geometries used

In this project, unwrapping of 18 part and 11 Part Rectangular and 18 part and 11 Part Spiral Swiss Roll Combustors are performed. First of all, the unwrapping of the 11 parts rectangular swiss roll which is illustrated in 3.1 is obtained.

In this process, the thickness of the wall of the swiss roll geometry is called as "ss" and the channel height is called as "m". Then every point that are located in the corners of the rectangular swiss roll system is defined in terms of m and ss. This condition provides a simplicity about passing through geometries without any distructions by only altering the m and s values. The rectangular Swiss Roll geometry and the points are illustrated in figure 3.1.

The Spiral Swiss Roll geometry is also unwrapped. The original illustrations of the unwrapped Spiral Swiss Roll geometries are represented for 11 part (in figure 3.2) and 18 part (in figure 3.3) Swiss rolls, respectively. But, the process is different from the rectangular one. In spiral systems, different parameters are used for generalizing the system.

These parameters are; r, a and θ . These parameters are related to each other by the equation represented below:

$$r = a\theta \qquad \frac{dr}{d\theta} = a \tag{3.1}$$

Also, length (L) is another important factor. Length is obtained by the formulas

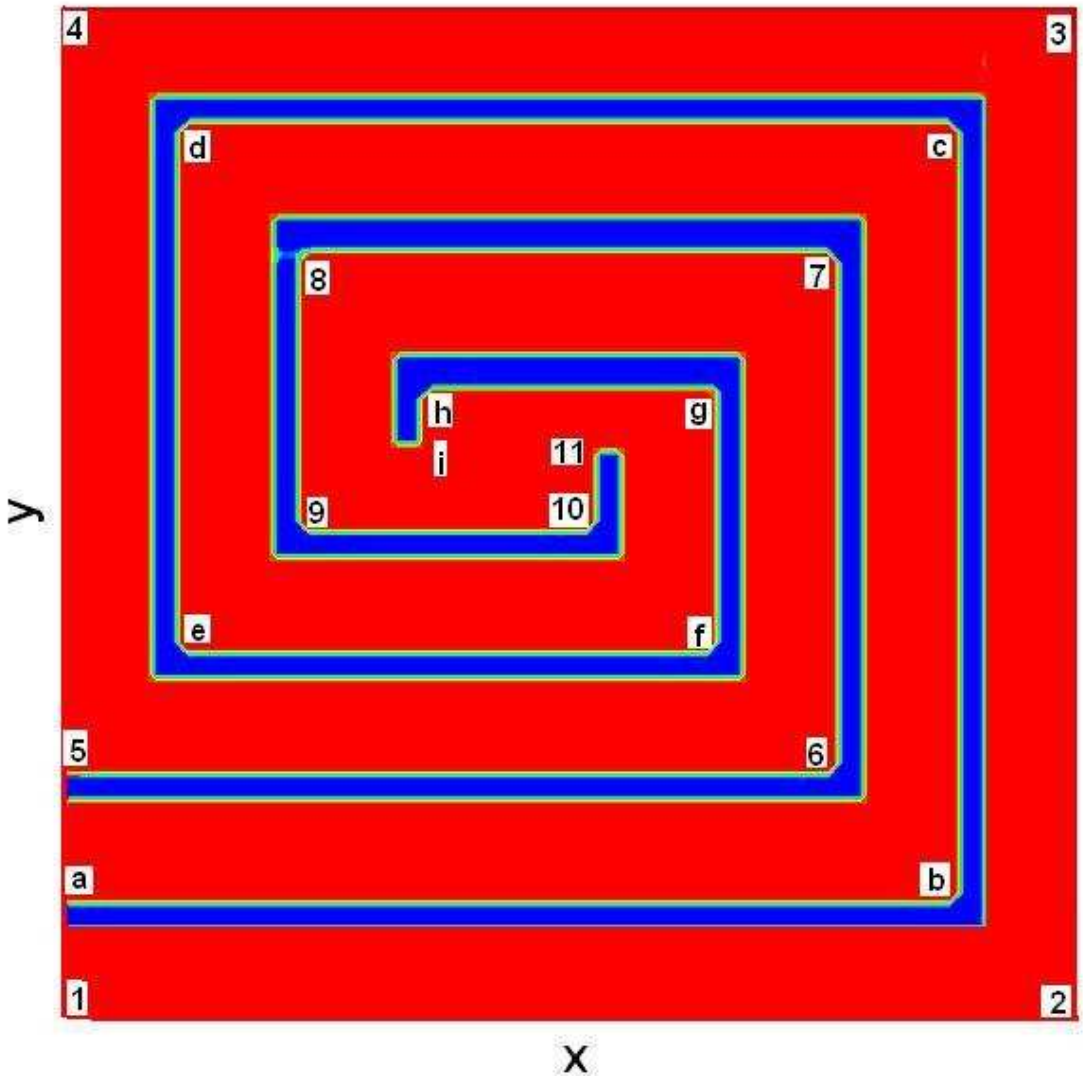

Figure 3.1. The 11 part Rectangular Swiss Roll Geometry

shown below.

$$L = \int_{\alpha}^{\beta} \sqrt{r^2 + \left(\frac{dr}{d\theta}\right)^2} d\theta = \int_{\alpha}^{\beta} \sqrt{a^2\theta^2 + a^2} d\theta$$
$$L = a \int_{\alpha}^{\beta} \sqrt{\theta^2 + 1} d\theta = a \left[\frac{\theta}{2}\sqrt{\theta^2+1} + \frac{1}{2}\ln\left(\theta + \sqrt{\theta^2+1}\right)\right]_{\alpha}^{\beta} \tag{3.2}$$

By using these formulas, different Swiss roll geometries with different channel heights can be created. In this project, "a" is regenerated for every significant channel length.

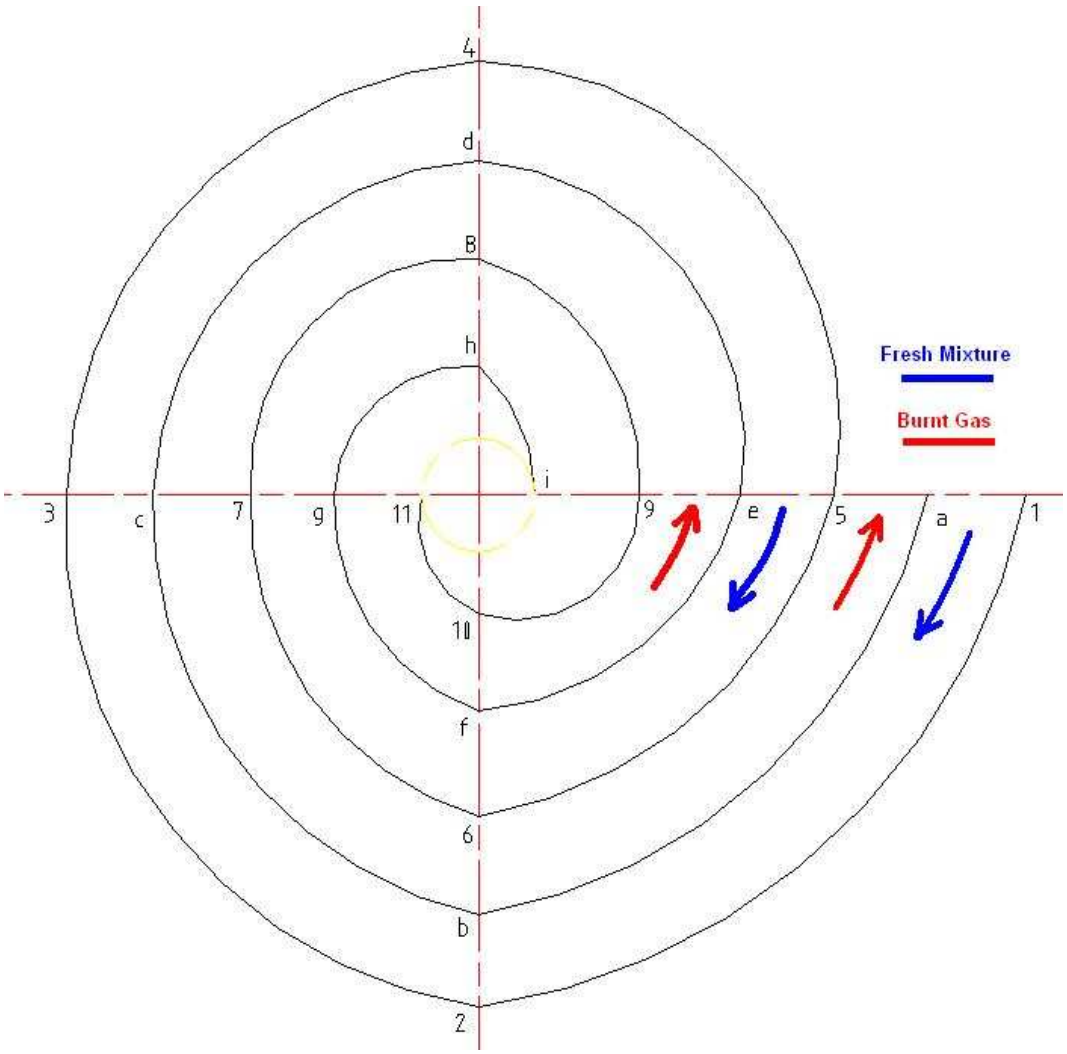

Figure 3.2. The 11 part Spiral Swiss Roll Geometry

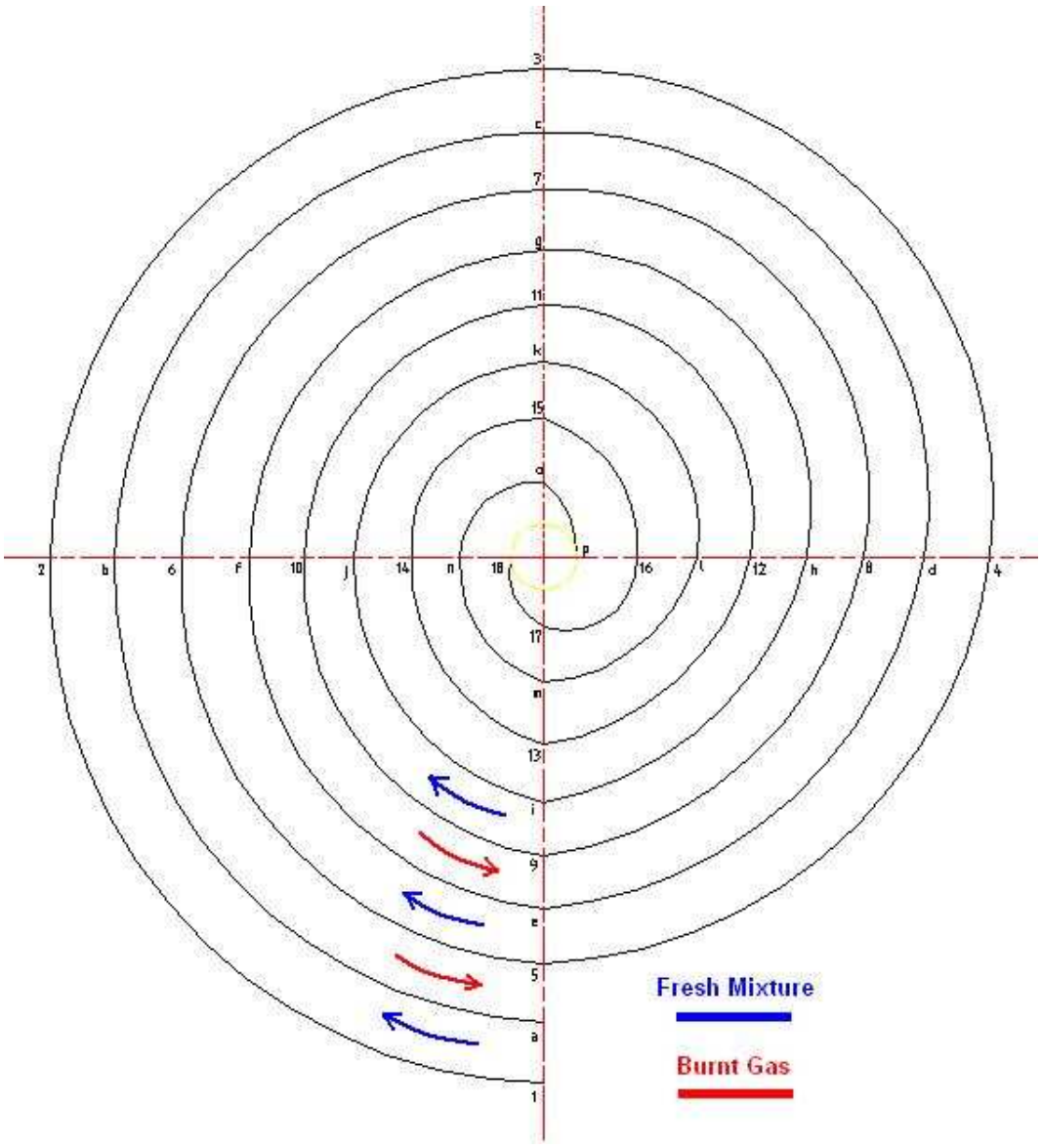

Figure 3.3. The 18 part Spiral Swiss Roll Geometry

3.2. The Unwrapping Process

For the unwrapping the Swiss roll geometry, most important reference is the article of Chen and Buckmaster [6]. In their research they investigate how Swiss roll geometry can be transformed into simple pipe system for avoiding the difficulties about modeling more complex geometry.

There may be various geometries about the unwrapped Swiss rolls. For example; 2-turn, 3- turn, 4 turn Swiss rolls, or 11 parts, 18 parts Swiss rolls, etc. Although, there are some differences between different types of Swiss rolls, the logic of the system is always same. As it is illustrated in the graph 3.4, the outer wall compromises 17 sections (i.e. 1-2, 2-3, 3-4, , 17-18); the inner wall compromises 15 sections (i.e. a-b, b-c, c-d, , o-p) for a 18-part Swiss roll geometry. Fillers are used to fix the wall sections to together and to prevent the heat balance errors in the system. It should be emphasized that; there exists burnt or fresh gas flow outside the unwrapped straight channel, but in the opposite direction to the flow of the channel.

In the numerical modeling; the Swiss roll geometry is unwrapped to a straight channel, with heat recirculation between the unburnt and burnt gas being appropriately taken into account. As it can be easily observed from the graph 3.4; a two-dimensional Swiss roll combustor is made of two separate conducting walls which are called as the outer wall and the inner wall. In this system; cold fuel and oxidizer enter from the channel and advances through it. By the advance of these reactants among the channel; they reach to the center of the geometry; where the chemical reaction is located. Then, by the effect of chemical reaction; the reactants are transformed into products. By this way, a large amount of energy is set free and makes the temperature of the gas maximum at that point. Then these products continue their advance throughout the geometry. The significant role of this geometry is the way how the conduction between separate walls is accomplished. The main idea of the system is; high temperature burnt gas flows towards the exit, transferring heat to warm up the unburnt gas along the way.

In the present model; the Swiss roll geometry is unwrapped into a simple pipe.

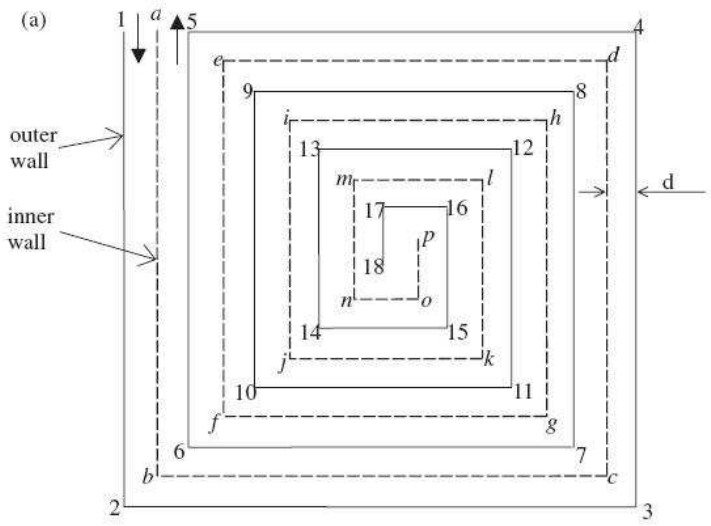

Figure 3.4. The Swiss Roll Geometry [6]

However it is appropriate to say that, the length of the walls are not the same. This condition can be examined by the graph 3.5. For example; the length of the outer wall section 1-2-3 is not equal to the length of the inner wall section a-b-c. This is because; the corners of the Swiss roll geometry do not obey the continuum of the system and cause to these length differences. On the other hand; that problem can be abolished by adding virtual wall sections which are called as "fillers" to solve this mismatch problem. As it is seen in the graph 3.5; b-b' is a filler. The fillers lengths differ due to the geometry. But the general approximation is to determine the length of the fillers from the locations of the walls.

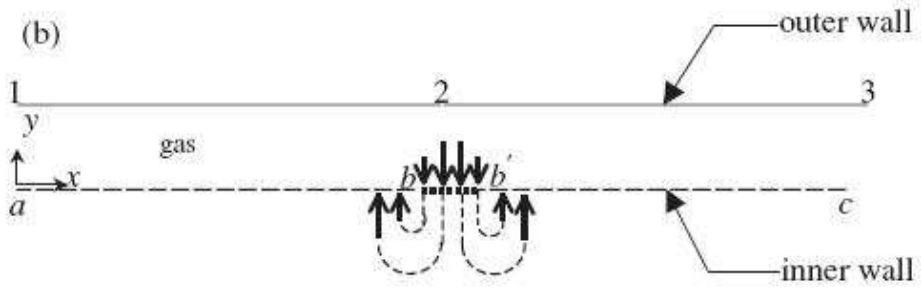

Figure 3.5. The Unwrapped appearance of Swiss Roll Geometry [6]

The temperature of the fillers is another important parameter. Since they belong to the same location in the original 2-d geometry, their temperature is set to be uniform and equal to that of the adjacent wall.

The main problem with adding fillers is that heat transfer between them and the gas can change the total energy balance and lead to errors. For compensating that problem; a heat source is added in the wall energy equation as illustrated by the energy flow through the filler b-b' in figure 3.5.

The most important problem for an unwrapped Swiss roll system is the lack of direct heat conduction between the channels including fresh mixture and burned mixture. However, in this study; this problem is abolished assuming there is an opposite gas flow with opposite temperature character out of the inner and the outer wall respectively. By this way, one can model the Swiss roll geometry, by using heat fluxes and transmitting them to the inherent wall section located in the opposite side of the flame. As it is shown in the graph 3.6; Q_a and Q_b are convective heat fluxes to the wall from the gas inside and outside the unwrapped channel, respectively. It should also be emphasized that, in such a system; the walls after and before the center are the same due to the symmetry. For example; 10-11 which is located before the center is the same with another wall section 11-10'. Since they are identical walls, the heat fluxes which are entering and abandoning them should be the same.

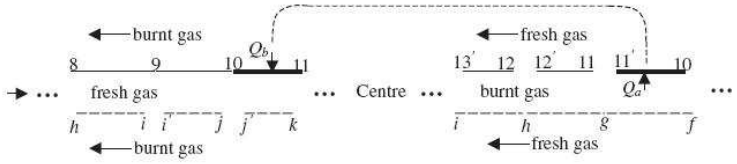

Figure 3.6. The Unwrapped appearance of Swiss Roll Geometry and The Transportation of fluxes [6]

The energy equation for the outer wall (y=1) at steady state is;

$$\delta \frac{\partial}{\partial x}\left(k_w \frac{\partial T_{w1}}{\partial x}\right) + Q_a + Q_b = 0 \qquad for\ 0 \leqslant x \leqslant L_1 \tag{3.3}$$

These fluxes can be represented in the mathematical form of;

$$Q_a = -k_g \left. \frac{\partial T_g}{\partial y} \right|_{y=d} \tag{3.4}$$

$$\begin{aligned} Q_b &= h(1 - T_{w1}), \text{ when } x < s \\ Q_b &= Q_a\,(\bar{x})|_{\bar{x}=L_1+s-x}\,, \text{ when } x > s \end{aligned} \tag{3.5}$$

The boundary conditions are;

$$\begin{aligned} \frac{\partial T_{w1}}{\partial x} &= \frac{h(T_{w1} - 1)}{k_w} \text{ at x = 0} \\ T_{w1} &= T_{w1}|_{x=s} \text{ at x = } L_1 \end{aligned} \tag{3.6}$$

It should be noted that; radiative heat fluxes to the wall from the gas inside and outside the unwrapped channel and the heat gain from the environment in the z-direction via convection and radiation are neglected.

The energy equation for the inner wall (y=0) is;

$$\delta \frac{\partial}{\partial x}\left(k_w \frac{\partial T_{w2}}{\partial x}\right) + Q_c + Q_d = 0 \quad for\ 0 \leqslant x \leqslant L_2 \tag{3.7}$$

$$Q_c = -k_g \left. \frac{\partial T_g}{\partial y} \right|_{y=0} \tag{3.8}$$

$$Q_d = Q_c\,(\bar{x})|_{\bar{x}=L_2-x} \tag{3.9}$$

The boundary conditions are;

$$\begin{aligned} \frac{\partial T_{w2}}{\partial x} &= \frac{h(T_{w2}-1)}{k_w} \text{ at x} = 0 \\ \frac{\partial T_{w2}}{\partial x} &= -\frac{h(T_{w2}-1)}{k_w} \text{ at x} = \mathrm{L}_2 \end{aligned} \tag{3.10}$$

3.3. Governing Equations

The governing equations of fluid flow represent mathematical statements of the conservation laws of physics. In writing the governing equations the following assumptions are made;

1. Flow is steady.
2. The flow is modeled as two dimensional.
3. Radiation is neglected.
4. The gas mixture is an ideal gas.
5. In simulating heat conduction in the walls, the temperature gradient across the wall thickness is neglected. This simplification is valid when the Biot number is less than 0.1 [6].
6. Conductivities and specific heat values of the fluid and the solid are assumed to be constant.
7. Viscosity of the flow is assumed to be constant.
8. One step global reaction mechanism is used.
9. The gravity is neglected.
10. The binary diffusion coefficient of each species assumed to be constant.

With these assumptions, the governing equations for two dimensional laminar steady flow are as follows.

Continuity Equation;

$$\frac{\partial(\rho u)}{\partial x} + \frac{\partial(\rho v)}{\partial y} = 0 \tag{3.11}$$

X-momentum equation;

$$\frac{\partial(\rho uu)}{\partial x} + \frac{\partial(\rho vu)}{\partial y} = \frac{\partial}{\partial x}\left(\mu\frac{\partial u}{\partial x}\right) + \frac{\partial}{\partial y}\left(\mu\frac{\partial u}{\partial y}\right) - \frac{\partial p}{\partial x} + S_U \tag{3.12}$$

Y-momentum equation;

$$\frac{\partial(\rho uv)}{\partial x} + \frac{\partial(\rho vv)}{\partial y} = \frac{\partial}{\partial x}\left(\mu\frac{\partial v}{\partial x}\right) + \frac{\partial}{\partial y}\left(\mu\frac{\partial v}{\partial y}\right) - \frac{\partial p}{\partial y} + S_V \tag{3.13}$$

Energy equation;

$$\rho c_p\left(u\frac{\partial T}{\partial x} + v\frac{\partial T}{\partial y}\right) = k\left(\frac{\partial^2 T}{\partial x^2} + \frac{\partial^2 T}{\partial y^2}\right) - \sum h_k w_k \tag{3.14}$$

Species mass continuity equation;

$$\frac{\partial(\rho u Y_k)}{\partial x} + \frac{\partial(\rho v Y_k)}{\partial y} = \frac{\partial}{\partial x}\left(\rho D\frac{\partial Y_k}{\partial x}\right) + \frac{\partial}{\partial y}\left(\rho D\frac{\partial Y_k}{\partial y}\right) + \dot{w}_k \tag{3.15}$$

The source terms S_u and S_v are explained in detail in the Appendix D. The reaction rate w_i is given by the phenomenological reaction rate expression;

$$w_i = M w_i \sum_{k=1}^{M} (v_{i,k}^{''} - v_{i,k}^{'}\ ) B_k T^{\alpha_k} \exp\left(-\frac{E_{ak}}{R_u T}\right) \prod_{j=1}^{N}\left(\frac{X_j p}{R_u T}\right)^{v_{j,k}^{'}} \tag{3.16}$$

Where M is the total number of chemical reactions occurring and N is the total number of chemical species present. $\sum_{k=1}^{M}(v_{i,k}^{''} - v_{i,k}^{'})$ is the stoichiometric coefficient of a species. In Table 3.1, global reaction constants for fuels that are used in this study are illustrated.

Table 3.1. Global Reaction constants for Propane and Methane

Properties	B_k	E (kcal/gmole)	R (cal/gmole.K)	p (atm)	v'_{fuel}	$v'_{oxidizer}$
Propane	$8.6.10^{11}$	30.0	1,987	1	0.1	1.3
Methane	$8.6.10^{12}$	48.4	1,987	1	-0.3	1.65

3.4. Equation of State

The ideal-gas equation of state for a multi-component system can be written as;

$$p = \rho R_u T \sum_{i=1}^{N} \frac{Y_i}{Mw_i} \tag{3.17}$$

The relationship between X_i and Y_i is;

$$X_i = \frac{Y_i/Mw_i}{\sum_{j=1}^{N} (Y_j/Mw_j)} \text{ or } Y_i = \frac{X_i/Mw_i}{\sum_{j=1}^{N} (X_j/Mw_j)}, \text{ i = 1,2, . . ., N} \tag{3.18}$$

3.5. Boundary Conditions

The boundary conditions for momentum equations are represented in equation 3.19 and figure 3.7.

$$\begin{aligned} &\text{At x = 0 (inlet), } u = \text{constant}, v = 0 \\ &\text{At x = L (exit), } \frac{\partial u}{\partial x} = 0, \frac{\partial v}{\partial x} = 0 \\ &\text{At y = 0 (inner wall), u = 0, v = 0} \\ &\text{At y = 1 (outer wall), u = 0, v = 0} \end{aligned} \tag{3.19}$$

The boundary conditions for energy equation are represented in equation 3.20

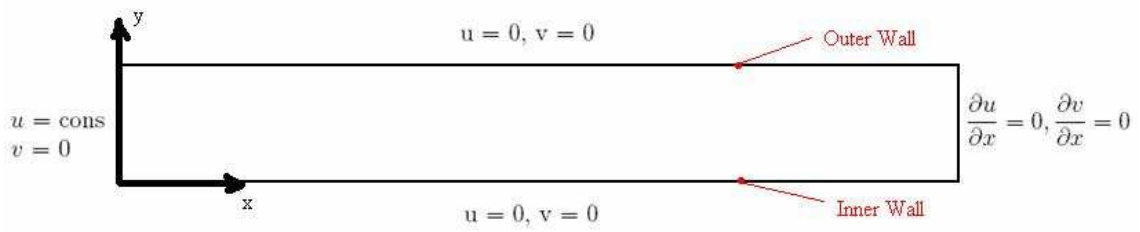

Figure 3.7. Boundary conditions for momentum equation

and figure 3.8.

$$\begin{aligned}
&\text{At x = 0 (inlet), } T_g = 300 \text{ K (environmental temperature)} \\
&\text{At x = L (exit), } \frac{\partial T}{\partial x} = 0 \\
&\text{At y = 0 (inner wall), T} = T_{w2} \\
&\text{At y = 1 (outer wall), T} = T_{w1}
\end{aligned} \tag{3.20}$$

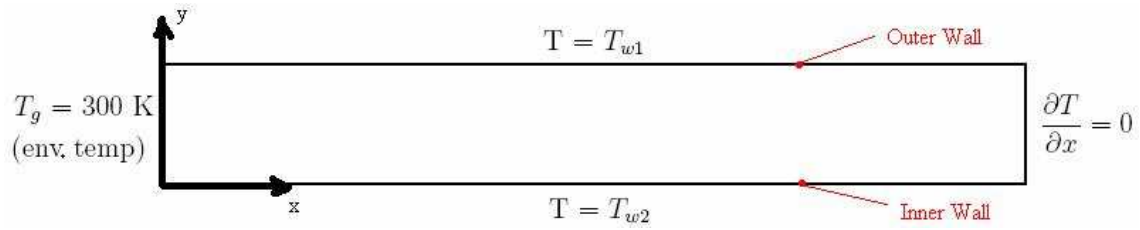

Figure 3.8. Boundary conditions for energy equation

The boundary conditions for species equation are represented in equation 3.21 and figure 3.9.

$$\begin{aligned}
&\text{At x = 0 (inlet), } Y_f = \text{constant}, Y_o = \text{constant} \\
&\text{At x = L (exit), } \frac{\partial Y_f}{\partial x} = 0 \\
&\text{At y = 0 (inner wall), } \frac{\partial Y_f}{\partial y} = 0 \\
&\text{At y = 1 (outer wall), } \frac{\partial Y_f}{\partial y} = 0
\end{aligned} \tag{3.21}$$

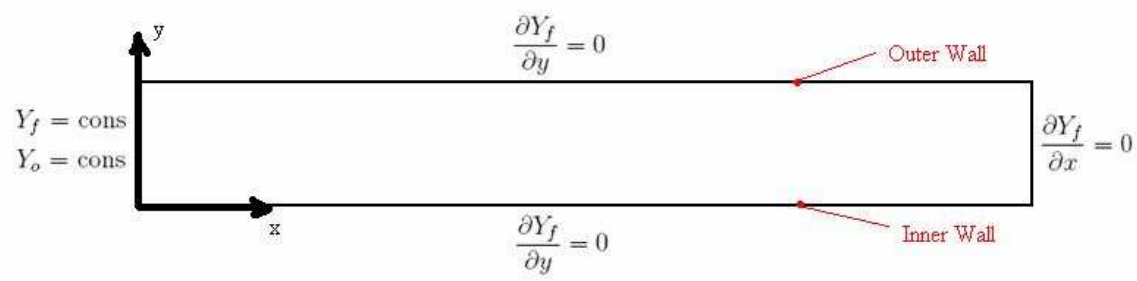

Figure 3.9. Boundary conditions for species equation

3.6. Computational Model

3.6.1. Code Development

In the computational model, these are the milestones.

1. Finite Volume Method is used.
2. The Hybrid Differencing Scheme is used.
3. TDMA (Tri-diagonal Matrix Algorithm is used for solving equations.
4. The Staggered Grid is used for evaluating scalar variables and velocity components.
5. The Simple Method is employed [6]. In figure 3.10; the SIMPLE Algorithm is illustrated.

3.6.2. The Staggered Grid

If the velocities are defined at the scalar grid nodes, the influence of pressure is not properly represented in the discretised momentum equations. A remedy for this problem is to use a staggered grid for the velocity components. (Harlow and Welch, 1965). The idea is to evaluate scalar variables, such as pressure, density, temperature etc., at ordinary nodal points but to calculate velocity components on staggered grids centered around the cell faces.

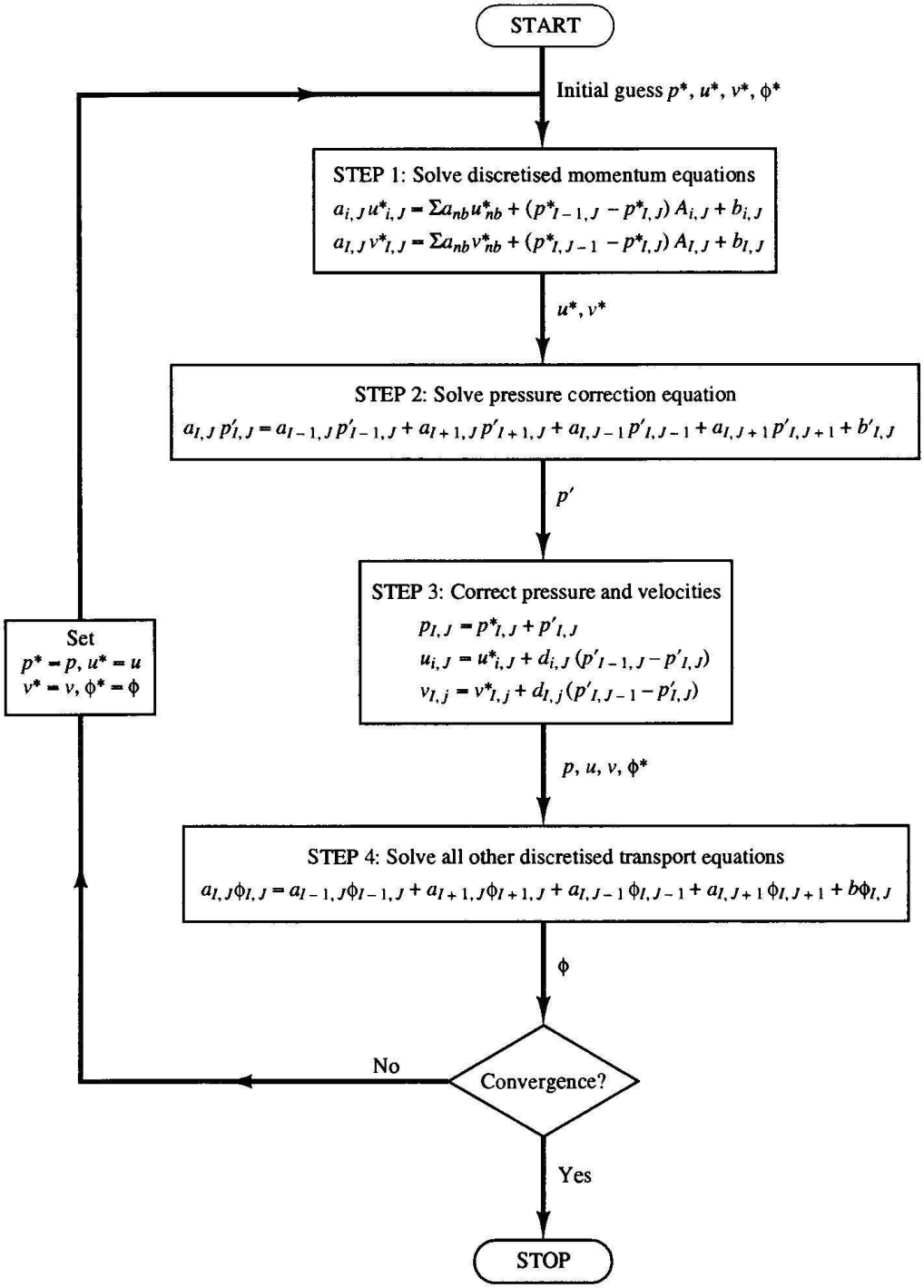

Figure 3.10. The SIMPLE Algorithm

The scalar variables, including pressure, are stored at the nodes marked (.). the velocities are defined at the (scalar) cell faces in between the nodes and are indicated by arrows. Horizontal arrows indicate the locations for u-velocities and vertical ones denote those for v-velocities.

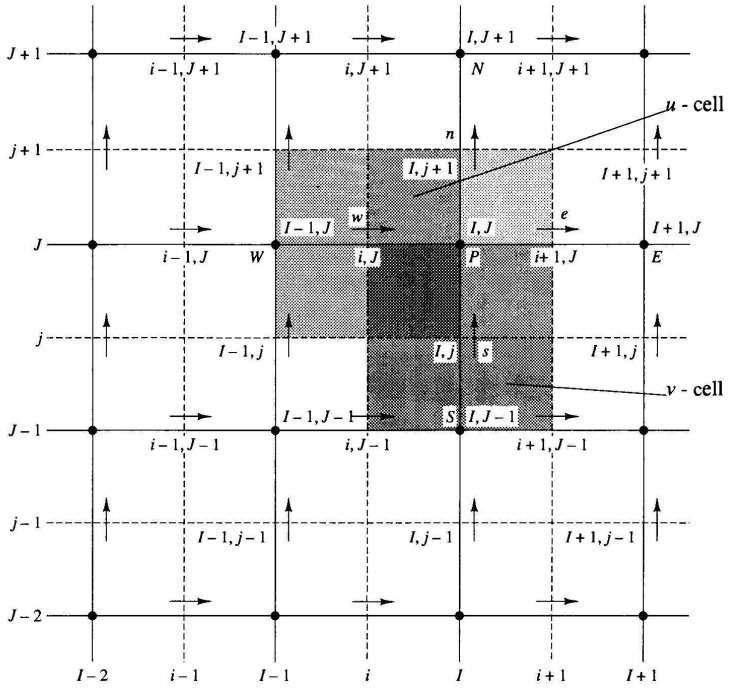

Figure 3.11. The staggered grid [11]

3.6.3. The Residual Theorem

Residual is the value which is used for investigating the convergence. In many numerical analyzes, it is the absolute value of the difference between the left hand side and the right hand side of an equality. It is generally used as a criteria of convergence.

On a computer with infinite precision, these residuals will go to zero as the solution converges. On an actual computer, the residuals decay to some small value (round-off) and then stop changing (level out). For single-precision computations (the default for workstations and most computers), residuals can drop as many as six orders of magnitude before hitting round-off. Double-precision residuals can drop up to twelve orders of magnitude.

3.6.4. Definition of Residuals for the Pressure Based Solver

$$a_P \phi_P = \sum_{nb} a_{nb} \phi_{nb} + b \tag{3.22}$$

The Residual Theorem which is preferred in this thesis is the one which FLUENT uses. In this manner, the residual R^{ϕ} computed by the code is the imbalance in the (3.22) summed over all the computational cells P. This is referred to as the "unscaled" residual. It may be written as;

$$R^{\phi} = \sum_{cellsP} \left| \sum_{nb} a_{nb} \phi_{nb} + b - a_P \phi_P \right| \tag{3.23}$$

In general; it is difficult to judge convergence by examining the residuals defined by (3.23) since no scaling is employed. This is especially true in enclosed flows such as natural convection in a room where there is no inlet flow rate of with which to compare the residual. By this way, the residual can be scaled by using a scaling factor representive of the flow rate of through the domain. This "scaled" residual is defined as

$$R^{\phi} = \frac{\sum_{cellsP} \left| \sum_{nb} a_{nb} \phi_{nb} + b - a_P \phi_P \right|}{\sum_{cellsP} p \left| a_P \phi_P \right|} \tag{3.24}$$

For the momentum equations $a_P \phi_P$ is replaces by $a_P v_P$, where v^P is the magnitude of the velocity at cell P. The scaled residual is a more appropriate indicator of convergence for most problems. For the continuity equation, the unscaled residual for

the pressure- based solver is defined as

$$R^c = \sum_{cells P} |\text{rate of mass creation in cell P}| \tag{3.25}$$

The pressure-based solvers scaled residual for the continuity equation is defined as;

$$\frac{R^c_{iteration\ \mathrm{N}}}{R^c_{iteration\ 5}} \tag{3.26}$$

The denominator is the largest absolute value of the continuity residual in the first five iterations. In conclusion, it can be easily said that, the scaled residuals described above are useful indicators of solution convergence.

3.7. The Material properties of the Swiss Roll

Inconel 718 is used as the material of the combustors. This alloy is a precipitation-hardenable nickel-chromium alloy containing significant amounts of iron, niobium, and molybdenum along with lesser amounts of aluminum and titanium. It combines corrosion resistance and high strength with outstanding weldability, including resistance to postweld cracking. The alloy has excellent creep-rupture strength at temperatures up to 700 C (1300 F). Inconel 718 is generally used in gas turbines, rocket motors, spacecraft, nuclear reactors, pumps and tooling.

Table 3.2. The Material (physical) properties of the Swiss Roll

Properties and Materials	*Inconel-718*	*Aluminum*
Specific Heat:	435 J/kg.K	897.0 J/kg.K
Density	8.19 g/cm^3	2.719 g/cm^3
Thermal Conductivity	11.4 W/m.K	237.40 W/m.K

4. RESULTS AND DISCUSSIONS

4.1. Rectangular Swiss Roll Combustor

The momentum, continuity and energy equations are solved for with an assumed constant temperature at the center of the Swiss Roll. In figure 4.1 flow field is shown in contour and vectorial form for $u = 10^{-1}$ m/s.

In the model the system is solved by the manner that a heat generator is located in the center which result as the constant temperature, 1000 K in the center. The aluminum walls are conductive. The results that are obtained for two different velocities ($u = 10^{-1}$ and $u = 10^{-2}$ m/s) are shown in the figure; 4.2. The figure shows the effect of increased convective heat transfer.

As it is seen by the figure 4.2, it is appropriate to say that, increasing velocity increases the convection and the distribution of temperature increases. On the other hand, in lower velocity solutions, diffusive effects dominate over the convective ones and the distribution is barren.

4.2. The comparison of temperature distribution in unwrapped and Rectangular Swiss Roll Burners

For investigating the accuracy of the unwrapping process, a numerical experiment is performed. In this experiment, firstly the temperature field for an 11 part Rectangular Swiss Roll burner is calculated. In the calculation a constant heat source is placed in the center of the burner. The calculated temperature field is illustrated in figure 4.3. Since the main purpose of this experiment is to investigate the temperature distribution; species and chemical reaction rate are not solved in the process. Secondly; the temperature field for the unwrapped burner geometry is solved via giving a constant heat source in the center as well. The comparison of the calculated temperatures at the solid walls and at gas along the centerline are given in figure 4.4. Notice that; even

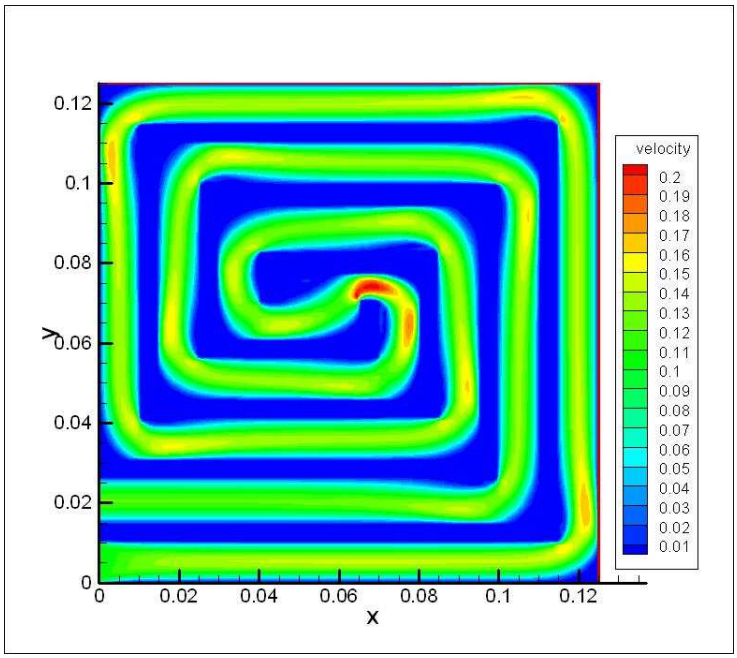

(a)

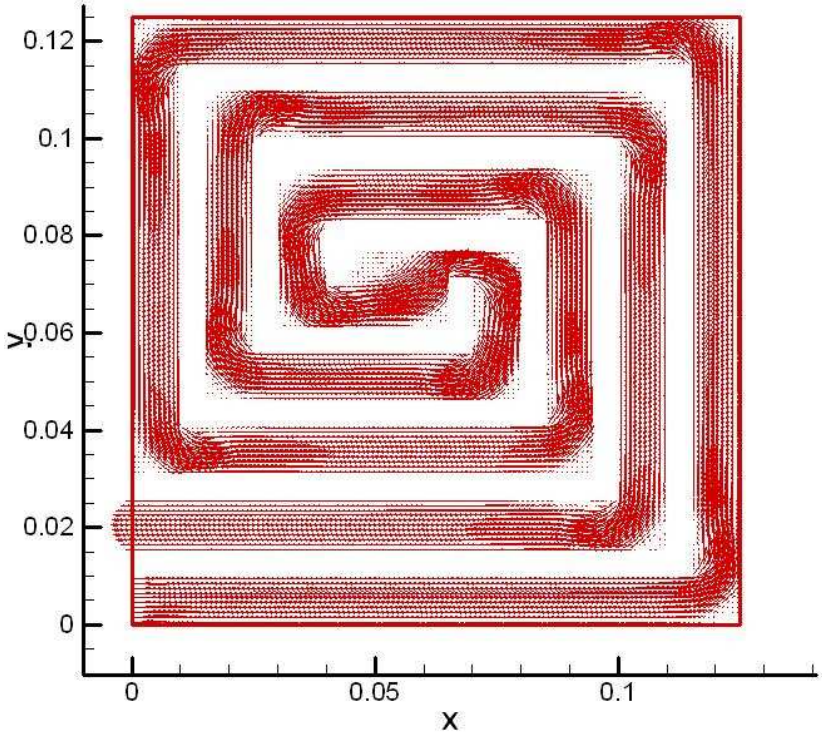

(b)

Figure 4.1. The flow field of a Swiss roll geometry with inlet velocity of 1×10^{-1} m/s in (a) contour form (b) vectorial appearance

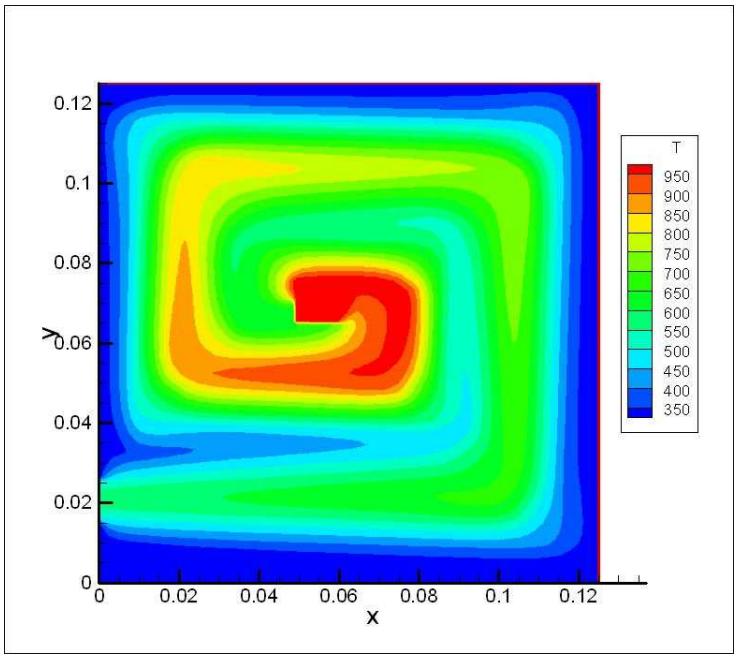

(a)

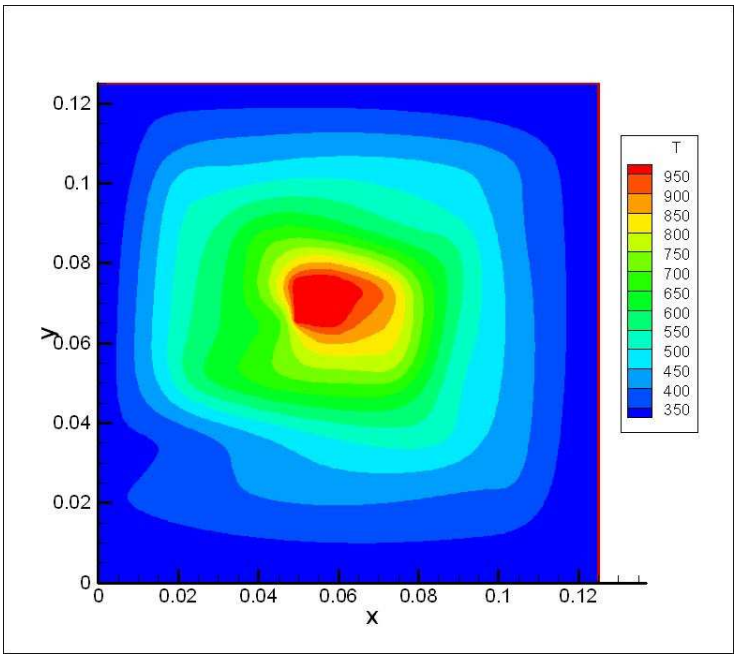

(b)

Figure 4.2. Temperature contours of a Swiss Roll geometry with inlet velocity of (a) 1×10^{-1} m/s and (b) 1×10^{-2} m/s

though there are small differences between the calculations the unwrapped geometry gives satisfactory results.

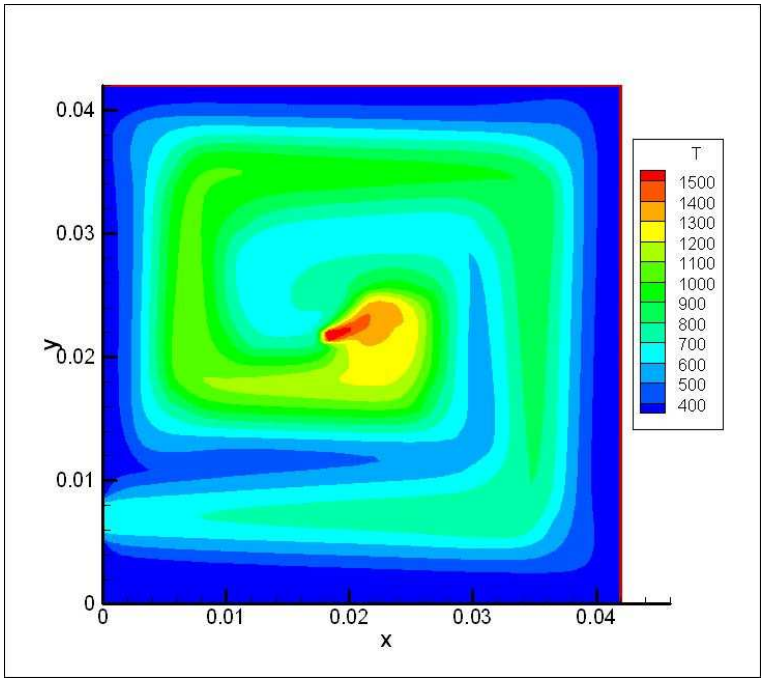

Figure 4.3. The temperature distribution in 11 part Rectangular Swiss Roll geometry

4.3. The comparison of 18 part Rectangular Swiss Roll Combustor model with literature

To investigate the validity of the results, they are compared with the results in the literature [6]. The comparison of calculated temperature values (following literature data temperature is non-dimensionalised with the ambient temperature of 300 K and the length is non-dimensionalised with channel height of d=3.5 mm.) and the literature data for the solid walls and the gas along the centerline is shown in the figure 4.5. The comparison of chemical reaction rates is illustrated in 4.6. The chemical reaction rate in the [6] is also non-dimensionalised by these expressions:

$$w = Da\ Y_f\ \rho_g\ exp(-\frac{\theta}{T_g}); \qquad Da = \frac{B\ d^2}{\alpha_{gr}}; \qquad \theta = \frac{E}{R\ T_\infty} \tag{4.1}$$

To be compatible same non-dimensionalization also used in our calculations. As it is easily seen in the figures, the results are similar. Although there is some difference in the

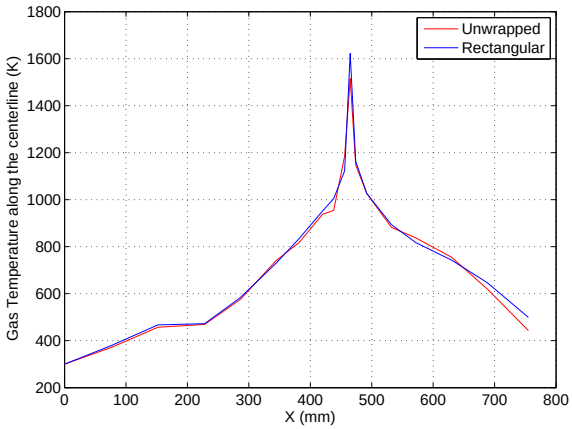

(a)

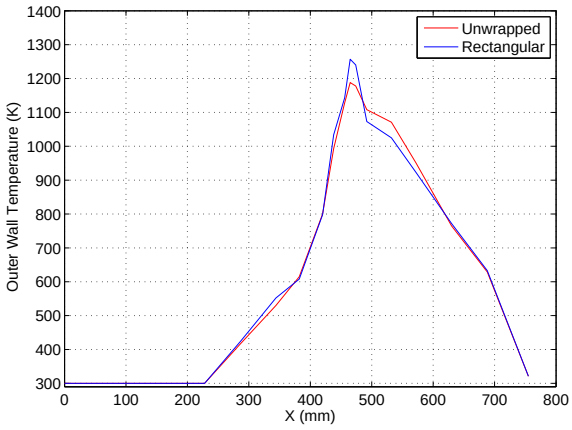

(b)

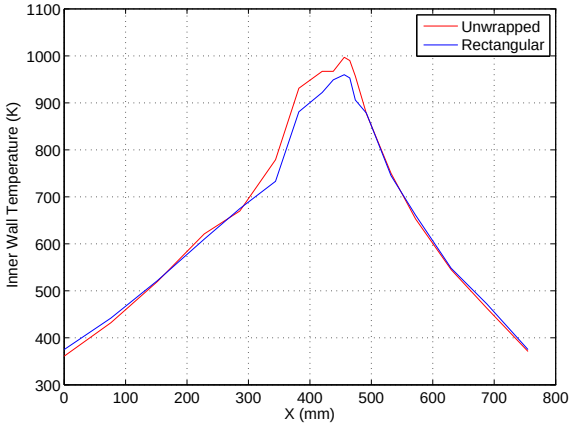

(c)

Figure 4.4. Comparison of the original and the unwrapped SRCs for (a) gas temperature (b) outer wall temperature (c) inner wall temperature

appearance of the reaction rate values, this probably occur because of two differences in the way the center of the burner is unwrapped. In the literature work; the center is the same with figure 2.2, however, in the simulations that are performed in this study, the wall parts do not overlap each others end point. Also, another difference between these two sources is the approach to the momentum equations. Chen and Buckmaster [6] assumed a fully developed velocity profile. However, in the present work, momentum equations are solved and it is observed that, in the center part, the velocity values differ.

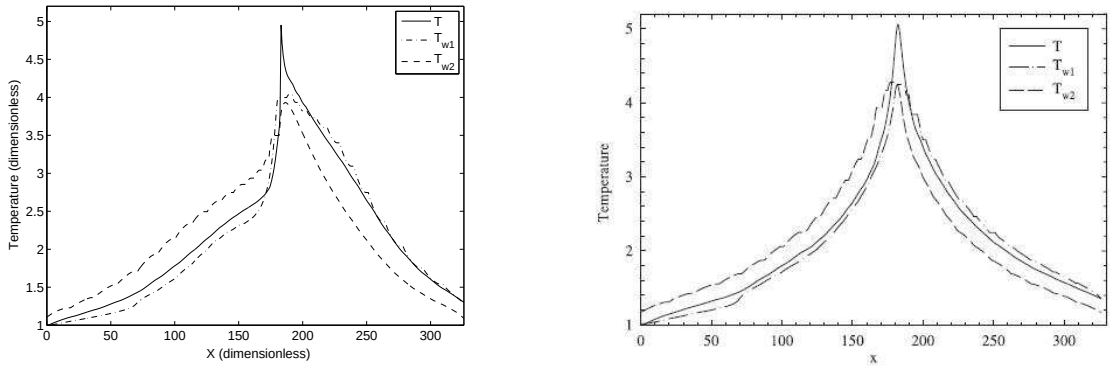

(a) (b)

Figure 4.5. The temperature distribution (a) generated by the code, (b) obtained from [6]; for 18 Part Rectangular SRC at Re=100 and $\phi = 0.415$

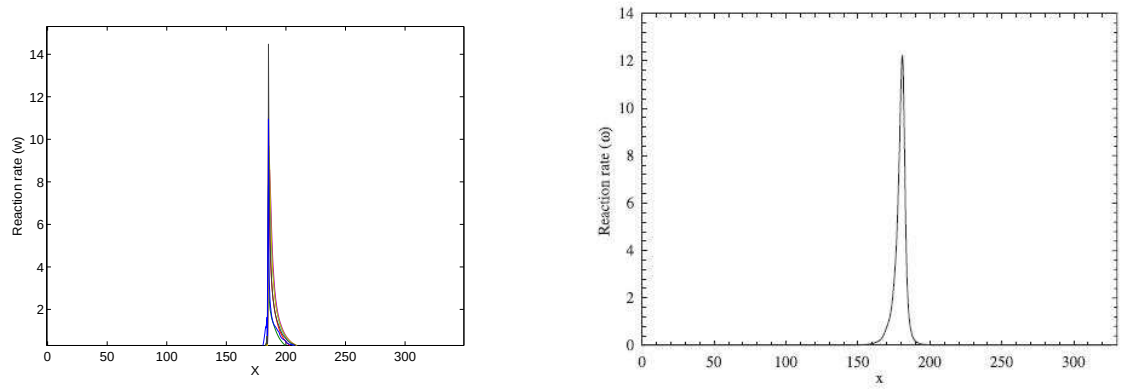

(a) (b)

Figure 4.6. The reaction rate values (a) generated by the code, (b) obtained from [6]; for 18 Part Rectangular SRC at Re=100 and $\phi = 0.415$

4.4. The comparison of 18 part Spiral and Rectangular Swiss Roll Combustors

Burner type is another important parameter. Since simulations can be performed in both unwrapped Spiral and Rectangular SRC's, the comparison of these two different geometries is investigated for examining which geometry is more effective.

For the simulation, Re=100 and $\phi = 0.415$ is selected. As it is seen in the figure 4.7; 18 Part Spiral and Rectangular Swiss Roll combustors have almost same values at these conditions. However; although the outlet temperature values are closer, the maximum temperature value for Spiral Swiss roll is higher than the other one. The difference is about 40 K. Differences are observed in favor of Spiral SRC. It should be noted that the length of the Spiral SRC is 943 mm and the Rectangular one is 1141 mm and the results shown are use non-dimensional length.

4.5. The results for the unwrapped 18 part Spiral Swiss Roll combustor

The details of the results are shown for unwrapped Spiral Swiss Roll Burner are explained in this section. In this burner the global chemical reaction is as follows:

$$C_3H_8 + 5(O_2 + 3.76N_2) \rightarrow 4H_2O + 3CO_2$$

The conditions are such that for Re=100, Lx=943 mm, d=3.5 mm (Channel Height), $\phi = 0.41$. This equivalence ratio is the extinction limit under these conditions.

In the figure 4.8 the temperature distribution in the Spiral Swiss Roll Burner is illustrated. The contours shown are for the gas phase. The two different lines exhibits the outer and the inner wall temperatures. The gas temperature and the density distribution in line form at several channel heights are shown in figure 4.9. Notice that; because of high temperature differences, the density of the flow changes significantly.

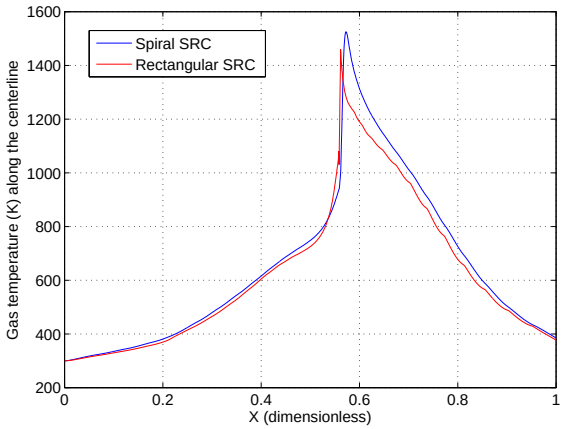

(a)

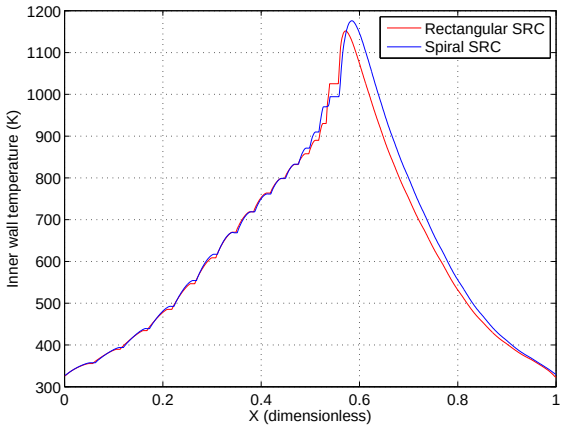

(b)

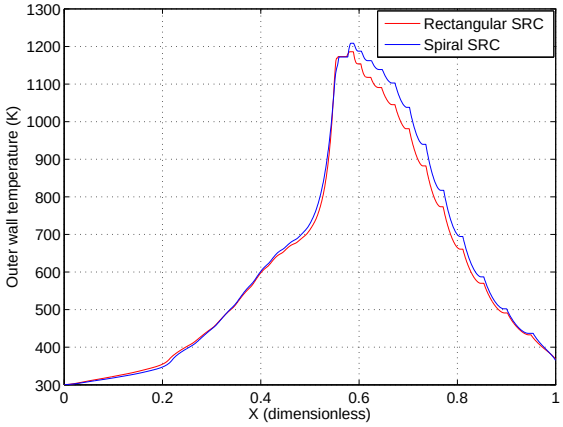

(c)

Figure 4.7. Comparison of the Spiral and Rectangular SRCs for (a) gas temperature (b) inner wall temperature (c) outer wall temperature

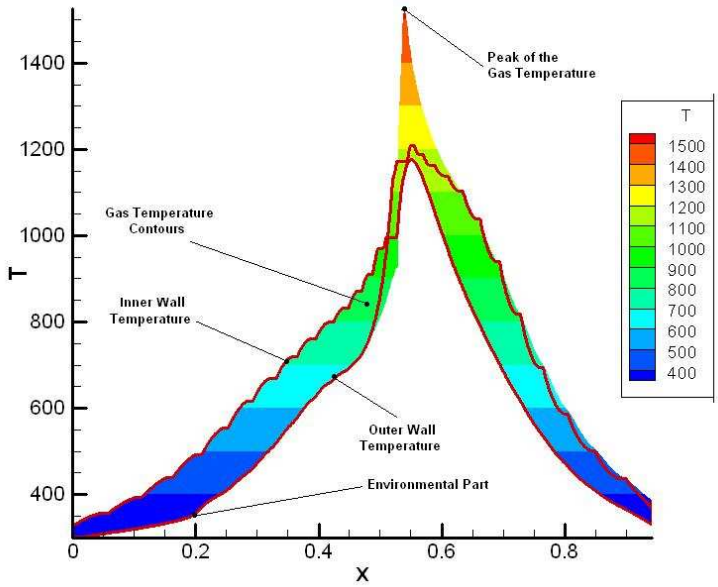

Figure 4.8. The temperature distribution in the Spiral Swiss Roll Burner

In the Spiral Swiss Roll system; the fresh fuel-oxidizer mixture flows into the roll and moves in the channels to the center. As it flows, the fresh mixture is heated by the heat flux from the hot walls. Hence, by the time the fresh mixture arrives to the center of the burner, it has higher temperature relatively to the inlet value.

After combustion which is happening in the center, the hot burnt product flows out of the burner in the exit channels. However, it transfers heat to the bounding walls along the way. Hence, the temperature of the walls are increased. The increased temperature of these walls is used to preheat the incoming fresh mixture.

In the figure 4.10 the temperature distributions in the Spiral Swiss Roll Burner in some critical locations are exhibited. As it is seen from the figures, before the combustion, the inner wall temperature is higher than the outer wall temperature. Because, a significant part of the outer wall is opened to the environment. Also at that part the gas is cooler than the inner wall and hotter than the outer wall. In the flame region; the gas temperature is higher than the temperatures of inner and outer walls. After combustion, the outer wall temperature is higher than the inner wall temperature. Hence, beyond the flame region, the energy flow is from the outer

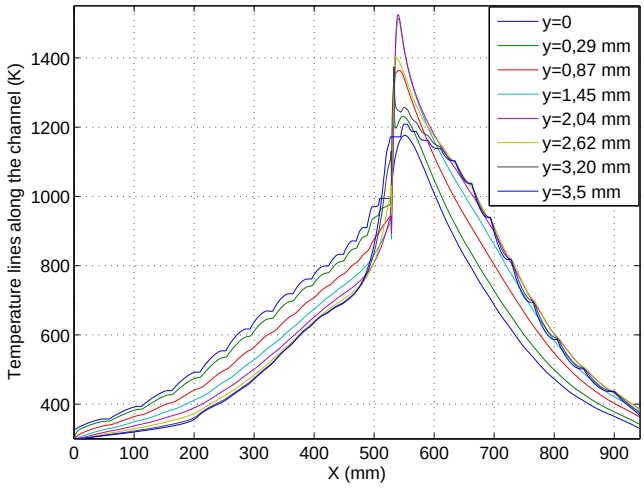

(a)

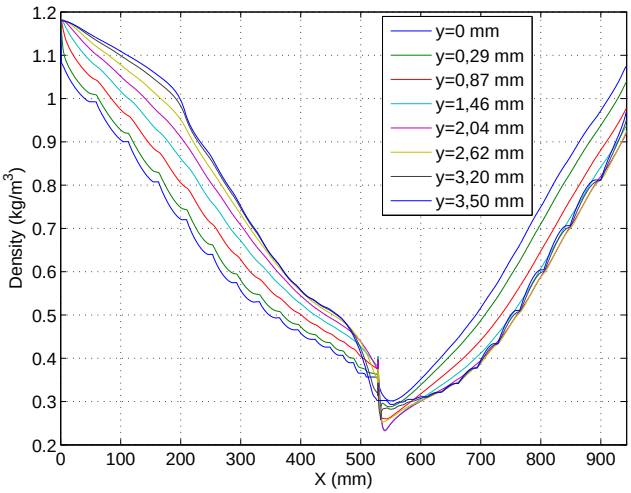

(b)

Figure 4.9. (a) The temperature and (b) The density distributions in line form for Spiral SRC

wall to the gas. Also it should be emphasized that, as it is clear to see in the figure 4.8, there is a kink which is located on the outer wall at x=0 vs x=0.2 m. The reason is, the outer wall is exposed to the environment at that span.

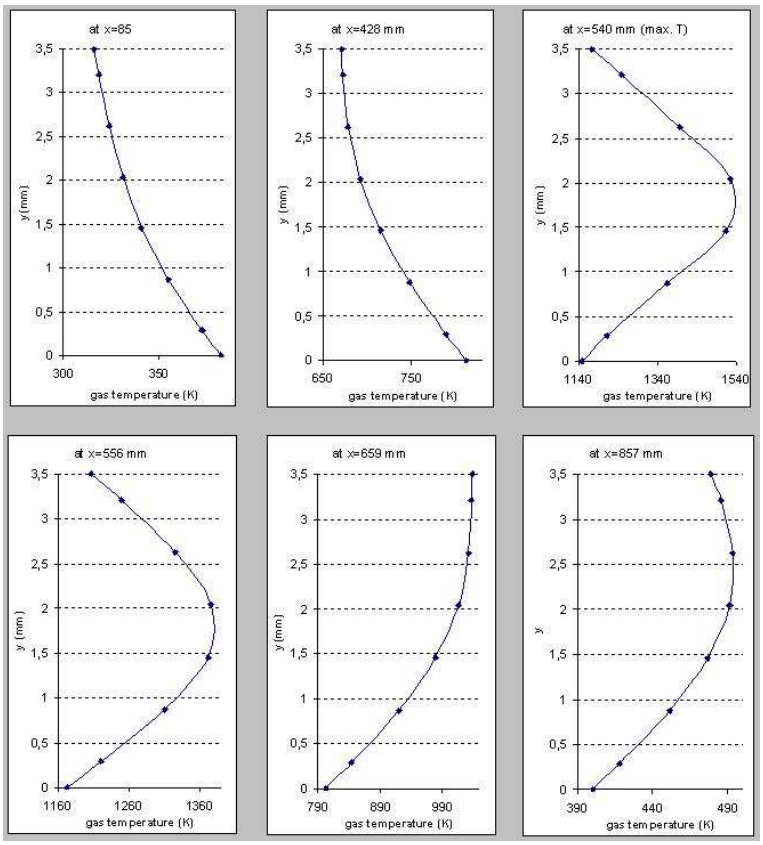

Figure 4.10. The temperature distribution in the Spiral Swiss Roll Burner in some critical locations

From the gas energy equation, the preheating of gas along the channel is related to the mass flow rate (Reynolds number), streamwise gas heat conduction and heat flux between the gas and the walls. The figure 4.11 shows the conduction in the streamwise direction (Q_{gas}), on the outer wall (Q_a) and on the inner wall (Q_c). The expression for the heat fluxes are;

$$\begin{aligned} Q_{gas} &= -k_g \left.\frac{\partial T_g}{\partial x}\right|_{y=d} \\ Q_a &= -k_g \left.\frac{\partial T_g}{\partial y}\right|_{y=d} \\ Q_c &= -k_g \left.\frac{\partial T_g}{\partial y}\right|_{y=0} \end{aligned} \tag{4.2}$$

By investigating the figure 4.11; it can be easily said that; the gas-wall heat transfer is roughly one order of magnitude stronger than streamwise heat conduction. The contour plot of reaction rate close to the region where the reaction rate is maximum is shown in figure 4.12 which is located in 0.537 m of the unwrapped geometry. For the same location the density and gas temperature contours are also shown in figure 4.13.As it is easily seen in the figure 4.13 the density decreases by the increased value of gas temperature. That process, of course, results as the higher x- direction velocity at the center.

In figure 4.13, the contours for the chemical reaction rate and mass fractions of reactants and products are also shown. As it is seen easily in the figure; transformation of products from reactants is maximum at the point where the chemical reaction rate is maximum.

In figure 4.14 the mass fraction values of reactants and products at the centerline of the channel are observed. The main reason why the oxidizer is not depleted where the fuel is finished is equivalence ratio.

4.5.1. The results for different channel heights

In this section the effects of the channel height to temperature distribution is investigated. In many cases, the channel height is selected as 3.5 mm. So, to observe the differences arising from channel height, the geometries of the Spiral Swiss Roll combustor is changed. Since the length of wall parts are symmetrical and the length of the roll depends directly o the channel height, assigning a new channel height is enough for obtaining new geometries. Hence; two different channel heights, d=0.5 mm and d=1.0 mm are chosen. The length of these burners are; Lx= 134 mm and Lx=269 mm, respectively. It should be noted that, in both experiment, Re=100 and the equivalence ratio is (ϕ=0.47).

The temperature distribution for d=0.5 mm is illustrated in the figure 4.15. The maximum reaction rate is located at x=0.075 m and 893th mesh point in the

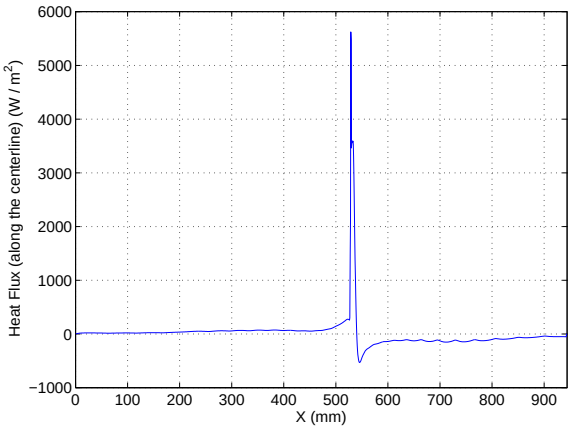

(a)

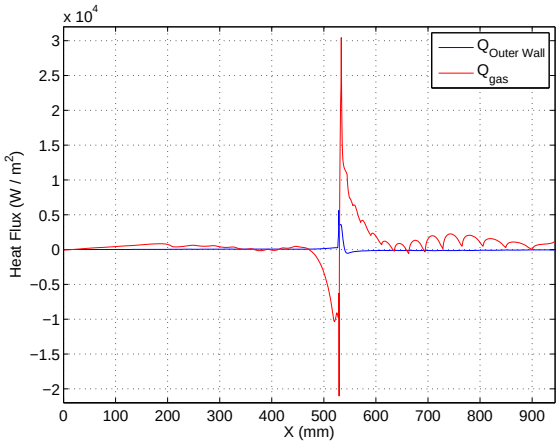

(b)

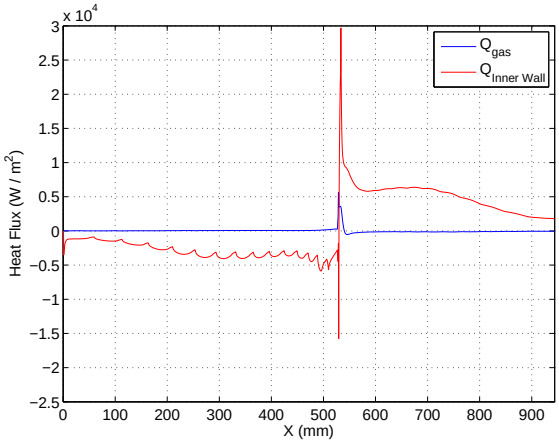

(c)

Figure 4.11. The heat flux values (a) referring to the streamwise gas heat conduction (b) between the gas and outer wall (Q_a) (c) between the gas and inner wall (Q_c)

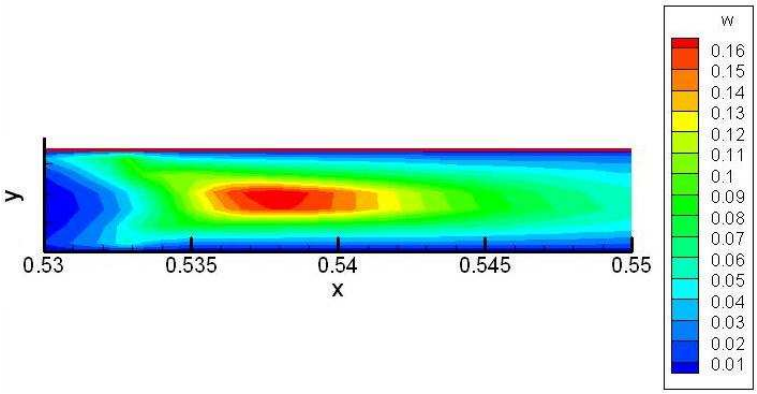

Figure 4.12. The chemical reaction rate

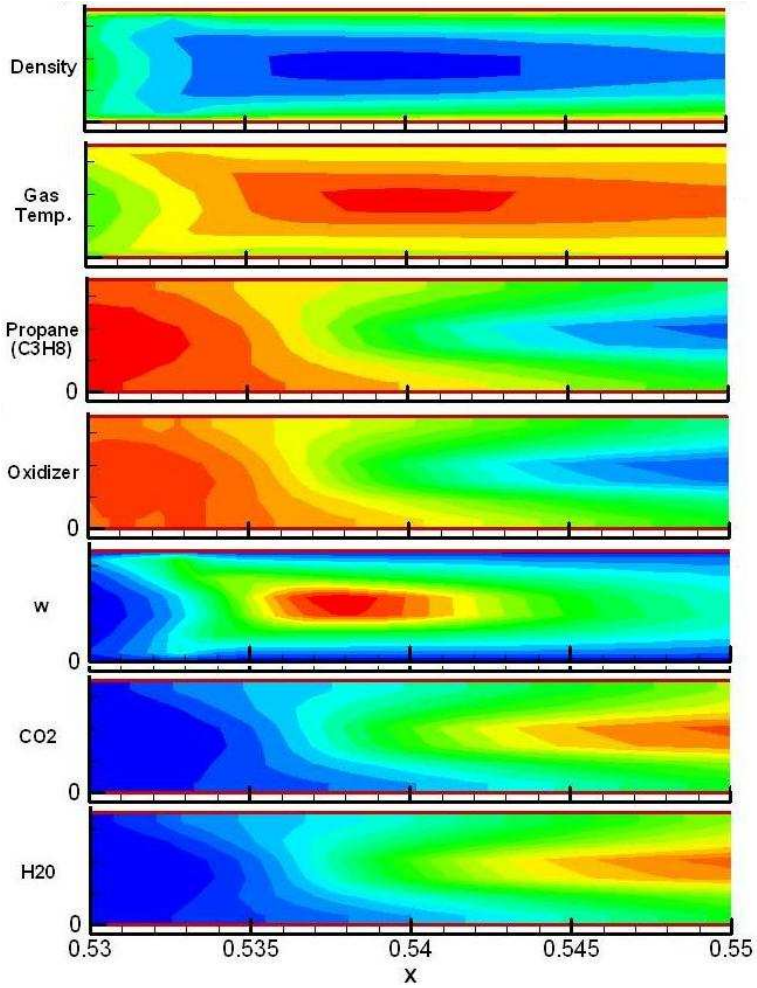

Figure 4.13. The contours for the chemical reaction rate and mass fractions of reactants and products

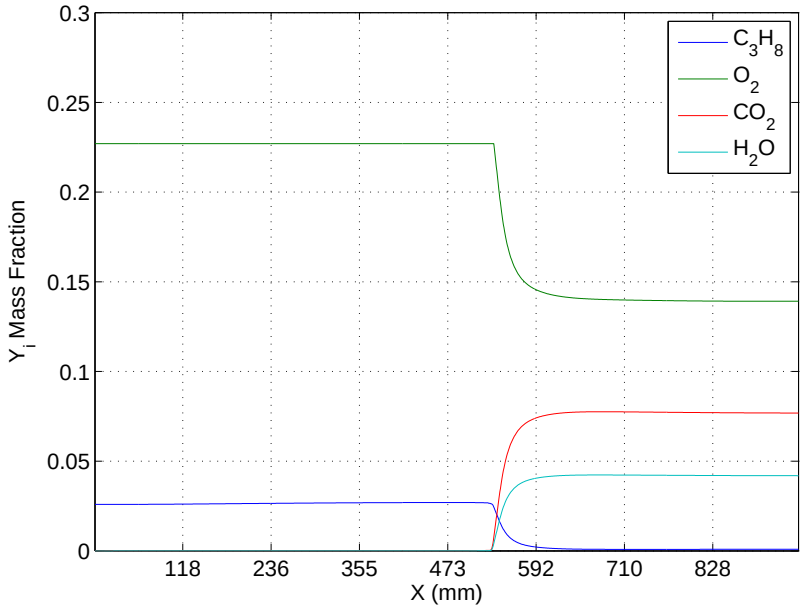

Figure 4.14. The mass fraction values of reactants and products

x-direction. The temperature distribution for d=1.0 mm is illustrated in the figure 4.16. The maximum reaction rate is located at x=0.1505 m and 893th mesh point in the x-direction.

As it is displayed in the figures 4.15 and 4.16, a temperature difference always exists between two walls and the gas temperature varies between them, in different channel heights. Also, a significant result which is drawn from figures 4.15 and 4.16; is decreasing the channel height would result with higher temperature values; when the equivalence ratio and the inlet velocity profile are the same.

4.5.2. Effect of Reynolds number on the temperature distribution and chemical reaction rate

The effect of Reynolds number on the temperature and chemical reaction rate distribution is studied. The observations obtained for different values of Reynolds number, Re=50, Re=60, Re=70 and Re=80. The equivalence ratio is selected as $\phi = 0.58$. This value is chosen because, it is the extinction limit of Propane for Re=50, d=3.5 mm. As it is seen easily from the figure 4.17; the increase in Reynolds number

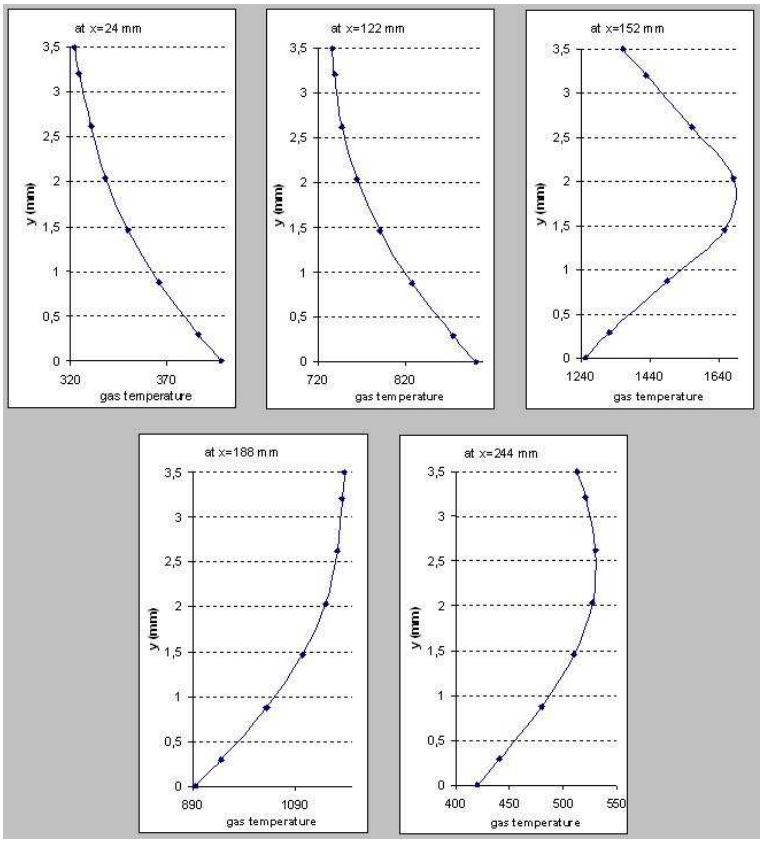

Figure 4.15. The temperature distribution in Swiss Roll Combustor, channel height=0.5 mm

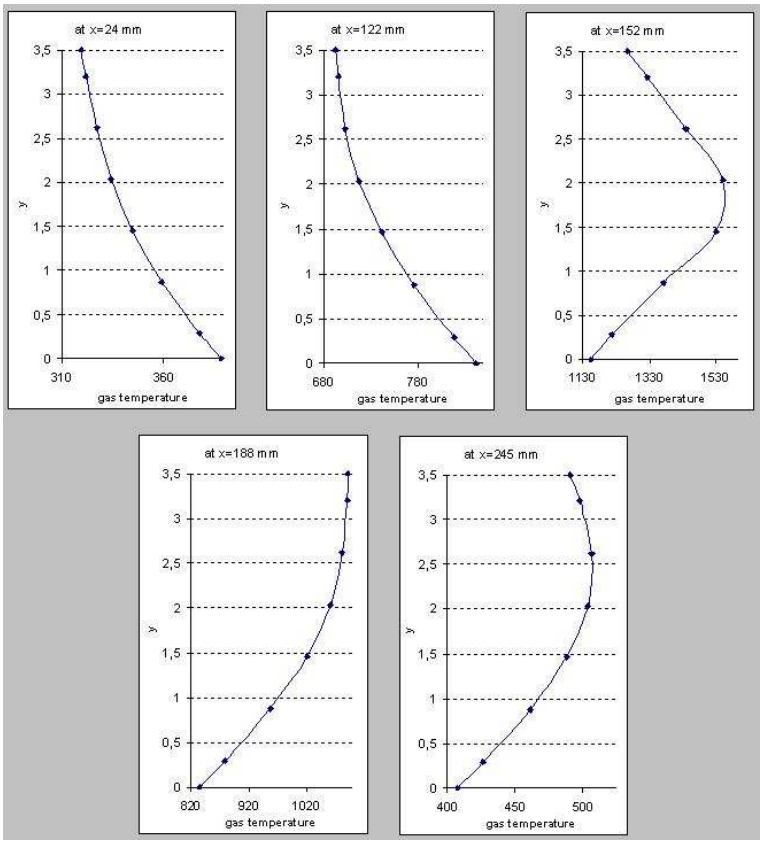

Figure 4.16. The temperature distribution in Swiss Roll Combustor, channel height=1.0 mm

results in an increase in gas temperature, wall temperature and chemical reaction rate.

Another observation that is significant in the figures, is the location of the flame zone. It moves away from the center of the Swiss roll toward the inlet when the Reynolds number increase. Here, there are two different effects on the location of the temperature and reaction rate peaks. The first effect is the mass flow rate. The increase in Re number means higher velocities and mass flow rates. Higher mass flow rate means much more cold fresh mixture advancing to the center to decrease the temperature and make the peak advance to the outlet. On the other hand; a higher value of Reynolds number result in an increase in the heat circulation which is the fundamental supporter of enhanced convective heat transfer between the walls and fuel-oxidizer mixture. It would be valid to say that there is a rivalry between these factors.

But there is some other secondary factors which are concluding the competition in favor of heat circulation. One of them is the magnitudes of streamwise heat conduction and heat flux between the gas and the walls. Since the temperature gradient between the wall and gas is much more than the gradient of gas temperature in streamwise direction; the magnitude of heat flux between the gas and the walls has more dominant effect which is the reason of the increment in heat circulation. Besides; higher mass flow rate also means more fuel and oxidizer advancing to the center to increase heat release. Another important factor is the range of Reynolds number. As it is easily obtained from the figure; the increase of mass flow rate is insufficient to play a dominant role for determining the location of temperature peak. However, for that span, the heat circulation increases in a more quick behavior relatively to the mass flow rate does. Last but not least; the effect of selecting constant equivalence ratio ($\phi = 0.58$) is another effect. This equivalence ratio is close to the extinction limit of Re=50 case and higher than the extinction limits at the other Re numbers studied. This can be assumed as a secondary reason for why the escalation of temperature peak and chemical reaction rate occurs by an increment in Reynolds number.

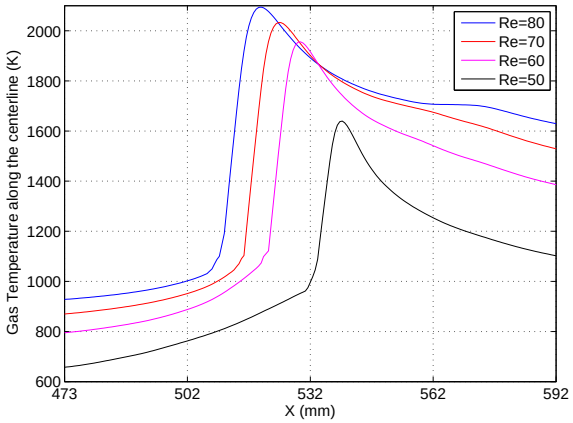

(a)

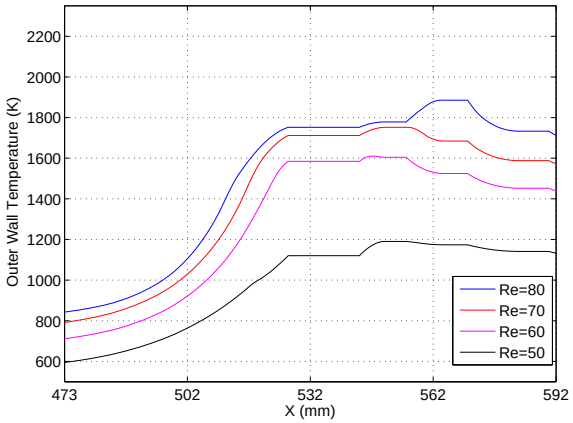

(b)

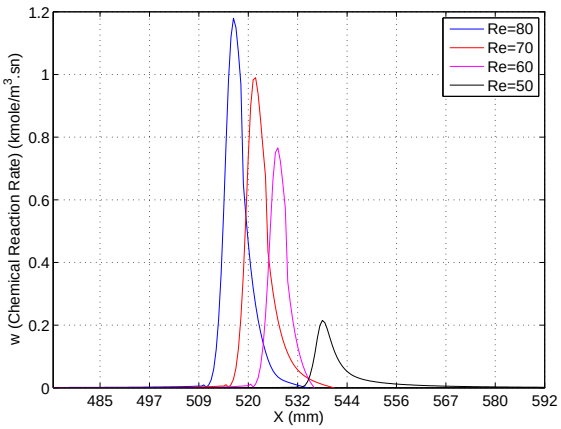

(c)

Figure 4.17. Effect of Reynolds number on (a) gas temperature (b) outer wall temperature (c) reaction rate along the centerline

4.5.3. Effect of Equivalence ratio on the temperature distribution and chemical reaction rate

The effect of equivalence ratio on the temperature distribution and chemical reaction rate is also investigated. For observing the effect; different equivalence ratios; ($\phi = 0.43$, $\phi = 0.45$, $\phi = 0.47$ and $\phi = 0.51$) are used. The Reynolds number is taken as Re=100 which has x-direction inlet velocity of u=0.596 m/s. As expected; it is found that, the increase in equivalence ratio results in an increase of the gas temperature peak value. As the equivalence ratio increases, heat circulation is enhanced because of increased total energy release. Hence; as it is seen the figure, the gas temperature and the wall temperature become higher. This condition; of course, would help preheating. Also, all other effects, as mentioned in the previous section, which are playing dominant role for enhancing heat circulation, are active, again. Since heat circulation increases as the equivalence ratio increases; the combustion zone will shift from the center to the upstream. The results are illustrated in figure 4.18.

4.5.4. Extinction limits for different channel heights and Re numbers

The extinction limits for different Reynolds numbers and channel height are obtained and illustrated in the figure 4.19. The Reynolds number span is between 40 to 500. There are three different channel heights in the figure. These are; d=3.5 mm, d=1.0 mm and d=0.5 mm.

As it is seen easily seen in the figure, the most important result is; the extinction limits become lower when the Reynolds number increase for all channel heights. Another results is; the extinction limit increases by the decrease in channel height. This is an expected result.

Besides, it is observable that, although the extinction limits for d=3.5 and d=1.0 mm has same value at some points, the extinction limits for d=0.5 mm is higher at every Reynolds values from the two other channel heights.

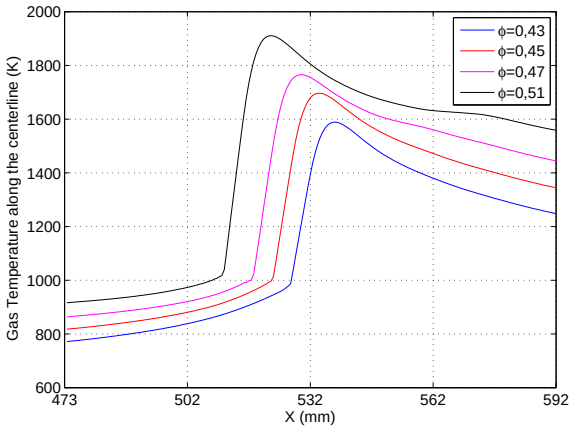

(a)

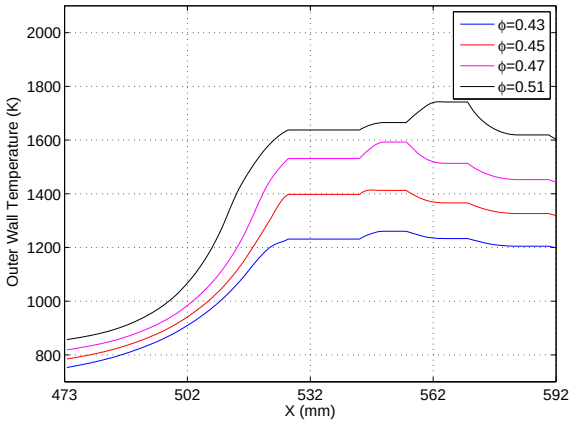

(b)

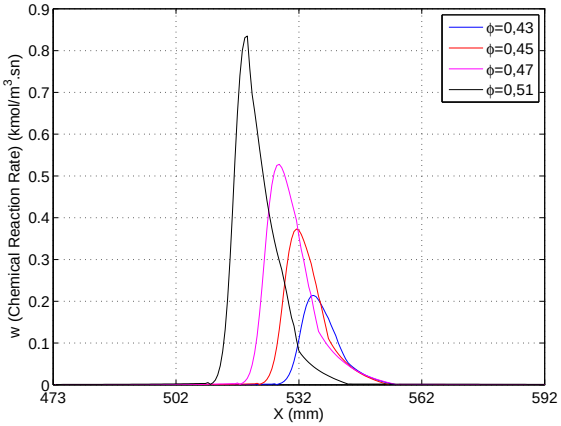

(c)

Figure 4.18. Effect of Equivalence ratio on (a) gas temperature (b) outer wall temperature (c) reaction rate along the centerline

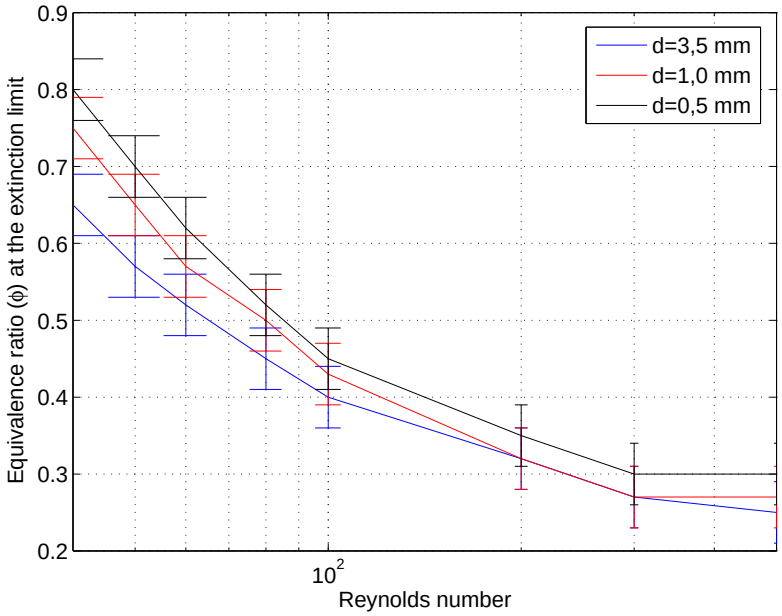

Figure 4.19. Effect of wall thermal conductivity on the extinction limit for different Reynolds numbers

As a final point at this section; it should be emphasized that; in some works it is argued that d=1.0 mm is the border for obtaining a sustainable combustion and the combustion in a straight channel would not survive because of the natural cooling if the channel height is less than 1.0 mm. However; after taking the points that are mentioned before; it would be appropriate to say that, by the Swiss Roll type geometry, the heat circulation is stronger relatively to a simple pipe. Hence, it is valid to say that; even lower channel height values would give stable combustion in the absence of radiative effects.

4.5.5. Effect of thermal conductivity on the extinction limit for different Reynolds numbers

The effect of the wall thermal conductivity on the extinction limit is exhibited in figure 4.20. Here, the other parameters for the system remains constant and only wall thermal conductivity differs. It is normalized with the thermal conductivity of Inconel-718. The difference ratio varies from 0.1 to 10. As it is seen in the figure 4.20, as the wall conductivity increases, the extinction limit increases, too. Because, as

the wall conductivity increases, the heat transfer from the combustion zone to walls, increases. As a result of that event, the reaction weakens and needs more fuel. Hence; the increase in the wall conductivity value results as the increase in extinction limits. It should be noted that, the values are obtained with a error span of $\phi = \pm 0.03$.

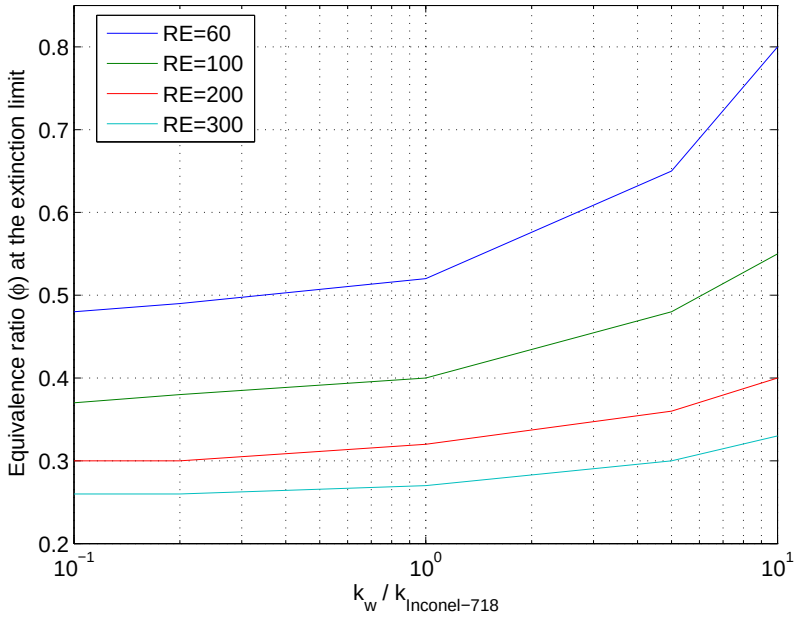

Figure 4.20. Effect of thermal conductivity on the extinction limit for different Reynolds numbers

As it can be easily seen in the figure 4.20, the increase in Reynolds number diminished the equivalence ratio at the extinction limit. This condition can be argued as the Reynolds number increases, the effect of heat conduction on the convective heat transfer between the wall and the gas along the walls diminishes.

Also, it should be emphasized that; since Biot number is always less than 0.1; the temperature gradient across the wall thickness is always negligible for the range of thermal conductivities. The expressions below is the proof for the simplification:

Bi= $h_0\delta^*/k_w$ since; $k_{Inconel-718}$ = 11.40 W/m.K and h_0 is considered as 10 $W/m^2.K$ and $\delta^* = 0.0035$ m; Biot number can be calculated as; Bi= 0.00307 which is less than 0.1. So the simplification can be used.

4.5.6. Effect of wall thickness on the temperature distribution

As it is seen in the wall equations, wall thickness is another important parameter that has significant effect on the temperature distribution. It is quiet simple to obtain the information from the wall heat conduction equations that the wall thickness plays the same role as the wall thermal conductivity. Hence, it would be valid to say that, its effect on the extinction limits will be very similar to the figure 4.20.

The wall thickness parameter is changed due to its ratio to the channel height, d. As it is seen in the figure 4.21; 3 different thickness values are investigated. These are d/4, d/7 and d/12. The equivalence ratio is the same value for the cases d/7 and d/12 and equal to $\phi = 0.42$. It should be noted that, for ensuring a stable combustion; the equivalence ratio of d/4 case is higher, $\phi = 0.43$. Since the extinction limit becomes higher as the thickness diminishes, the equivalence ratio is selected due to the d/12 model.

As it is illustrated in the figures; when the wall thickness decreases the heat circulation increases and as a result, higher temperature values are obtained. Working in the same equivalence ratio is a strong reason for that temperature rise, since in lower thickness values, the equivalence ratio is much higher than the extinction limit respectively to higher thickness values. This of course enhance the temperature in the center and in the walls.

4.5.7. The results for Methane-air mixture

In the present project; the differences arising from the fuel is investigated. As a secondary fuel, Methane (CH_4) is chosen.

Methane is a colorless, odorless gas which is lighter than air. It is formed by the decomposition of organic carbons under anaerobic conditions and is commonly found in near swamps and wetland areas, peat deposits, woodwastes such as hogfuel, or in the area of old landfills.

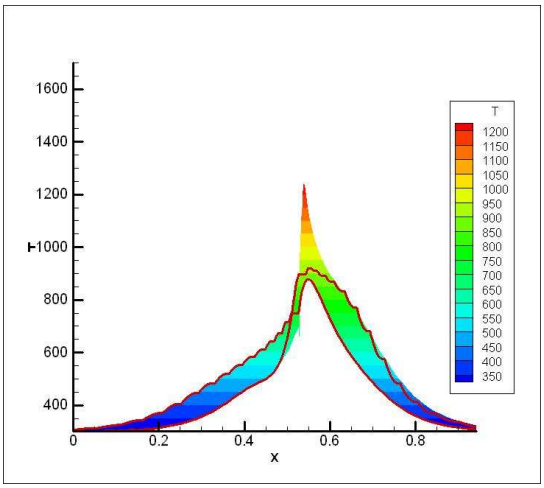

(a)

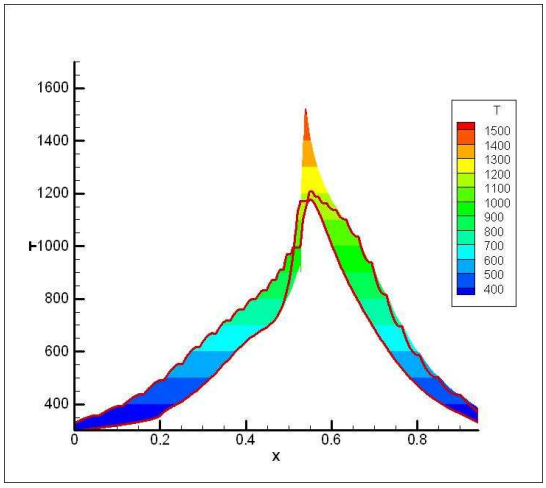

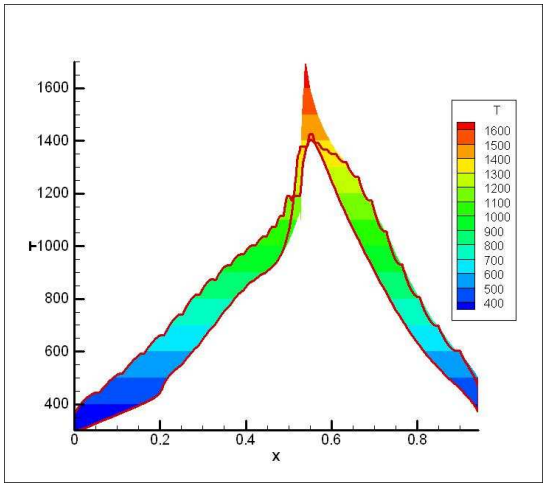

(b) (c)

Figure 4.21. The temperature distribution when the wall thickness is (a) d/4, (a) d/7 and (a) d/12

It is a chemical compound with the molecular formula CH_4. It is the simplest alkane,and the principal component of natural gas. The relative abundance of methane and its clean burning process makes it a very attractive fuel.

In the combustion of methane, the main step is;

$$CH_4 + 2O_2 \rightarrow CO_2 + 2H_2O + 809KJ$$

The results for the combustion of methane-air mixture are illustrated in the figures 4.22-4.29

In the figure 4.22 and 4.23 the temperature distribution for the combustion of methane-air mixture is exhibited. The results are obtained at Re=100 and $\phi = 0.50$ which is located near the extinction limit. When the result is compared with 4.8; which is the temperature distribution for the combustion of propane-air mixture, it can be easily observed that, although the two figures have almost same distribution, the value of the temperature peak differs from each other. At that point, it should be emphasized that, the reasons why they have similar figures are that; they have the same geometry and the same walls which is made from Inconel-718. This condition provides a similar temperature distribution. On the other hand, since the heat of combustion for methane-air mixture is lower than the propane-air mixture; lower temperature values are achieved in simulations which the methane is used as fuel.

In the figure 4.24 the chemical reaction rate values are shown. When it is compared with figure 4.12 it is observed that the methane-air mixture have narrower chemical reaction rate distribution.

In the figure 4.26; the mass fraction values of reactants and products are displayed. The distribution is obtained at Re=100 and $\phi = 0.50$. Since, the oxidizer is more than the required amount; although the fuel is completely consumed; there are still remains of oxidizer.

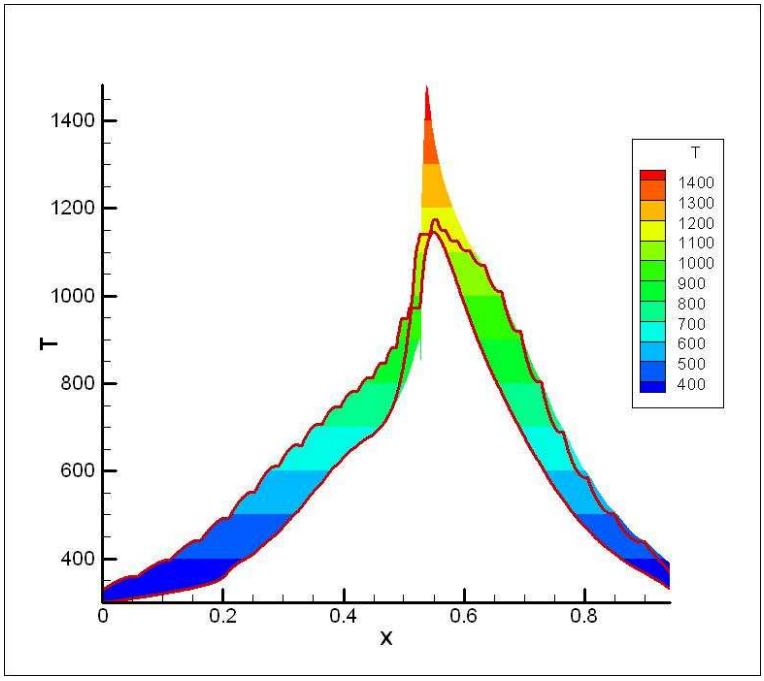

Figure 4.22. Temperature distribution for Methane- air mixture at Re=100 and $\phi = 0.50$ with gas temperature contour

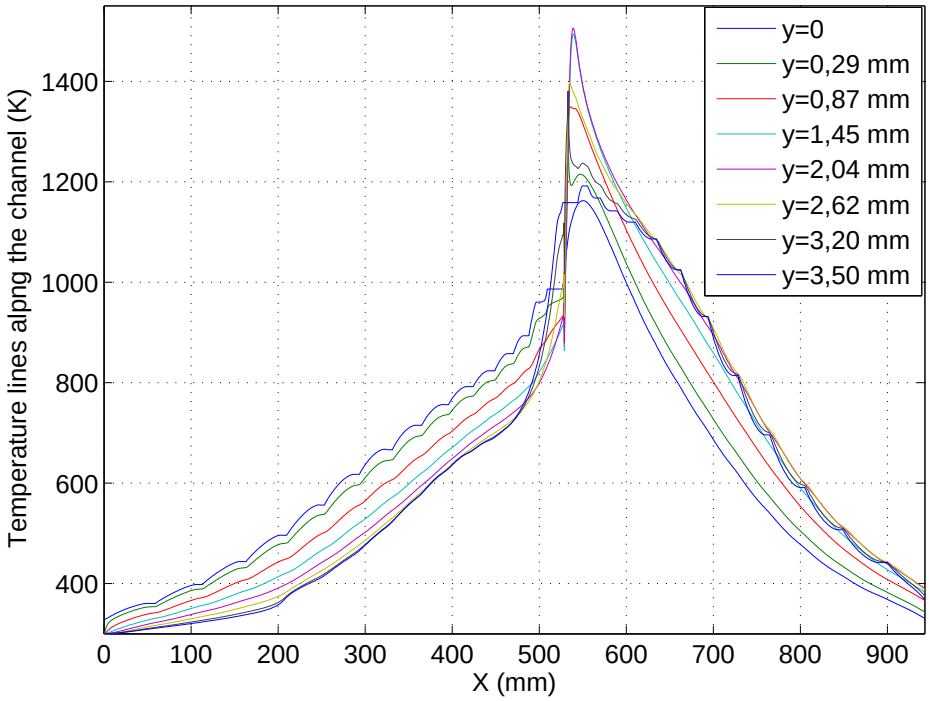

Figure 4.23. Temperature distribution for Methane- air mixture at Re=100 and $\phi = 0.50$ with gas temperature lines

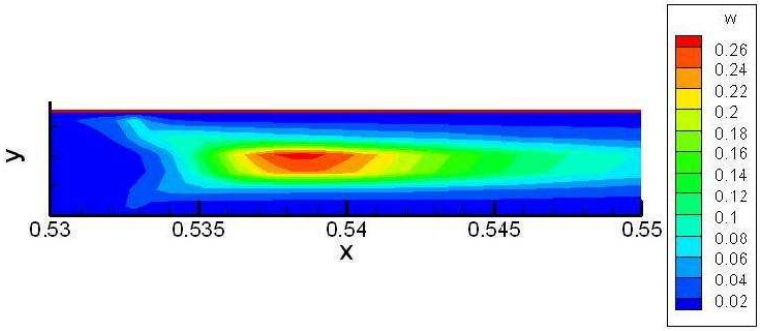

Figure 4.24. The chemical reaction rate for Methane-air mixture at Re=100 and $\phi = 0.50$

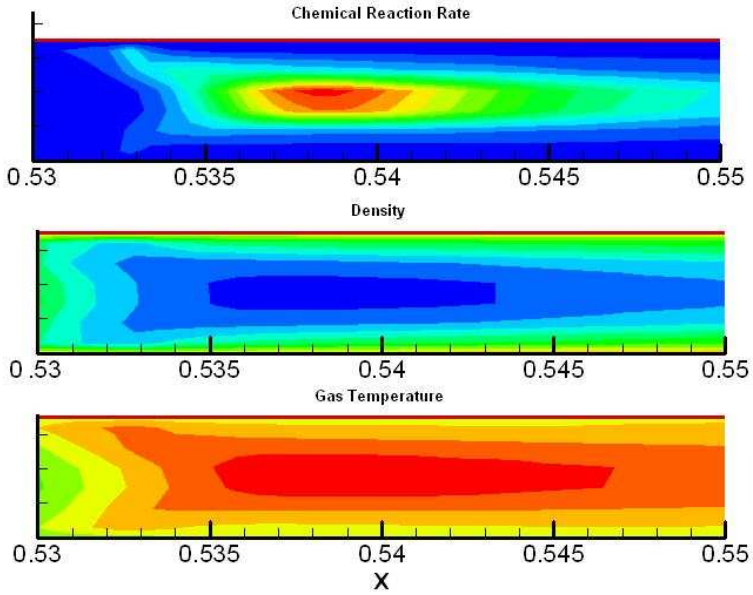

Figure 4.25. The chemical reaction rate, density and gas temperature contours for Methane- air mixture at Re=100 and $\phi = 0.50$

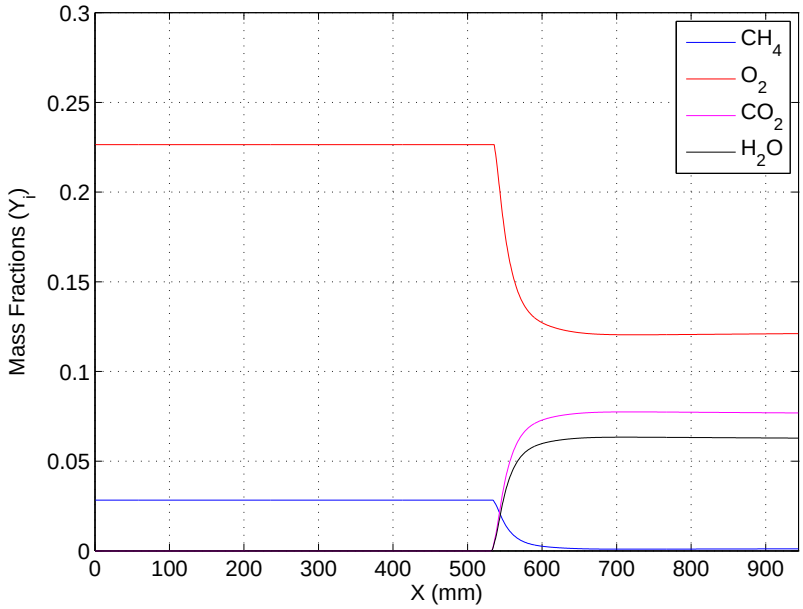

Figure 4.26. Mass fraction values for Methane- air mixture at Re=100 and $\phi = 0.50$

The effect of equivalence ratio is investigated in the figure 4.27. As it is seen in the figures, by the increase of equivalence ratio, the amount of fuel advancing to the flame zone increases and this condition makes the heat release enhanced. As a result, higher temperature values and stronger heat circulation through the conducting wall are achieved. These conditions make the fuel to burn closer to the inlet.

In the figure 4.28 the extinction limits of Methane-air mixture for different channel heights are exhibited. As it is seen from the figures, as it is expected; the increased channel height results as the lower extinction limits.

In the figure 4.29 the extinction limits of Methane-air mixture and Propane-air mixture is compared. As it is seen in the figure; the extinction limit values increases when methane is used as the fuel. The primary reason for that difference is; the heat of combustion values of these fuels. Although heat of combustion value of Propane is approximately 2220 kJ/mol, heat of combustion value of Methane is 809 kJ/mol. Because of this difference, the heat release of propane is higher at same conditions. As a result, higher equivalence ratios of methane is required.

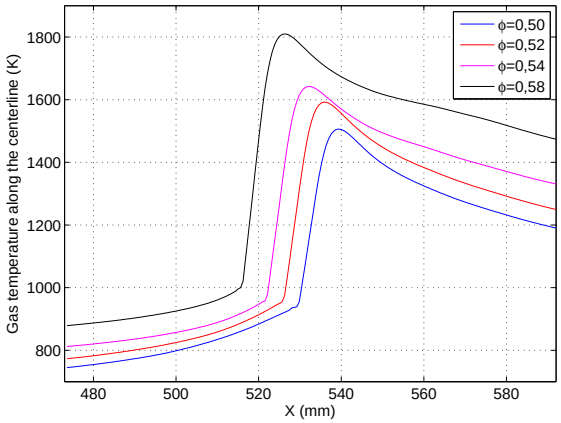

(a)

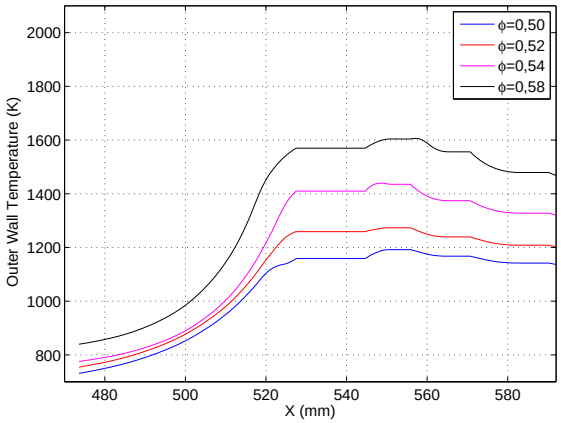

(b)

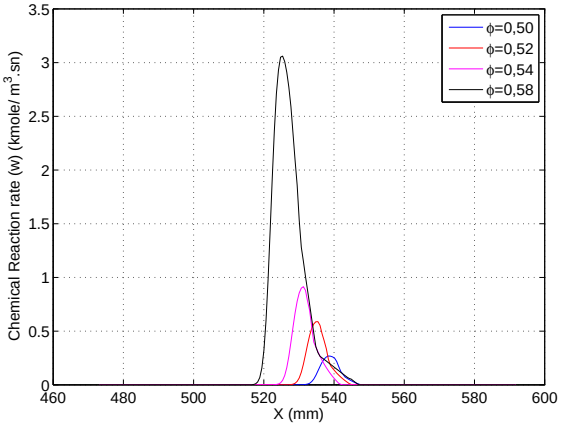

(c)

Figure 4.27. Effect of Equivalence ratio on (a) gas temperature (b) outer wall temperature (c) reaction rate along the centerline for Methane-air mixture

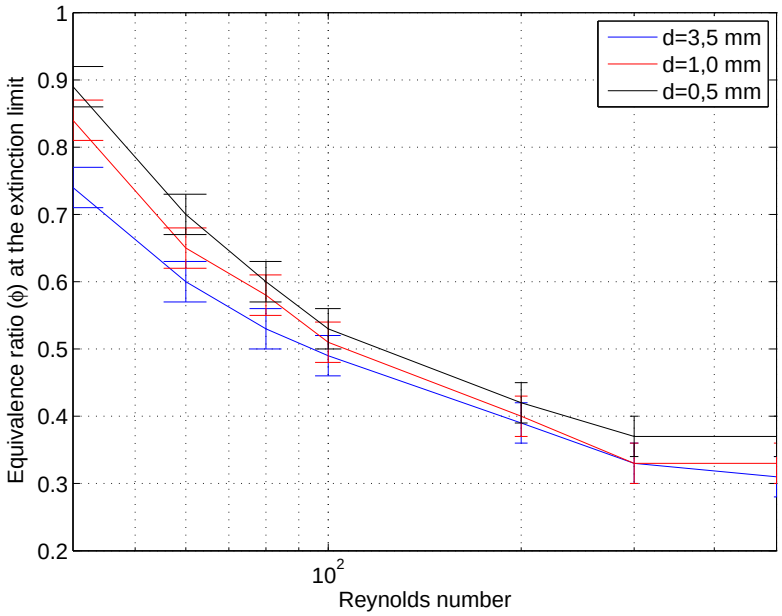

Figure 4.28. The extinction limits of Methane-air mixture for different channel heights

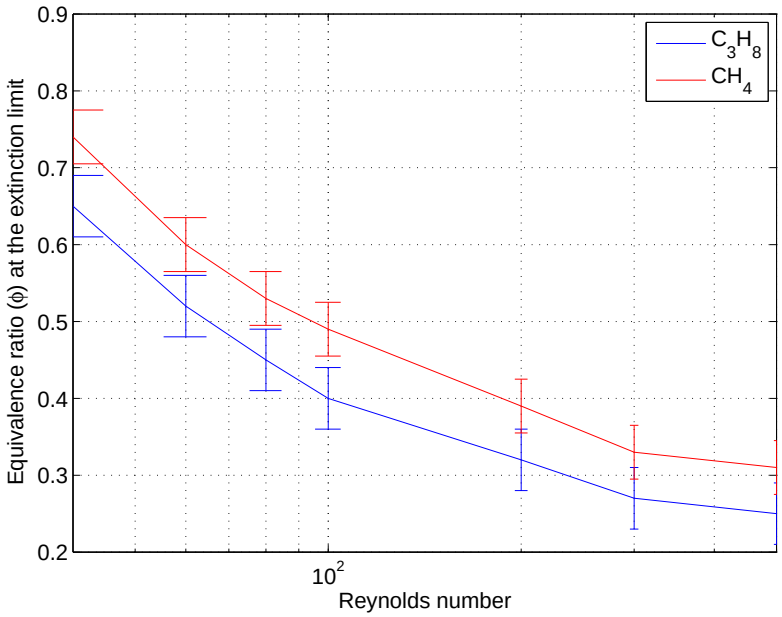

Figure 4.29. The comparison for the extinction limits of Methane-air mixture and Propane-air mixture for d=3.5 mm

5. CONCLUSIONS AND FUTURE WORK

In this study a simplified model is generated for simulating the heat transfer and combustion in a Swiss Roll Combustor by unwrapping the geometry into a straight channel. In this model; two-dimensional momentum, continuity, energy, species equations are solved.

Besides; the model is used to solve different kind of Swiss roll geometries, such as Spiral and Rectangular Swiss Roll combustors. It is observed that, although the outlet temperatures of both SRCs are closer, the maximum temperature of the Spiral one is higher. By also considering that the length of the 18 part Spiral SRC is lower than the Rectangular one, it is valid to state that, for the same conditions and same lengths, the Spiral SRC is more effective.

Different fuels are used in the present study. Fuel lean propane-air mixture and methane-air mixtures are selected as fuels. In the simulations, it is observed that, propane-air mixtures has higher maximum temperature value than the methane-air mixtures under same conditions. Also it is found that, the extinction limits of methane-air mixture is higher than the propane-air mixture.

Effect of channel height, Reynolds number, equivalence ratio, wall thickness, wall conductivity and fuel type on the temperature distribution and chemical reaction rate is investigated. For the range of Reynolds numbers and equivalence ratios examined in the present work; it is found that, higher values of Reynolds number or equivalence ratios result as the increase in the reaction rate and temperature values. Also, the reaction front moves from center to upstream direction. The main reason for that event is, the increase of heat circulation. Because, as the equivalence ratio increases, heat release increases and this result as the higher heat circulation. Also, higher Re numbers are another reason for enhanced heat circulation. Increased heat circulation makes the fresh mixtures temperature higher. So, the reaction zone moves from the center in the direction of inlet.

The extinction limits are investigated for different channel height values such as, d=3.5 mm, d=1.0 mm and d=0.5 mm. Also, the effect of the wall thickness, conductivity constant and fuel type on the extinction limits are observed. It is observed that; higher values of wall conductivity and wall thickness result as higher extinction limits.

APPENDIX A: SOURCE CALCULATION IN COMPRESSIBLE FLOW

A.1. Computing source values

The equation of motion for x direction is;

$$\rho\left(u\frac{\partial u}{\partial x}+v\frac{\partial u}{\partial y}\right)=-\frac{\partial p}{\partial x}+\frac{\partial}{\partial x}\left[\mu\left(2\frac{\partial u}{\partial x}-\frac{2}{3}\left(\frac{\partial u}{\partial x}+\frac{\partial v}{\partial y}\right)\right)\right]+\frac{\partial}{\partial y}\left[\mu\left(\frac{\partial u}{\partial y}+\frac{\partial u}{\partial x}\right)\right] \tag{A.1}$$

If the system is incompressible then divV will be zero. Hence, the equation A.1 becomes;

$$\rho\left(u\frac{\partial u}{\partial x}+v\frac{\partial u}{\partial y}\right)=-\frac{\partial p}{\partial x}+\frac{\partial}{\partial x}\left[\mu\left(2\frac{\partial u}{\partial x}\right)\right]+\frac{\partial}{\partial y}\left[\mu\left(\frac{\partial u}{\partial y}+\frac{\partial u}{\partial x}\right)\right] \tag{A.2}$$

The equation A.1 can also be written as;

$$\rho\left(u\frac{\partial u}{\partial x}+v\frac{\partial u}{\partial y}\right)=-\frac{\partial p}{\partial x}+\frac{\partial}{\partial x}\left[\mu\left(\frac{\partial u}{\partial x}\right)\right]+\frac{\partial}{\partial y}\left[\mu\left(\frac{\partial u}{\partial y}\right)\right]+\frac{\partial}{\partial y}\left[\mu\left(\frac{\partial u}{\partial x}\right)\right]+\frac{\partial}{\partial x}\left[\mu\left(\frac{\partial u}{\partial x}\right)\right] \tag{A.3}$$

The general form of equation of motion is;

$$\frac{\partial}{\partial x}\left(\rho u u\right)+\frac{\partial}{\partial y}\left(\rho v u\right)=-\frac{\partial p}{\partial x}+\frac{\partial}{\partial x}\left[\mu\left(\frac{\partial u}{\partial x}\right)\right]+\frac{\partial}{\partial y}\left[\mu\left(\frac{\partial u}{\partial x}\right)\right]+S_u \tag{A.4}$$

By comparing the equation (A.3) with the equation (A.4), it can be easily seen that,

$$S_u=\frac{\partial}{\partial x}\left[\mu\left(\frac{\partial u}{\partial x}\right)\right]+\frac{\partial}{\partial y}\left[\mu\left(\frac{\partial v}{\partial x}\right)\right] \tag{A.5}$$

However if the system is compressible, then the divV will not be equal to zero and as a result, the source value that is evaluated before is not valid for that case.

In compressible form; the equation (A.3) becomes;

$$\rho\left(u\frac{\partial u}{\partial x}+v\frac{\partial u}{\partial y}\right)=-\frac{\partial p}{\partial x}+\frac{\partial}{\partial x}\left[\mu\left(\frac{4}{3}\frac{\partial u}{\partial x}\right)\right]+\frac{\partial}{\partial x}\left[\mu\left(-\frac{2}{3}\frac{\partial v}{\partial y}\right)\right]+\frac{\partial}{\partial y}\left[\mu\left(\frac{\partial u}{\partial y}\right)\right]+\frac{\partial}{\partial y}\left[\mu\left(\frac{\partial v}{\partial x}\right)\right] \tag{A.6}$$

This equation can be arranged as;

$$\rho\left(u\frac{\partial u}{\partial x}+v\frac{\partial u}{\partial y}\right)=-\frac{\partial p}{\partial x}+\frac{\partial}{\partial x}\left[\mu\left(\frac{\partial u}{\partial x}\right)\right]+\frac{\partial}{\partial y}\left[\mu\left(\frac{\partial u}{\partial y}\right)\right]+\frac{\partial}{\partial x}\left[\mu\left(\frac{1}{3}\frac{\partial u}{\partial x}\right)\right]+\frac{\partial}{\partial x}\left[\mu\left(-\frac{2}{3}\frac{\partial v}{\partial y}\right)\right]+\frac{\partial}{\partial y}\left[\mu\left(\frac{\partial v}{\partial x}\right)\right] \tag{A.7}$$

By comparing the equation A.11 with the general form, S_u can be easily written as;

$$S_u=\frac{\partial}{\partial x}\left[\frac{\mu}{3}\left(\frac{\partial u}{\partial x}\right)\right]+\frac{\partial}{\partial x}\left[\mu\left(-\frac{2}{3}\frac{\partial v}{\partial y}\right)\right]+\frac{\partial}{\partial y}\left[\mu\left(\frac{\partial v}{\partial x}\right)\right] \tag{A.8}$$

The equation of motion for y direction is;

$$\rho\left(u\frac{\partial v}{\partial x}+v\frac{\partial v}{\partial y}\right)=-\frac{\partial p}{\partial x}+\frac{\partial}{\partial y}\left[\mu\left(2\frac{\partial v}{\partial y}-\frac{2}{3}\left(\frac{\partial u}{\partial x}+\frac{\partial v}{\partial y}\right)\right)\right]+\frac{\partial}{\partial x}\left[\mu\left(\frac{\partial u}{\partial y}+\frac{\partial v}{\partial x}\right)\right] \tag{A.9}$$

If the system is incompressible then divV will be zero. Hence, the equation above

becomes;

$$\rho\left(u\frac{\partial v}{\partial x}+v\frac{\partial v}{\partial y}\right)=-\frac{\partial p}{\partial x}+\frac{\partial}{\partial y}\left[\mu\left(2\frac{\partial v}{\partial y}\right)\right]+\frac{\partial}{\partial x}\left[\mu\left(\frac{\partial u}{\partial y}+\frac{\partial v}{\partial x}\right)\right] \tag{A.10}$$

The equation can also be written as;

$$\rho\left(u\frac{\partial v}{\partial x}+v\frac{\partial v}{\partial y}\right)=-\frac{\partial p}{\partial x}+\frac{\partial}{\partial y}\left[\mu\left(\frac{\partial v}{\partial y}\right)\right]+\frac{\partial}{\partial x}\left[\mu\left(\frac{\partial u}{\partial y}\right)\right]+\frac{\partial}{\partial x}\left[\mu\left(\frac{\partial v}{\partial x}\right)\right]+\frac{\partial}{\partial y}\left[\mu\left(\frac{\partial v}{\partial y}\right)\right] \tag{A.11}$$

The general form of equation of motion is;

$$\frac{\partial}{\partial x}\left(\rho uv\right)+\frac{\partial}{\partial y}\left(\rho vv\right)=-\frac{\partial p}{\partial y}+\frac{\partial}{\partial x}\left[\mu\left(\frac{\partial v}{\partial x}\right)\right]+\frac{\partial}{\partial y}\left[\mu\left(\frac{\partial v}{\partial y}\right)\right]+S_v \tag{A.12}$$

By comparing the equation (A.11) with the equation above, it can be easily seen that,

$$S_v=\frac{\partial}{\partial y}\left[\mu\left(\frac{\partial v}{\partial y}\right)\right]+\frac{\partial}{\partial x}\left[\mu\left(\frac{\partial u}{\partial y}\right)\right] \tag{A.13}$$

Because of the fact that if the system is compressible, the divV will not be equal to zero and as a result, the source value that is evaluated before is not valid for that case.

In compressible form; the quotation (A.9) becomes;

$$\rho\left(u\frac{\partial v}{\partial x}+v\frac{\partial v}{\partial y}\right)=-\frac{\partial p}{\partial y}+\frac{\partial}{\partial x}\left[\mu\left(\frac{\partial u}{\partial y}+\frac{\partial v}{\partial x}\right)\right]+\frac{\partial}{\partial x}\left[\frac{4\mu}{3}\left(\frac{\partial v}{\partial y}\right)-\frac{2\mu}{3}\left(\frac{\partial u}{\partial x}\right)\right] \tag{A.14}$$

This equation can be arranged as;

$$\rho\left(u\frac{\partial v}{\partial x}+v\frac{\partial v}{\partial y}\right)=-\frac{\partial p}{\partial y}+\frac{\partial}{\partial x}\left[\mu\left(\frac{\partial u}{\partial y}\right)\right]+\frac{\partial}{\partial x}\left[\mu\left(\frac{\partial v}{\partial x}\right)\right]+\frac{\partial}{\partial y}\left[\mu\left(\frac{\partial v}{\partial y}\right)\right] +\frac{\partial}{\partial y}\left[\frac{\mu}{3}\left(\frac{\partial v}{\partial y}\right)\right]+\frac{\partial}{\partial y}\left[\frac{-2\mu}{3}\left(\frac{\partial u}{\partial x}\right)\right] \tag{A.15}$$

By comparing the equation A.15 with the general form, S_v can be easily written as;

$$S_v=\frac{\partial}{\partial x}\left[\mu\left(\frac{\partial u}{\partial y}\right)\right]+\frac{\partial}{\partial y}\left[\frac{\mu}{3}\left(\frac{\partial v}{\partial y}\right)\right]+\frac{\partial}{\partial y}\left[\frac{-2\mu}{3}\left(\frac{\partial u}{\partial x}\right)\right] \tag{A.16}$$

APPENDIX B: CODE VERIFICATION

First of all, for examining whether the code is giving the valid results after solving momentum, pressure and energy equation; a simple pipe system is designed and different velocity values are assigned to compare with the graphs which are generated at same conditions by FLUENT.

In these experiments four different velocities are used for the compare. These are; U=0.01 m/s, U=0.001 m/s, U=0.0001 m/s and U=0.00001 m/s. The results are plotted in the following figures.

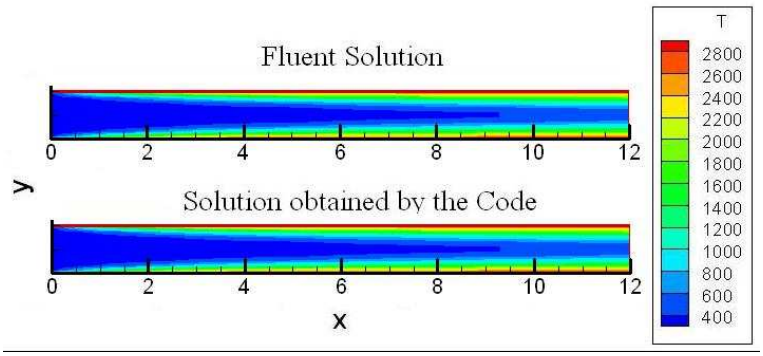

Figure B.1. Temperature contours in a simple pipe for 1×10^{-2} m/s inlet velocity and Re=590

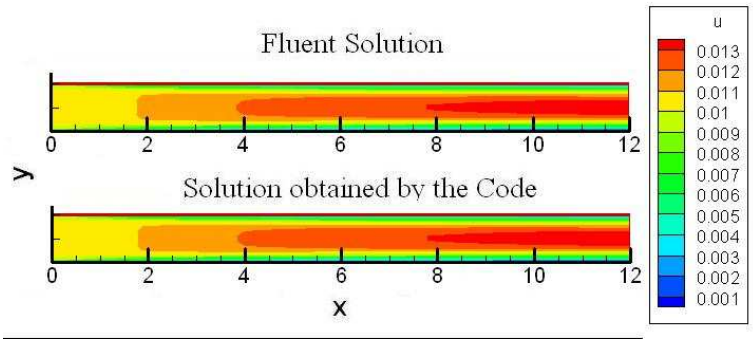

Figure B.2. x-velocity contours in a simple pipe for 1×10^{-2} m/s inlet velocity and Re=590

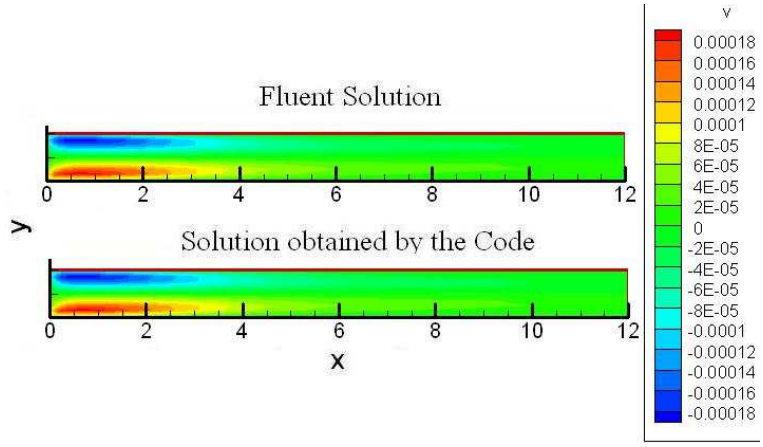

Figure B.3. y-velocity contours in a simple pipe for 1×10^{-2} m/s inlet velocity and Re=590

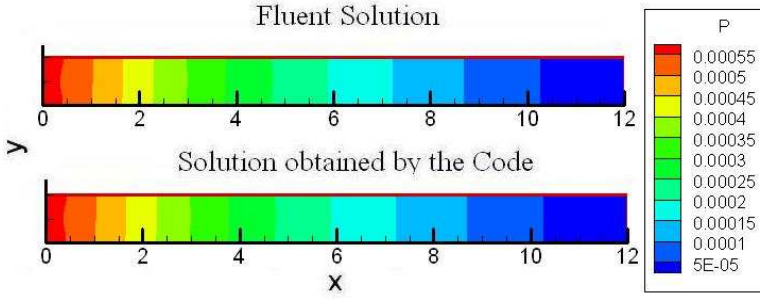

Figure B.4. Pressure contours in a simple pipe for 1×10^{-2} m/s inlet velocity and Re=590

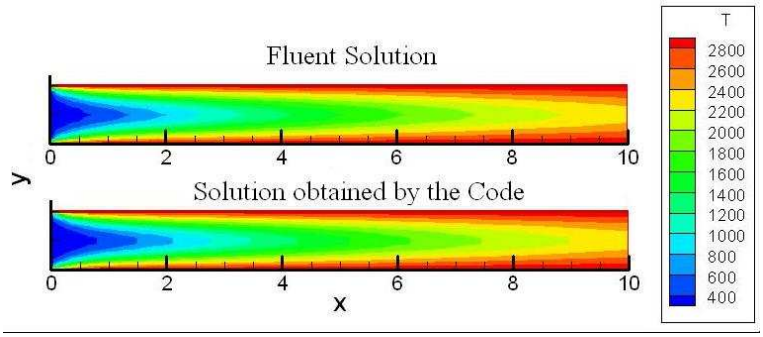

Figure B.5. Temperature contours in a simple pipe for 1×10^{-3} m/s inlet velocity and Re=59

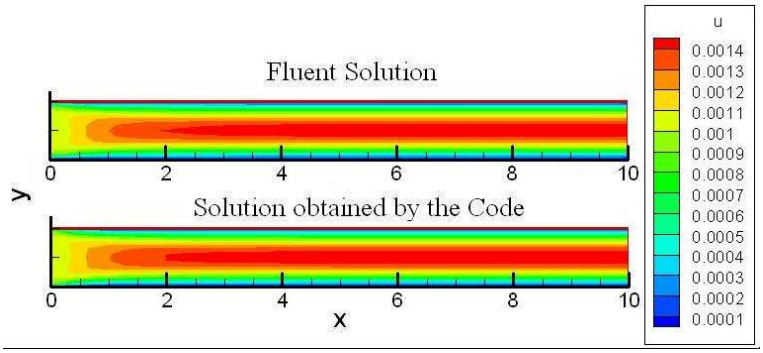

Figure B.6. x-velocity contours in a simple pipe for 1×10^{-3} m/s inlet velocity and Re=59

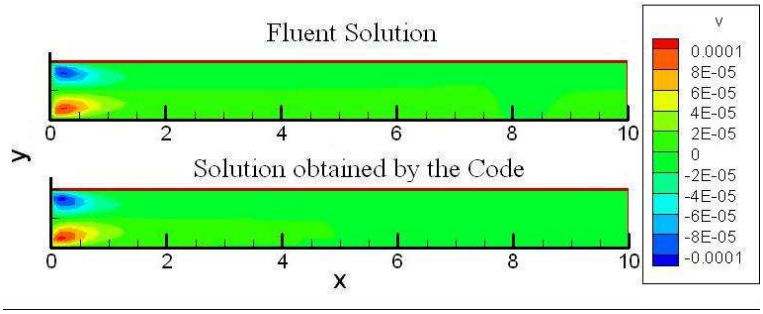

Figure B.7. y-velocity contours in a simple pipe for 1×10^{-3} m/s inlet velocity and Re=59

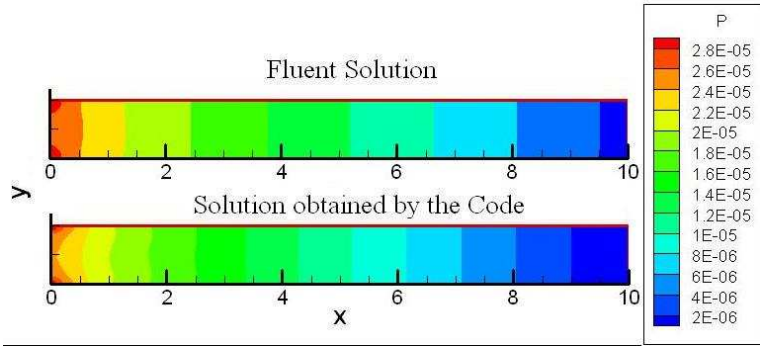

Figure B.8. Pressure contours in a simple pipe for 1×10^{-3} m/s inlet velocity and Re=59

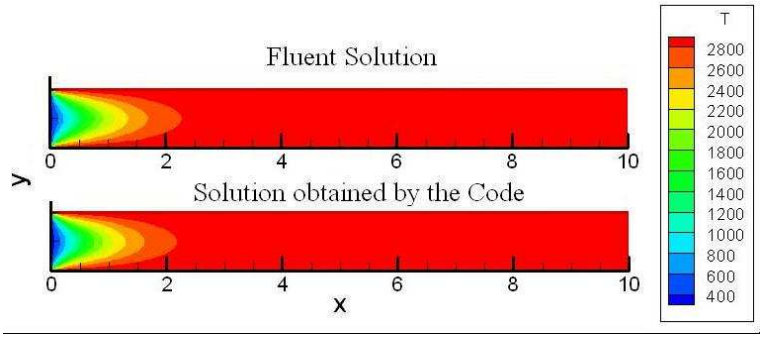

Figure B.9. Temperature contours in a simple pipe for 1×10^{-4} m/s inlet velocity and Re=5.9

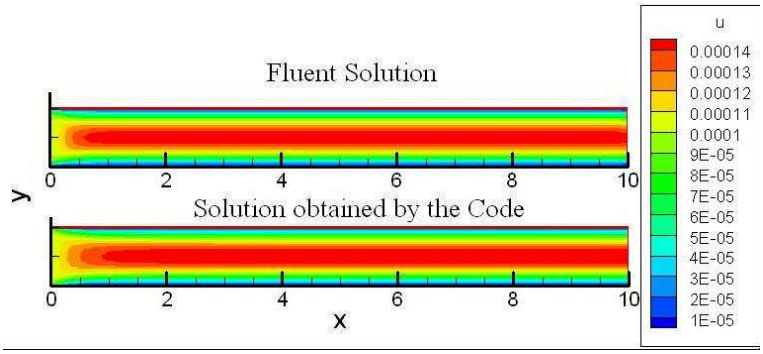

Figure B.10. x-velocity contours in a simple pipe for 1×10^{-4} m/s inlet velocity and Re=5.9

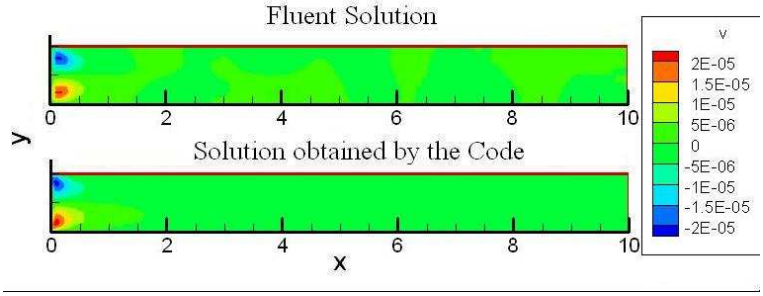

Figure B.11. y-velocity contours in a simple pipe for 1×10^{-4} m/s inlet velocity and Re=5.9

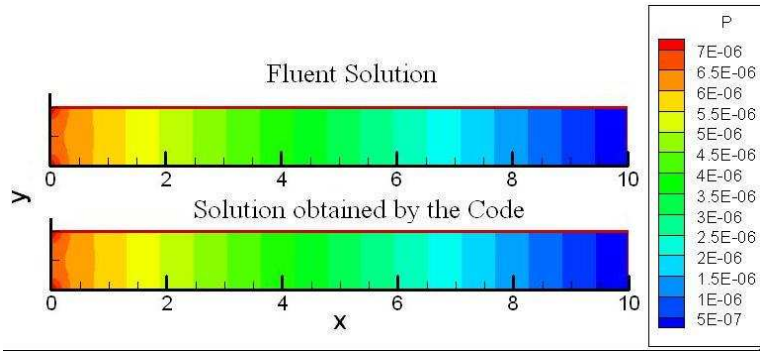

Figure B.12. Pressure contours in a simple pipe for 1×10^{-4} m/s inlet velocity and Re=5.9

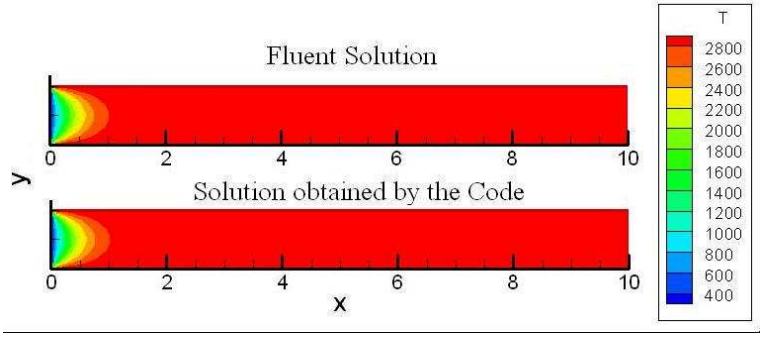

Figure B.13. Temperature contours in a simple pipe for 1×10^{-5} m/s inlet velocity and Re=0.59

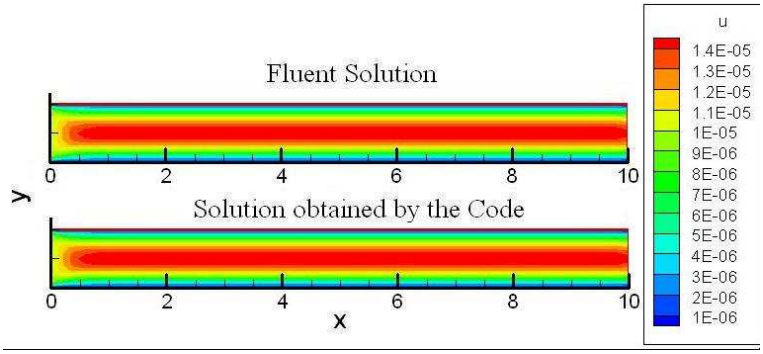

Figure B.14. x-velocity contours in a simple pipe for 1×10^{-5} m/s inlet velocity and Re=0.59

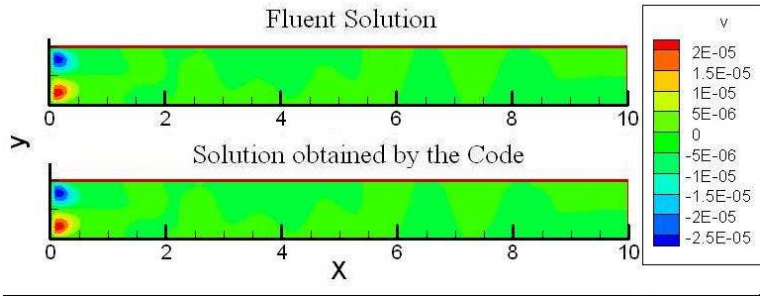

Figure B.15. y-velocity contours in a simple pipe for 1×10^{-5} m/s inlet velocity and Re=0.59

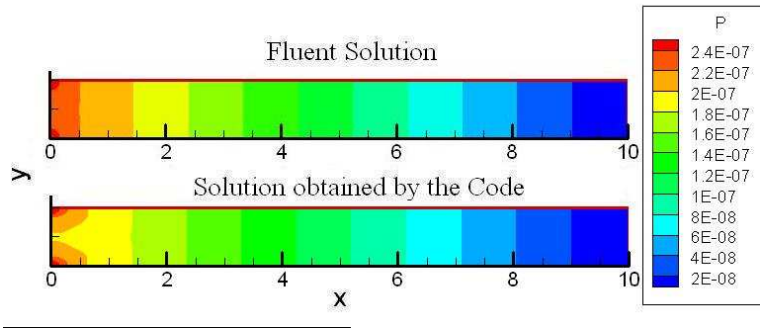

Figure B.16. Pressure contours in a simple pipe for 1×10^{-5} m/s inlet velocity and Re=0.59

B.1. Mesh Independency

B.1.1. The mesh independency in Simple pipe

A mesh independence study was done. Mesh independency is another important factor for proving the validity of the code. Hence; the code of double grid (20x200=4000 finite volume mesh) is used for the approval. The comparison is accomplished below:

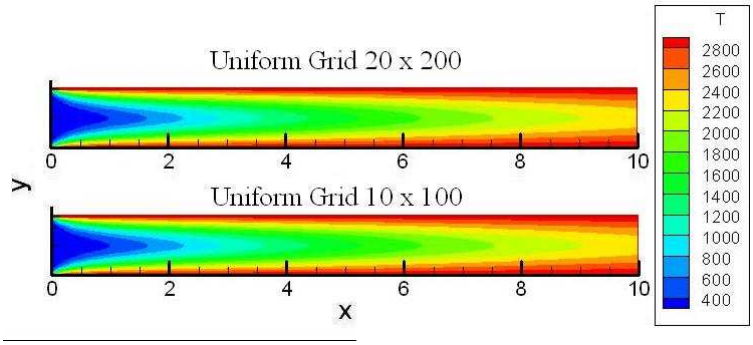

Figure B.17. Temperature contours in a simple pipe for 1×10^{-3} m/s inlet velocity and Re=59

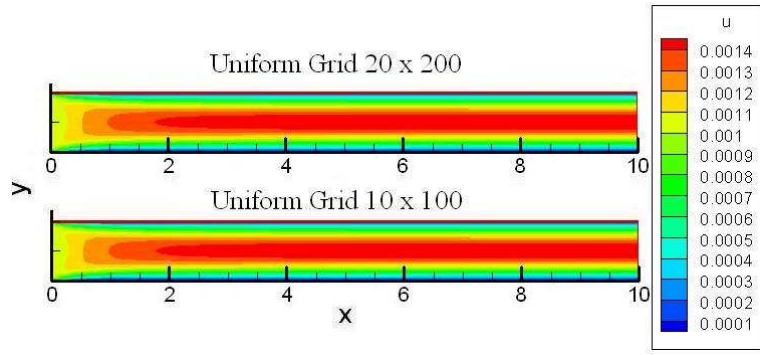

Figure B.18. x-velocity contours in a simple pipe for 1×10^{-3} m/s inlet velocity and Re=59

As it is easily seen in the figures B.17, B.18, B.19 and B.20; the mesh independency of the code is satisfied.

B.1.2. The mesh independency in the unwrapped Swiss Roll geometry

For investigating the mesh independency for the unwrapped geometry, one unwrapped Spiral Swiss Roll geometry is modeled with two different clusters of mesh

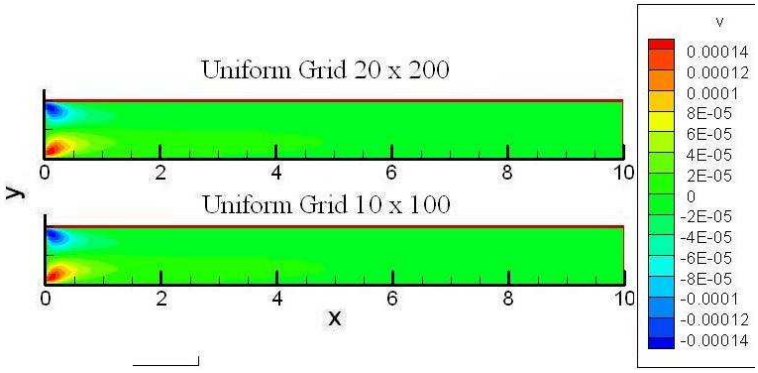

Figure B.19. y-velocity contours in a simple pipe for 1×10^{-3} m/s inlet velocity and Re=59

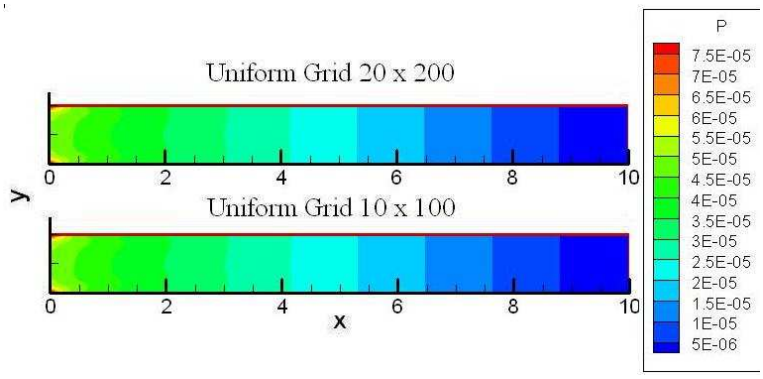

Figure B.20. Pressure contours in a simple pipe for 1×10^{-3} m/s inlet velocity and Re=59

points. Since this is an experiment for observing whether the unwrapping process is valid for double mesh, the system is only solved for temperature distribution. Since there is no chemical reaction, the temperature distribution is accomplished by locating a heat source in the center of the burner.

In general type, a uniform grid of 1594 (x-direction)by 8 (y-direction) is used. But in the double meshed type, a uniform grid of 3158 (x-direction)by 14 (y-direction) is used.

The figures for the first and the second type (double mesh) are represented in figures B.21 and B.22; respectively. Also a contour comparison between these two grids is exhibited in the figure B.23. As a result, it can be easily said that; a mesh

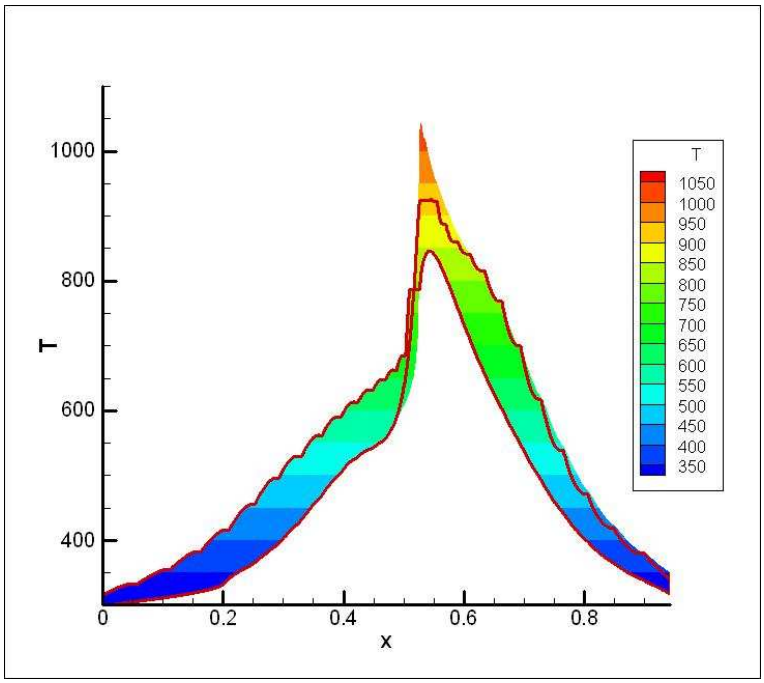

Figure B.21. The temperature distribution for single mesh geometry

independence study is accomplished.

B.2. Reversed, double, triple flow simple pipe solutions

Another condition that should be investigated is; the independency of the code about the Boundary conditions. For example; the location of starting velocity should

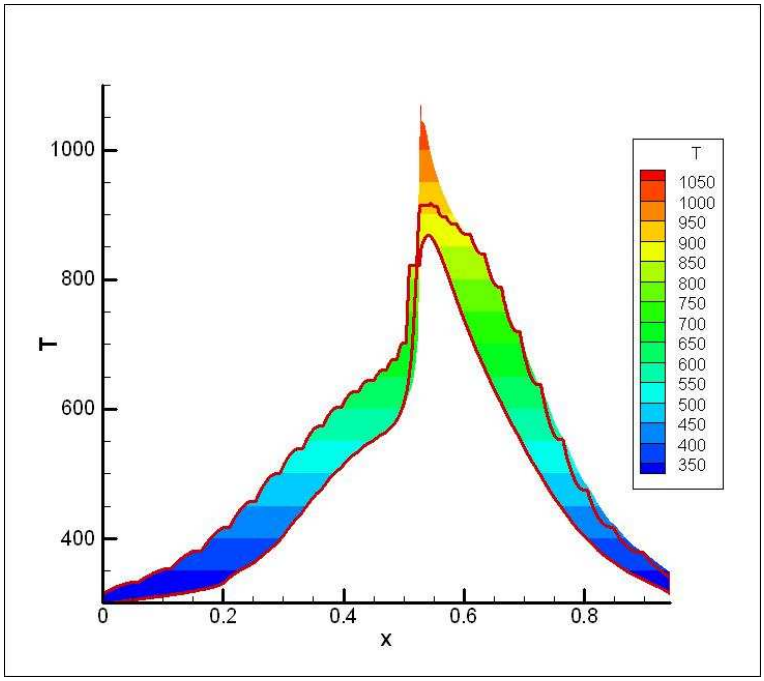

Figure B.22. The temperature distribution for double mesh geometry

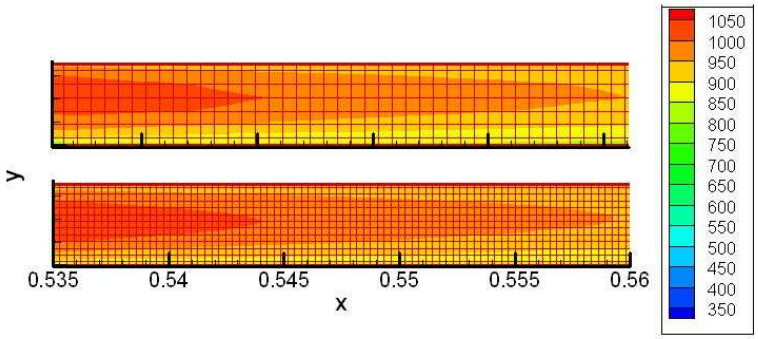

Figure B.23. The comparison of single and double meshed geometries in contour form

be investigated. For that examination; the simple pipe example reinvestigated for the reverse flow and vertical flow (without gravity), respectively.

The reverse flow can be examined in the following graphs:

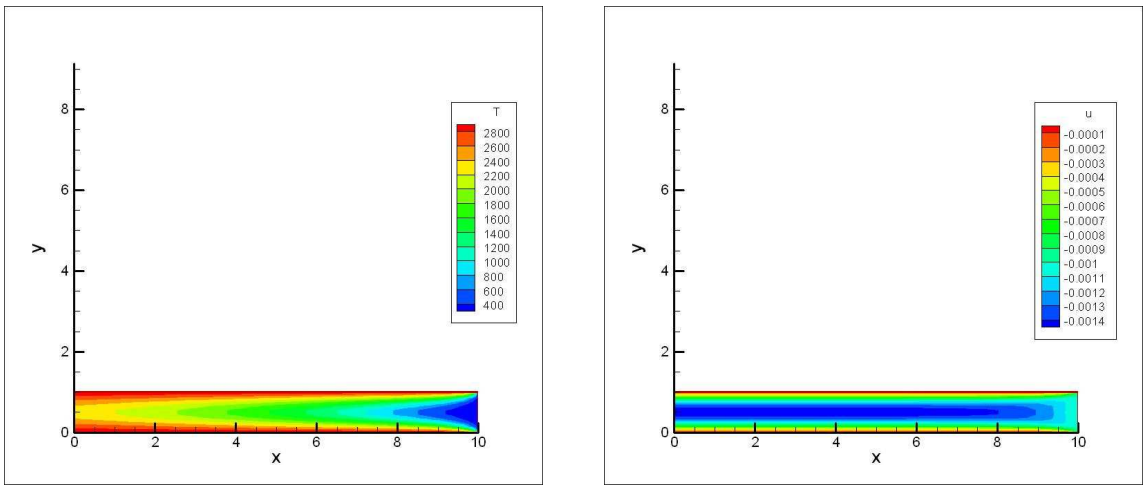

(a) (b)

Figure B.24. (a) The temperature and (b) x velocity values for the inlet velocity of 1×10^{-3} m/s in reverse flow

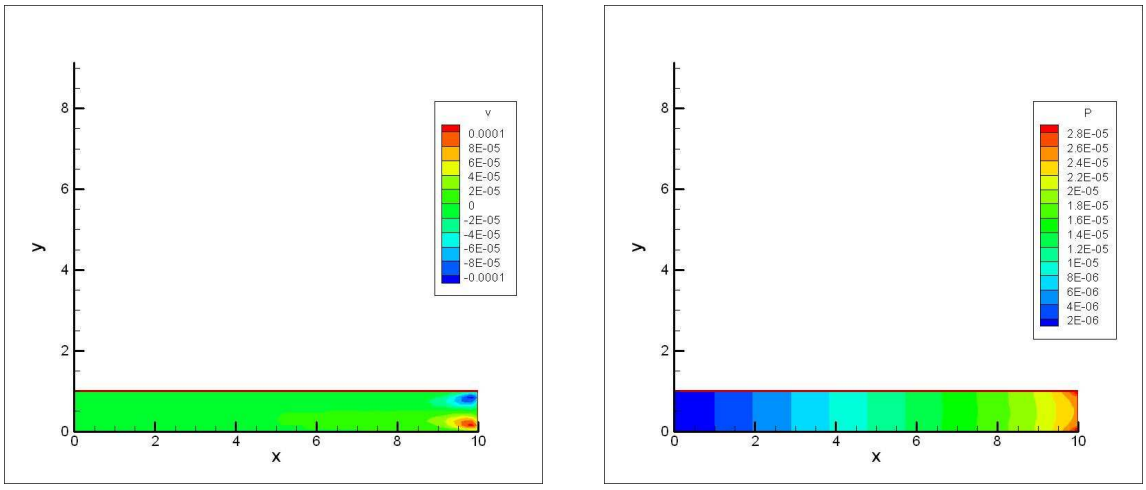

(a) (b)

Figure B.25. (a) The y velocity and (b) pressure values for the inlet velocity of 1×10^{-3} m/s in reverse flow

The vertical flow can be examined in the following graphs:

A lot of different geometries can be modeled by the existing code. In this section,

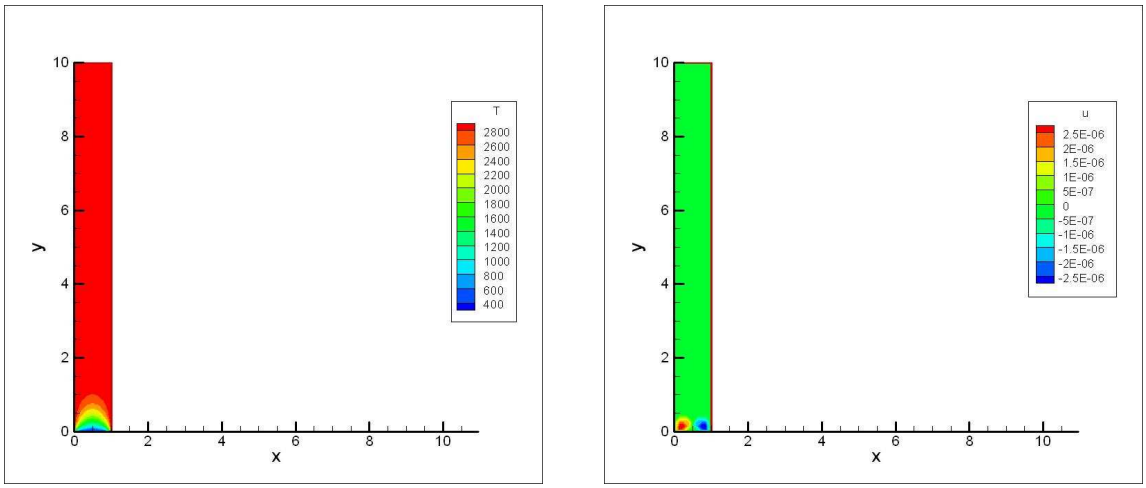

(a) (b)

Figure B.26. (a) The temperature and (b) x velocity values for the inlet velocity of 1×10^{-3} m/s in vertical flow

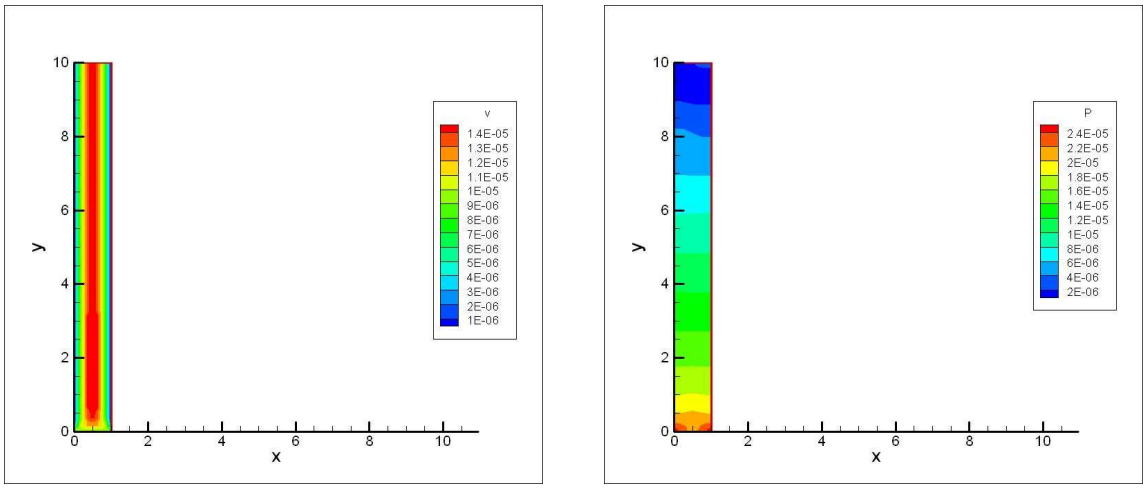

(a) (b)

Figure B.27. (a) The y velocity and (b) pressure values for the inlet velocity of 1×10^{-3} m/s in vertical flow

the models and the concerned graphs will be displayed. For that goal, a U-tube model, different kinds of double flow models and a triple flow model is generated.

In the following graphs that are generated for a U-Tube model can be investigated. In that model, the beginning velocity is $U = 10^{-3}$ m/s , there is a wall which is constructed by using Aluminum located on the center of the model , the flow temperature in the beginning is 300K and the outer wall temperature is 3000K.

Aluminum properties are given in table 4.1;

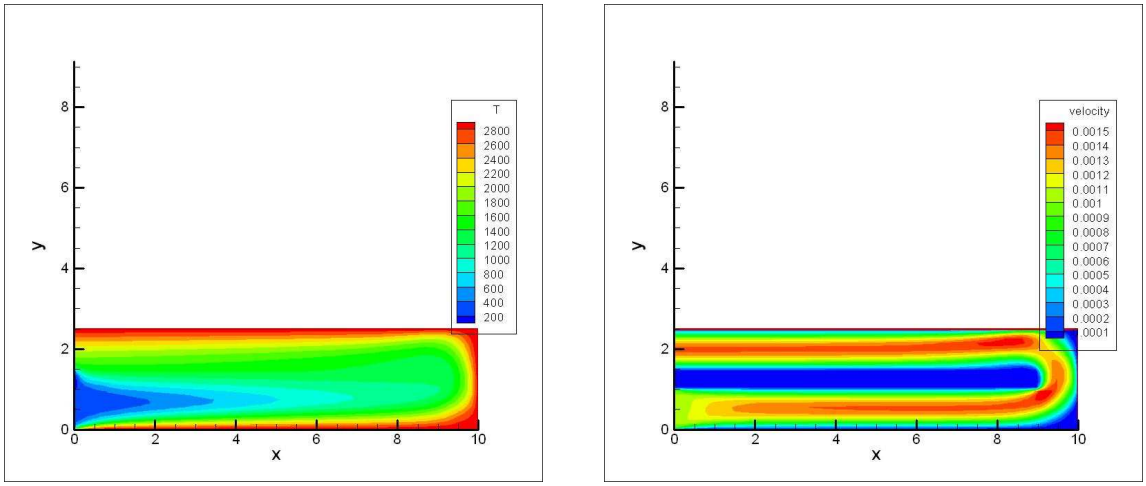

(a) (b)

Figure B.28. (a) The temperature and (b) total velocity values for the inlet velocity of $1 \times 10^{-3} m/s$ in simple u-tube burner

In the following graphs that are generated for Double Flow model can be examined. In that model, the beginning velocities of each flow are $U = 10^{-}3m/s$, there is a wall located on the centre of the model , the flow temperature in the beginning is 300 K and the outer wall temperature is 3000 K.

In the figure B.31, a comparison between the temperature graph of non-conductive wall and a conductive wall which is made of Aluminum.

As it is seen by the graph easily, temperature moves gradually among the conductive wall. In the other graph the wall is selected with constant temperature of

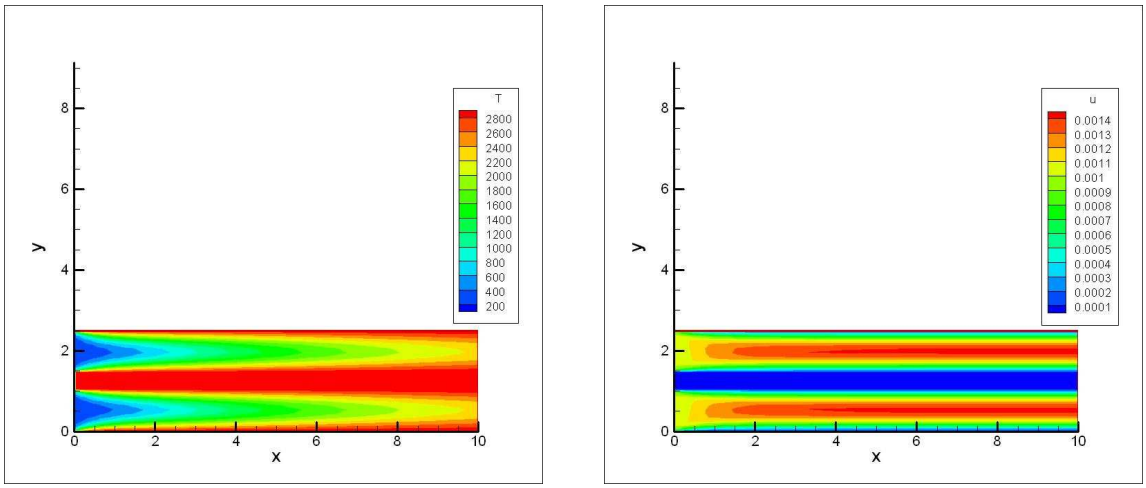

(a) (b)

Figure B.29. (a) The temperature and (b) x velocity values for the inlet velocity of $1 \times 10^{-3} m/s$ in double flow

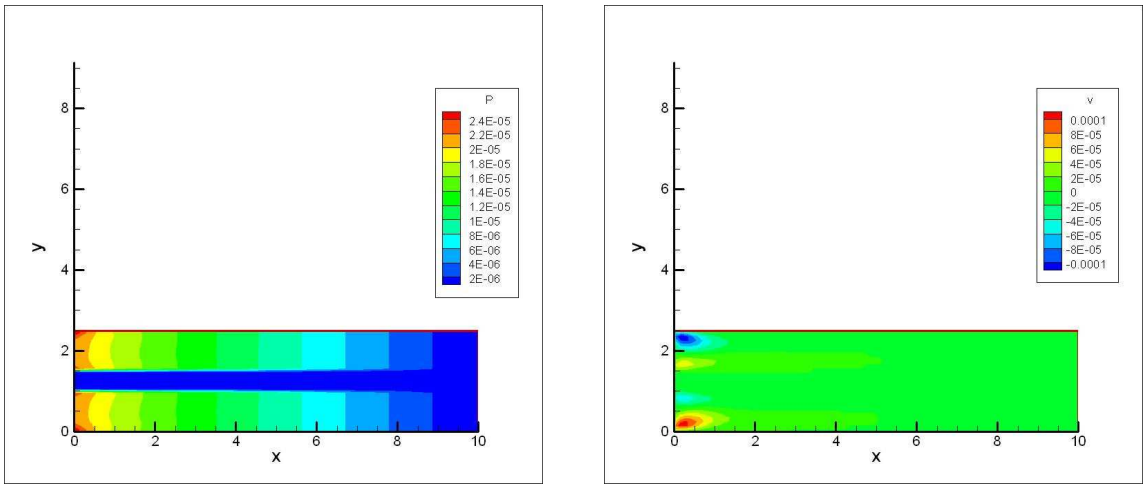

(a) (b)

Figure B.30. (a) The Pressure distribution and (b) y velocity values for the inlet velocity of $1 \times 10^{-3} m/s$ in double flow

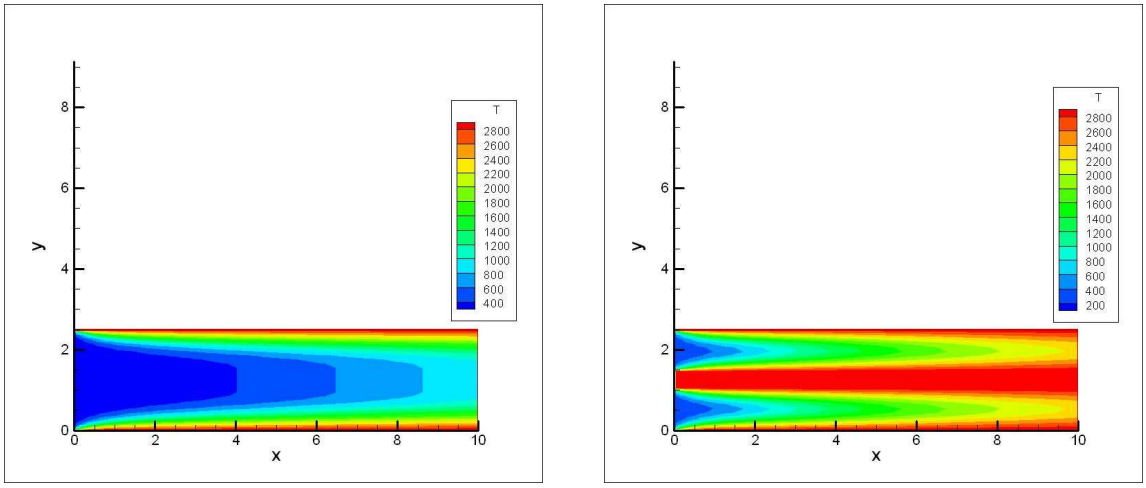

(a) (b)

Figure B.31. The temperature distribution in a burner (a) with and (b) without conductive walls

3000K.

Besides; a double flow problem with reverse flow directions is also solved by the code. In these graphs the boundary conditions and mechanical properties are same with the prior experiments.

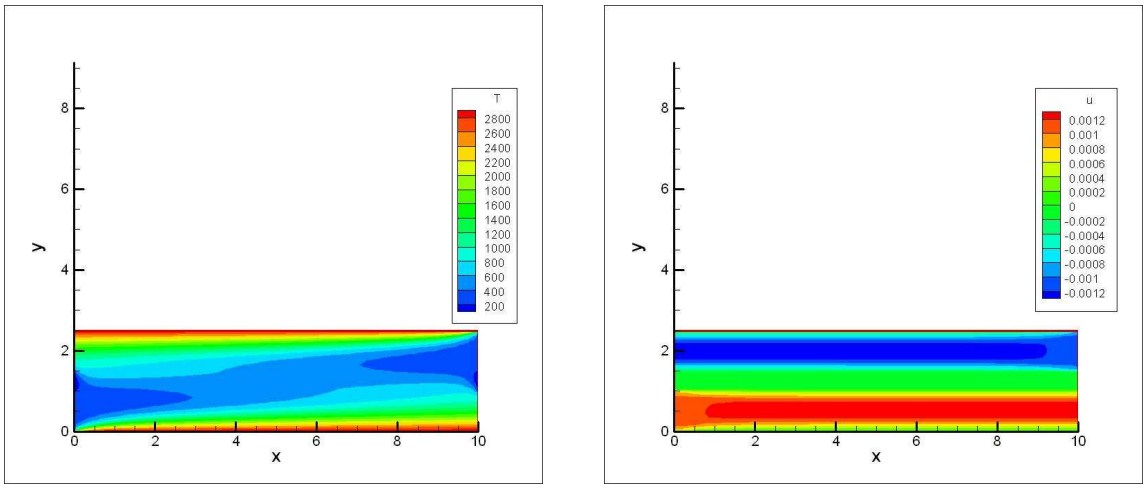

(a) (b)

Figure B.32. (a) The temperature and (b) x velocity values for the inlet velocity of $1 \times 10^{-3} m/s$ in reversed double flow

As it is exhibited by the graph a parabolic flow is obtained in the system.

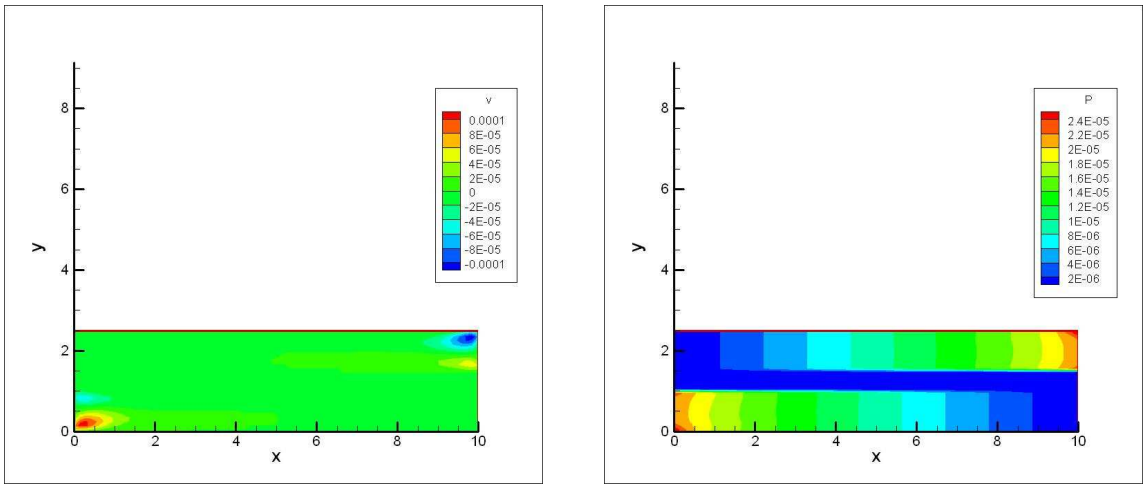

(a) (b)

Figure B.33. (a) The y velocity values and (b) pressure distribution for the inlet velocity of $1 \times 10^{-3} m/s$ in reversed double flow

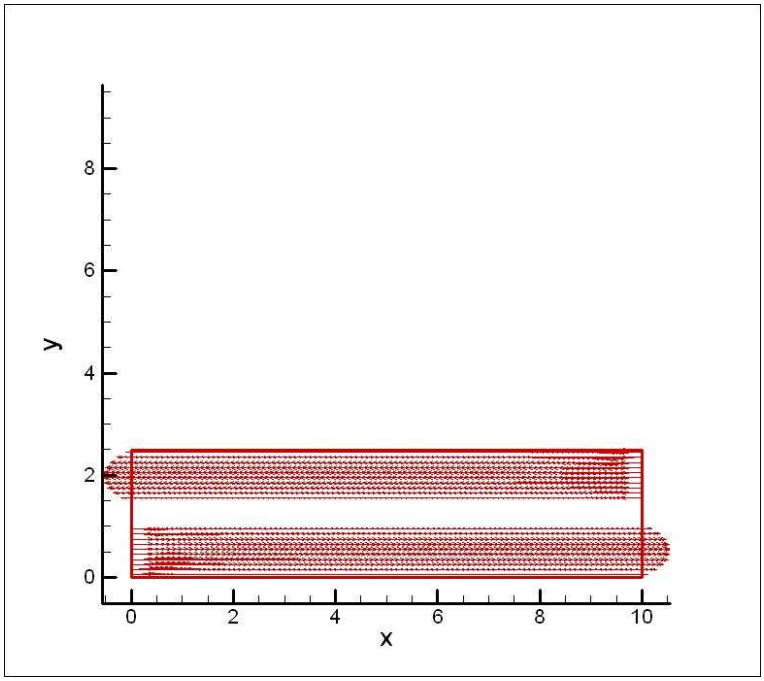

Figure B.34. The vectoral appearance of the flow

As an original geometry, a triple flow problem is solved in FORTRAN. In that problem; there exist a flow and two reverse flow which are divided by walls having the same constant temperature; 3000K. The starting temperature is 300 K. The Velocity is the same with the prior experiments; $U = 10^{-3} m/s$.

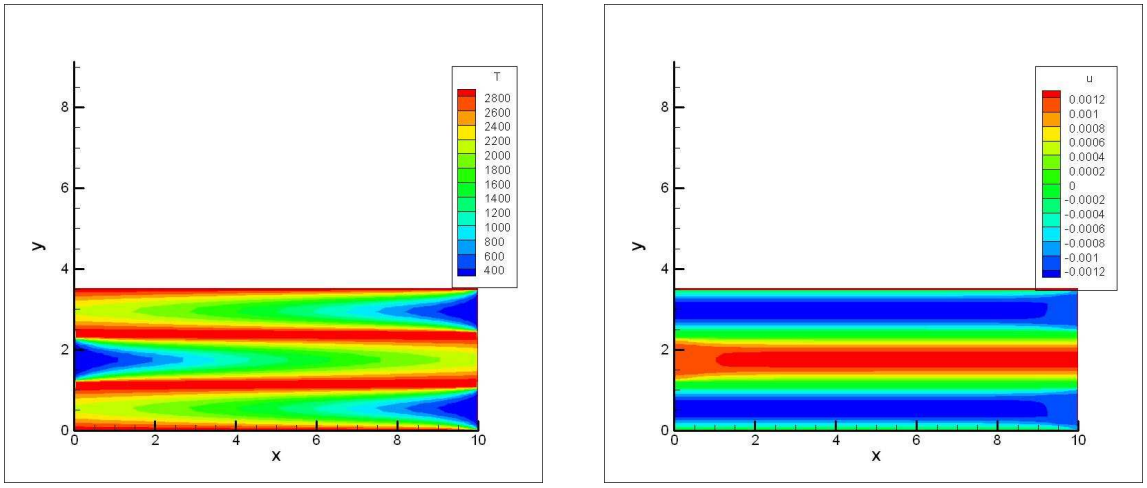

(a) (b)

Figure B.35. (a) The temperature and (b) x velocity values for the inlet velocity of $1 \times 10^{-3} m/s$ in triple flow

B.3. Contribution of Species Equation

In the first system; Methane and Oxygen are used for the experiment. By using the simple pipe and dividing it into two fictitious sections, it was easy to apply the boundary conditions for the problem. In the problem, from the upper part of the pipe, one of the species is given and from the lower part, other species is processed into the geometry. After redistributing among the geometry, it is easily seen that, a mixture of these species of the same mass fraction is obtained after a critical point.

In the example; Methane is given from the upper part of the geometry and denoted as Y_{one}; and Oxygen is given from the lower part and denoted as Y_{two}. Since ideal gas is solved; the momentum equations has given different values relatively to prior ones because of the varied density values.

In the second problem; Propane is given from the upper part of the geometry and denoted as Y_{one}; and Oxygen is given from the lower part and denoted as Y_{two}. The

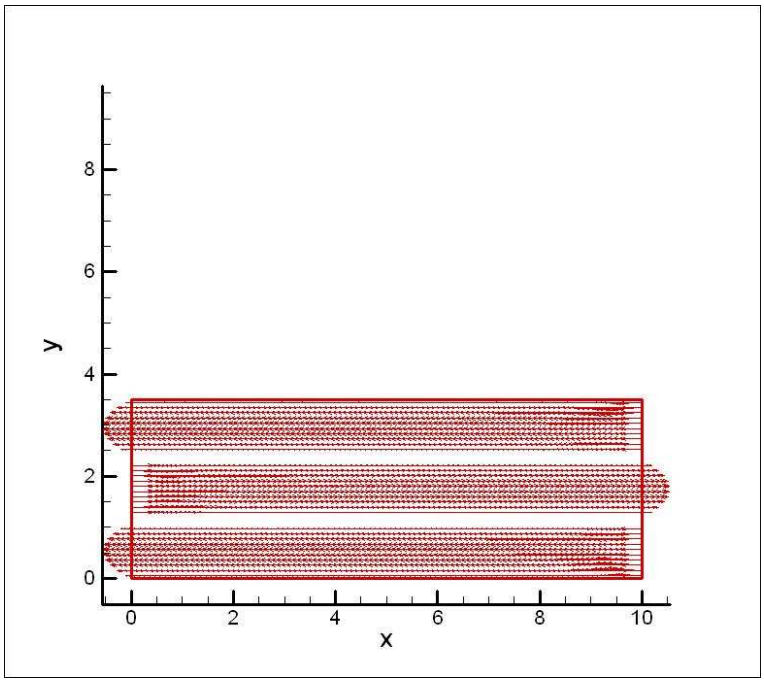

Figure B.36. The vectoral appearance of the triple flow

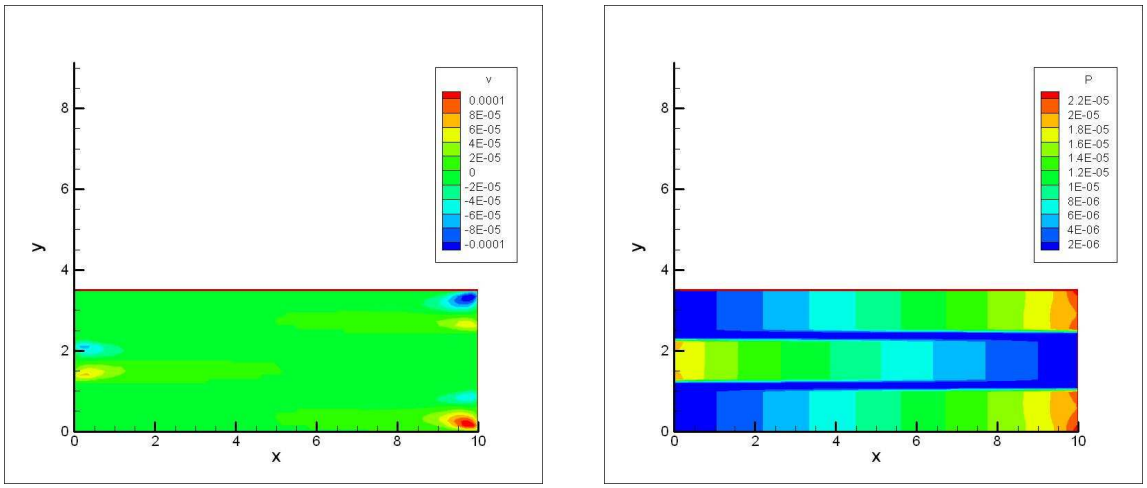

(a) (b)

Figure B.37. (a) The Y velocity values and (b) pressure distribution for the inlet velocity of $1 \times 10^{-3} m/s$ in triple flow

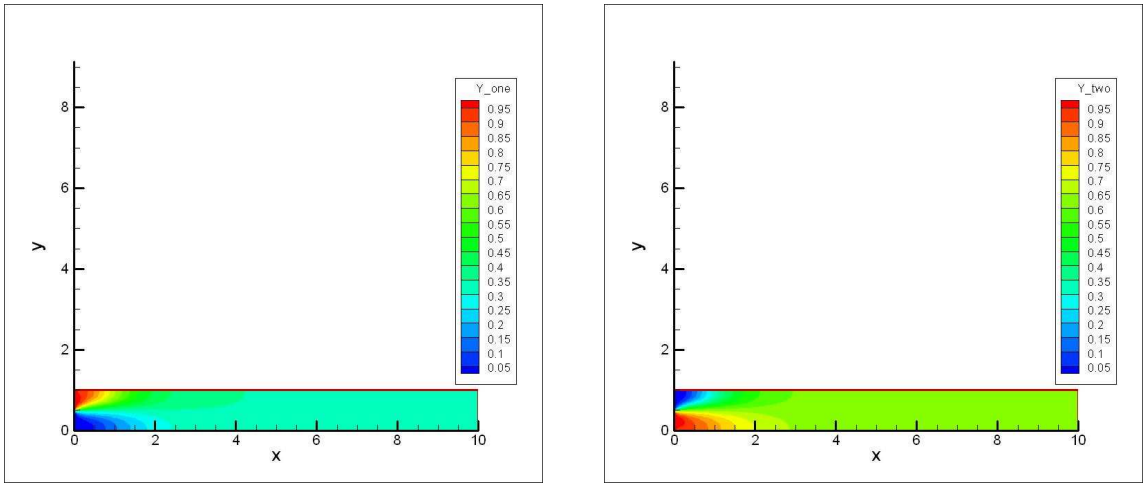

(a) (b)

Figure B.38. Mass fractions of (a) Methane and (b) Oxygen.

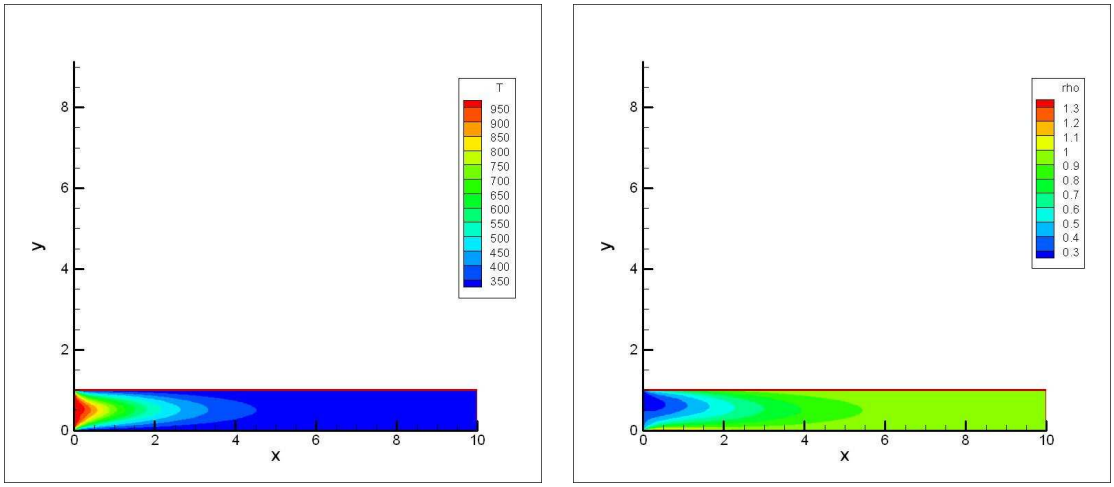

(a) (b)

Figure B.39. (a) The temperature and (b) density values.

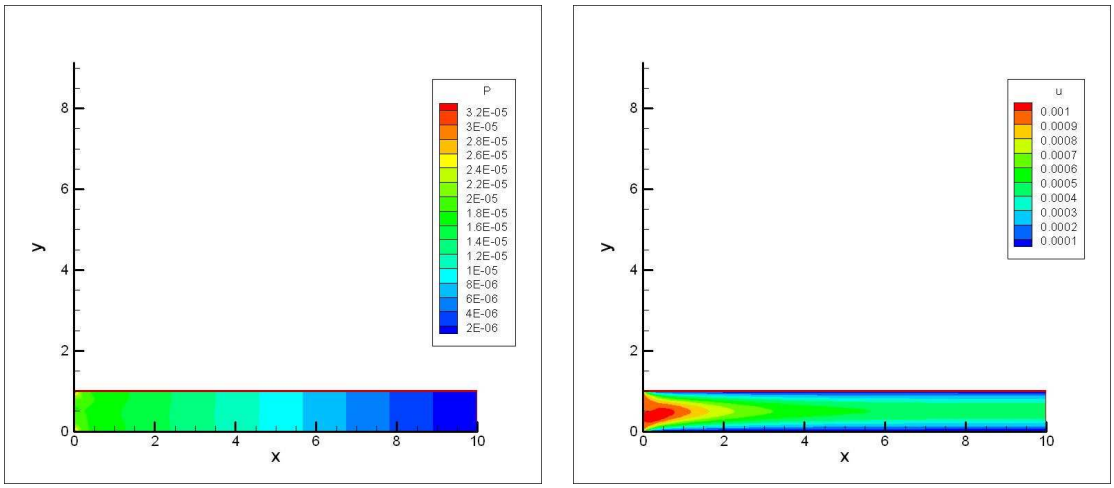

(a) (b)

Figure B.40. (a) The Pressure distribution and (b) density values.

results for that case are:

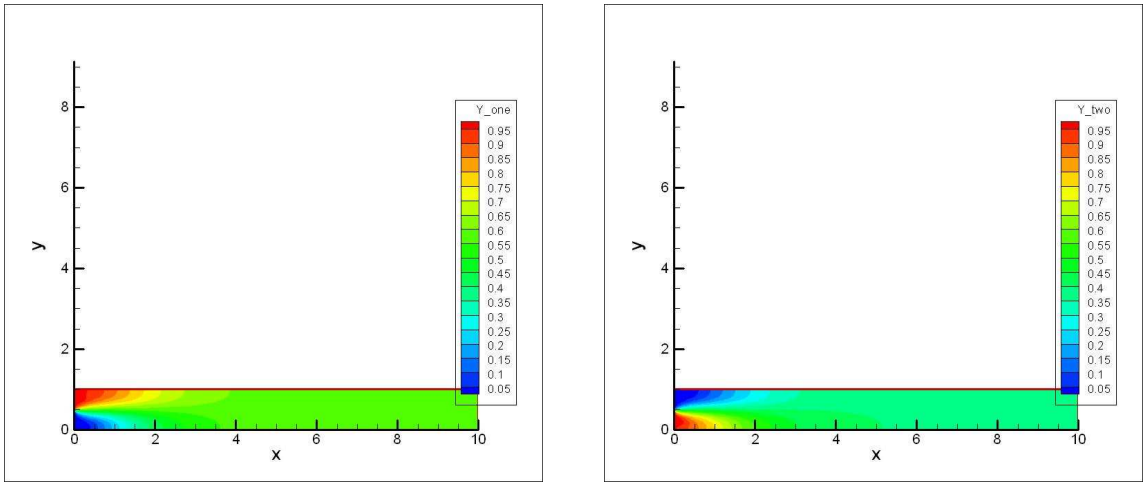

(a) (b)

Figure B.41. The mass fractions of (a) Propane and (b) Oxygen.

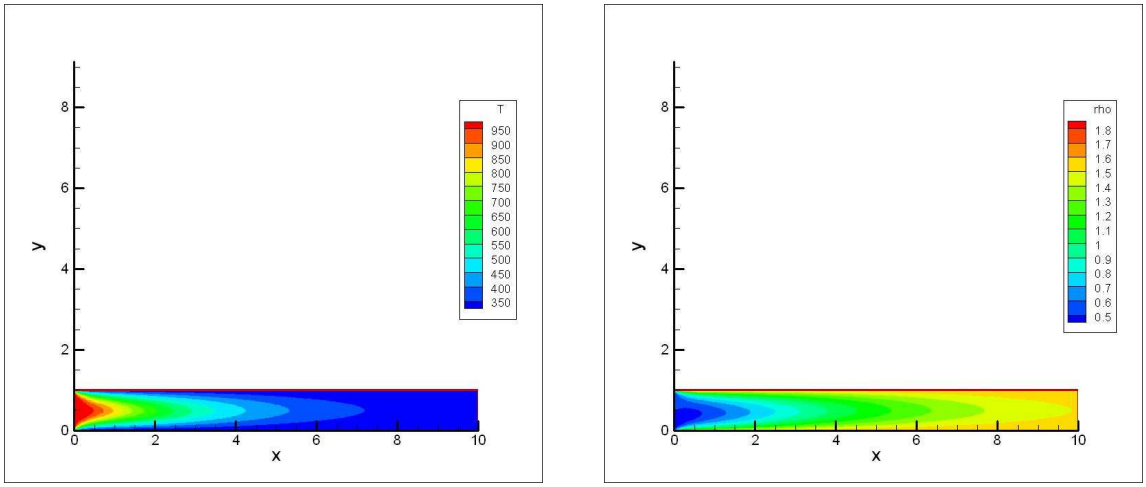

(a) (b)

Figure B.42. (a) The temperature and (b) density values.

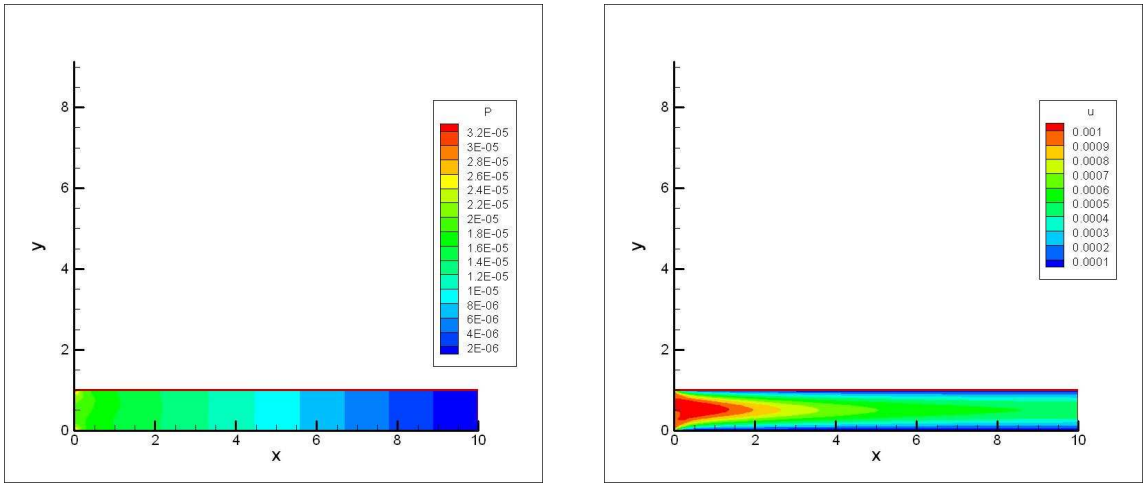

(a) (b)

Figure B.43. (a) The pressure and (b) x velocity values.

REFERENCES

1. L Sitzki, K Borer, E Schuster, P Ronney, S Wussow, The Third Asia- Pacific Conference on Combustion (2001) Seul Korea

2. J Vican, B F Gajdeczko, F L Dryer, D L Milius, I A Aksay, Proceedings of the Combustion Institute 29 (2002) 909-916

3. K Maruta, K Takeda, J Ahn, K Borer, L Sitzki, P D Ronney, O Deutschmann, Proceeding of the Combustion 29 (2002) 957-963

4. D Ronney, Combustion and Flame 135 (2003) 421-439

5. C Cui, M Matalon, J Daou, J Dold, Combustion Theory and Modeling 8 (2004) 41-64

6. M Chen, J Buckmaster, Combustion Theory Modeling 8 (2004) 701-720

7. K Maruta, J K Parc, K C Oh, T Fujimori, S S Minaev, R V Fursenko, Combustion, Explosion and Shock Waves 40 (2004) 516-523

8. J Ahn, C Eastwood, L Sitzki, P D Ronney, Proceedings of the combustion Institute 30 (2005) 2463-2472

9. N Kim, S Kato, T Kataoka, T Yokomori, S Maruyama, T Fujimori, K Maruta, Combustion and Flame 141 (2005) 229-240

10. Y Suzuki, Y Horii, N Kasagi, S MAtsuda, 17th IEEE Int. Conf. MEMS (2004) 312-315

11. Versteeg, Malalasakera, Introduction to computational fluid dynamics, 2007

12. Patankar, S.V., Numerical Heat Transfer and Fluid Flow Hemisphere Publishing

Corporation, 1980

13. L C Burmeister, Convective Heat Transfer, John Wiley Sons INC, 1993

14. K K Kuo, Principles of Combustion, John Wiley Sons INC, 2005

15. T Poinsot, D Veynante, Theoretical and Numerical Combustion, John Wiley Sons INC, 2005

16. C K Law, Combustion Physics, Cambridge University Press, 2006

17. W Bartok, A F Sarofim, Fossil Fuel Combustion: A source book, Cambridge University Press, John Wiley Sons INC, 1991